

AMERICAN UNIVERSITY OF BEIRUT

FULLY BIORESORBABLE AND FLEXIBLE
ELECTROCORTICOGRAPHY(ECoG) ARRAY FOR LOW
INVASIVE MONITORING OF EPILEPTIC SEIZURES

by
ISMAIL BABALE

A thesis
submitted in partial fulfillment of the requirements
for the degree of Master of Science
to the Biomedical Engineering Program
of the Maroun Semaan Faculty of Engineering and Architecture and Faculty of Medicine
at the American University of Beirut

Beirut, Lebanon
August 2022

AMERICAN UNIVERSITY OF BEIRUT

FULLY BIORESORBABLE AND FLEXIBLE
ELECTROCORTICOGRAPHY(ECoG) ARRAY FOR LOW
INVASIVE MONITORING OF EPILEPTIC SEIZURES

by

ISMAIL BABALE

Approved by:

Prof. Massoud Khraiche, Assistant Professor
Biomedical Engineering



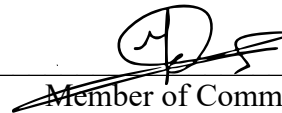
Advisor

Prof. Makram Obeid, Assistant Professor
Pediatrics and Adolescent Medicine



Co-Advisor

Prof. Firas Kobaissy, Associate Professor
Biochemistry and Molecular Genetics



Member of Committee

Prof. Ali Tehrani, Associate Professor
Bioproducts and Biosystems, Aalto University



Member of Committee

Prof. Mazen Saghir, Associate Professor
Electrical and Computer Engineering



Member of Committee

Date of thesis defense: August 19th, 2022

ACKNOWLEDGEMENTS

I would like to extend my profound gratitude to everyone that helped me in seeing this thesis progresses whether directly or indirectly. I would like to specially thank my advisor, Dr. Massoud Khraiche for his constant support and encouragement throughout my stay in the Lab. Additionally, I want to use this medium to thank my committee members for their support and contributions in seeing this thesis become a successful one.

I want to use this moment to thank my family and friends for their endless prayers and support. Many thanks to my Lab colleagues especially Sahera, Heba, Zeina, and Karen for supporting me and making my stay lively in the Lab.

ABSTRACT OF THE THESIS OF

Ismail Babale

for

Master of Science

Major: Biomedical Engineering

Title: Fully Bioresorbable and Flexible Electrocorticography (ECoG) Array for Low Invasive Monitoring of Epileptic Seizures

Implantable, bioresorbable, and flexible bioelectronics are leading the evolution towards non-invasive, high fidelity next-generation implanted devices, especially for recording acute/chronic neurophysiological signals from the brain. These devices promise to reduce foreign body response to implanted devices, saving neural tissue and improving recording fidelity and stability, extending implant life, and eliminating risks associated with surgical resection of implanted devices in acute recordings. Electrocorticography (ECoG) recordings are used in assessing the completeness of the treatment in patients with epilepsy. The latter is a central nervous system disorder in which brain activity becomes abnormal, causing seizures (a sudden, uncontrolled electrical disturbance in the brain) that lead to changes in behavior, movements, or feelings and sometimes loss of awareness. State-of-the-art devices for ECoG monitoring of seizures in patients with epilepsy are microelectrodes fabricated on rigid substrates with a high elastic modulus compared to the brain tissues. These implanted devices carry a high risk of failure and tissue damage due to mechanical mismatch with the soft brain tissue. Also, there is additional risk and cost to the patient when device resection is necessary. In this work, we designed and developed inkjet-printed microelectrode arrays on a flexible and biodegradable substrate for monitoring epilepsy. We fabricated the devices using a low-cost, additive inkjet printing process. The device has low-impedance gold microelectrodes on both polyimide (flexible substrate) and polycaprolactone (PCL, biodegradable substrate). We optimized the number of printed gold layers and parameters for a light-based sintering approach, achieving a minimum sheet resistance of 2.84 Ω /sq on PI at 3 layers and 2.54 Ω /sq at 9 layers on PCL. The mean impedance of 100 x 100 μ m electrodes on PI and 300 x 400 μ m electrodes on PCL measured 34.4 k Ω and 30.1 k Ω respectively. We recorded high fidelity epileptic seizure activity on multiple channels per device in an in vivo rat seizures model, where seizures were pharmacologically induced. Lastly, an accelerated degradation test was performed to assess the bioresorbable potential of our electrodes built on PCL. The work overall demonstrates the potential of inkjet printing for building low invasiveness, bioresorbable ECoG devices for applications in implanted neural interfaces. The scalability of the technology and approach used to build these devices also opens the door for potential near-future translation to clinical applications.

TABLE OF CONTENTS

ACKNOWLEDGEMENTS	1
ABSTRACT	2
ILLUSTRATIONS	6
TABLES	10
ABBREVIATIONS	11
INTRODUCTION	12
LITERATURE REVIEW	15
2.1. Measurable Neural signals	15
2.2. Neuron-electrode interface model	18
2.3. Neural Interface in Epilepsy	19
2.4. Neural Recording Challenges	20
2.5. Biodegradable/Bioresorbable Materials for Neural Prosthetics	21
2.6. Commercially available ECoG devices	24
2.7. Printing Technologies	26
2.8. Inkjet Printing technology	28
2.9. Drop Spacing	29
2.10. Nanoparticles	30
2.10.1 Biocompatibility of Nanoparticles in Biomedical Applications.....	31

2.10.2. Inkjettable Nanoparticles Ink Characteristics	32
2.10.3. Synthesis of Nanoparticles.....	33
2.10.4. Post-Printing Treatments of Nanoparticles ink.....	33
2.11. Dielectrics	34
SPECIFIC AIMS	36
METHODOLOGY	38
RESULTS	56
5.1.Surface Characterization.....	56
5.2. Printing of Gold Nanoparticles Ink on Polyimide substrate	59
5.3. Polyimide ink for insulation	61
5.4. Inkjet Printing of electrodes on PCL Substrate	67
5.5. Photonic Sintering of Gold electrodes on PCL.....	70
5.6. Electrical characterization.....	74
5.7. Printing on PCL & photonic sintering	76
5.8. Electrochemical Characterization	79
5.9. Electrochemical impedance of gold electrodes on PI.....	80
5.10. Electrochemical impedance of gold electrodes on PCL electrodes	81
5.11. In vivo Neurophysiological testing of electrodes	83
5.12. Degradation Test.....	90
DISCUSSION.....	93

CONCLUSION98

REFERENCES100

ILLUSTRATIONS

Figure

1. Placement of electrodes for extracellular recording at different depths. Over the scalp(EEG), onto the surface of the cerebral cortex (ECoG), and intracranial/intraparenchymal (Using depth electrodes).....	17
2. The three methods of electrophysiological recordings. Each method of signal recording is defined by the placement of the electrode: extracellular recording(outside the neuron), intracellular recording (inside the neuron), and patch clamp recording. Adapted from [14].....	18
3. Equivalent circuit model explaining measured extracellular brain signals. Adapted from[22]The schematic diagram shows a neuron (blue color) on a recording device (yellow) with one electrode contact site (orange). The recorded signals are sourced from the transmembrane currents, that flow through a seal resistance containing cleft, which ultimately results in the flow of current at the electrode site	19
4. Schematic diagram of neural interfaces and different electrode materials [33] .	20
5. Photolithography fabrication process using a positive photoresist. (a) Metal deposition,(b) spin coating of photoresist,(c)mask alignment and exposure of light, followed by resist development and hard baking,(d)etching of exposed metal,(e) removal of the remaining resist,(f) patterned metal on the substrate. Adapted from [65]	27
6. Schematic diagram of inkjet printing methods. (a) continuous inkjet printing and drop-on-demand-inkjet printing method(b).Adapted from[74]	29
7. Typical behavior of printed lines on a substrate.Individual drops(a), scalloped line(b), uniform line(c), bulging(d), and stacked coins (e).Drop spacing decreases from left to right (a-e). Adopted from[75].....	30
8. Schematic illustration of the sintering process of nanoparticles[92]	34
9. Schematic diagram of DMP-2850 inkjet printer.....	39
10. DMP-2850 inkjet printing workstation.....	40
11. Au in jetting waveform	42
12. PI ink jetting waveform	43
13. PCL electrode fabrication process	45
14. Top view of electrodes pattern 1	45
15. Top view of electrodes pattern 2.....	45

16. Flash sintering set up using camera flash.(a)Schematic diagram of the set-up (b)front view of the set up with Nikon Speedlight SB-28 (c)Lateral view with sample	47
17. Schematic diagram of four-point probe system (ossila) (a) and its equivalent circuit (b)[104]	48
18. EIS 3 electrode cell system set up. Adapted from [108].	50
19. Diagram of coronal section of the brain showing the intra-amygdala injection site. B- indicates the surface of the skull and A-indicates the surface of the brain.	53
20. In vivo recording set-up using the ME2100 system from multichannel systems. (a) Stereotaxic instrument,(b) Headstage,(c) Signal collector unit,(d)Interface board,(e) Computer for data visualization and analysis	54
21. SEM images of PCL films at different scales showing the topographical rough surface (a and b), PI films showing smoother surface(c and d).....	57
22. Optical microscopic images of PCL. (a) PCL film briefly subjected to heat on a hotplate having a less rough surface,(b)PCL film not subjected to heat, showing rougher surface, PI film surfaces(c and d).	58
23. Gold print on non-etched and etched PI substrate. (a and b) 100 μ m line on non-etched PI substrate at 20 μ m and 15 μ m drop spacing respectively, showing non-uniform spread of ink and poor printing quality, (c, d and e) 100 μ m line on 30 seconds plasma-etched PI substrate at 50 μ m,30 μ m and 20 μ m drop spacing respectively. Printing at this substrate condition yields well defined pattern	60
24. Printing quality of 2 layers of gold between 1-minute (a) and 30 seconds plasma etching(b).	61
25. Several layers of PI ink on a non-etched PI substrate at 15 μ m Drop spacing . (a) 2 layers,(b) 4 layers, (c) 6 layers, (d) 8 layers, and (e) 10 layers. Ink spread and concentration increased with increase in number of layers.	62
26. PI ink insulation on electrodes (pre-etched).Non-continuous PI ink deposition with areas devoid of ink due to hydrophobic nature of the gold printed pattern and non-etched PI substrate surface(a-e).	64
27. PI ink insulation on electrodes (Etched surface).Uniform and continuous distribution of PI ink. Optimum coverage of PI insulation layer on electrode tracks(a),uniform insulation ink distribution over the electrodes track with the exception of the electrode active contact site (b).....	64
28. Optical microscopic images of electrodes printed on PI.(a)Contact pads (b)Electrodes track (c)PI insulated electrodes showing exposed site (d) Electrodes without PI insulation	65
29. Images of PI electrodes array. PI six electrode array(a),flexed PI based electrode, PI electrode fixed in the connector for ME2100 head stage.	66

30. Optical microscopic images of electrodes printed on PCL.(a)Electrodes active site,(b)Contact pads ,(c)Electrodes track/leads,(d)PCL heat pressed electrodes with the exposed active site.	73
31. Images of PCL array. (a)and (b) PCL electrode with the connector(c)and (d) PCL electrodes conform on the surface of a pipette.....	74
32. Sheet resistance measurement between different number of gold layers on PI and corresponding electrical resistance.	75
33. Sheet resistance measurement between different number of gold layers on PCL at 3 flashes sintering condition.	77
34. Sheet resistance measurement of 9 layers of gold layers on PCL at 2, 3, and 4 flashes.	78
35. Sheet resistance measurement of 5 layers of gold on PCL at 2, 3, and 4 flashes.	79
36. Electrochemical Impedance Spectroscopy of PI electrodes before and after the experiment	81
37. Electrochemical impedance spectroscopy of PCL electrodes before and after 16 hours in PBS.	82
38. Continuous Electrochemical Impedance Spectroscopy of PCL Electrodes at 1KHz. There was a stable recording for over a period of 14 hours, after that a large drop in impedance was noticed which is likely due to delamination of the encapsulation layer (red arrow)	82
39. In vivo testing recording set-up	83
40. Microelectrode arrays implantation procedures in the rat brain.4mmx4mm craniotomy on the left side of the skull (a), where a 1µl Hamilton syringe is positioned over the injection site(b), axial view of polyimide electrodes over the exposed brain tissue(c), lateral view of electrode placement(d), Axial view of PCL electrodes placement (e).....	85
41. Signals from 3.....	87
42. Rhythmic beta activities before seizure discharge.....	Error! Bookmark not defined.
43. High frequency rhythmic sharp waves over the period of 4 seconds right after the large sharp wave as the point of seizure initiation (red arrow). This continues and evolve to the next stage of the seizure discharge as it progresses.....	87
44. Magnified image of high-frequency poly-spike like seizure discharge and transition from one burst of spikes to the next one. This is the third stage of our seizure discharge, and it is the continuous evolution of the high frequency rhythmic sharp waves which occurs immediately after the initial large sharp wave indicating the seizure initiation.	88

45. Figure. Low pass filtered signal at 200Hz and spectrogram over the period of 7 minutes. Seizure areas are seen as segments of increased activity and power (yellow) on the spectrogram, while the area of normal activities or baseline appear blue.	88
46. High-frequency oscillations (HFOs). Band passed signal between 80-600Hz Band passed signal between 80-600Hz over the period of 6 minutes(a),magnified HFOs from one of the seizure burst showing high amplitude seizure discharge(b)	89
47. High-frequency oscillations (HFOs) and its corresponding spectrogram. Baseline area represented as area of low activity(blue),while area of seizure discharge is seen as area of increased activity(yellow).	90
48. Spike and wave discharge. This is a characteristic manifestation of seizure. It appears as a sharp wave that is accompanied by an intermittent slow wave.	90
49. Series of images captured at different stages of accelerated degradation testing of PCL-based microelectrodes in buffer solution (pH 13) at 37 °C.....	92

TABLES

Table

1. Commercially available state-of-the-art ECoG devices	25
2. Physical properties of the ink used for printing at room temperature.	41
3. Inkjet printing parameters for ink deposition.	42
4. The sheet resistance of gold layers on PI.....	75
5. Sheet resistance measurement between different number of gold layers on PCL at 3 flashes sintering condition.	76
6. Sheet resistance measurement of 9 layers of gold layers on PCL at 2, 3, and 4 flashes.	77
7. Sheet resistance measurement of 5 layers of gold on PCL at 2, 3, and 4 flashes.	78

ABBREVIATIONS

AEDs	Antiepileptic drugs
DMSO	Dimethyl sulfoxide
ECOG	Electrocorticography
EEG	Electroencephalography
GABA	Gamma-aminobutyric acid
iEEG	Intracranial electroencephalography
MEAs	Microelectrode arrays
PBS	Phosphate buffer saline
PCL	Polycaprolactone
PDMS	Poly-di-methyl-siloxane
PEDOT:PSS	Poly(3,4-ethylene dioxythiophene)-poly(styrene sulfonate)
PLGA	Poly(lactide-co-glycolide)
PMF	Poly(melamineco-formaldehyde)
PPy	Poly-pyrrole
PVPh	Poly(4-vinyl phenol)
SNR	Signal to noise ratio
SRSs	Spontaneous recurrent seizures

CHAPTER 1

INTRODUCTION

Epilepsy is a chronic neurological disorder that causes recurrent unprovoked seizures, where abnormal, uncontrolled electrical activity of the brain that causes changes in behavior, movements or feelings, memory, and level of consciousness[1, 2]. Glutamate, a neurotransmitter in the central nervous system plays a major role in the excitatory activities of the central nervous system and has been linked to seizure initiation [3, 4]. The international league against epilepsy (ILAE) states that epilepsy syndrome diagnosis is made only after one unprovoked seizure and the patient has a probability of about sixty percent of developing subsequent seizures over the succeeding ten years, or when at least two unprovoked seizures happen for a period longer than twenty-four hours[5].

Following the diagnosis of a patient with epilepsy, the first round of therapy is antiepileptic drugs (AEDs), which modify the abnormal neuronal discharge in seizures without negatively impacting the nervous system. Over the past decades, about 12 different AEDs have been developed and classified based on their target of action. Some of these AEDs act by enhancing the inhibition of the synapse that is mediated by gamma-aminobutyric acid (GABA) like valproate receptors, voltage-gated sodium, and/or calcium blockers like lamotrigine, and glutamate receptors mediated synaptic excitation inhibitors like topiramate[6]. It has been reported that about thirty percent of epilepsy patients under AEDs show resistance to the drug and continue to have unprovoked seizures during the medication period [7]. Epilepsy patients are said to be drug-resistant epilepsy patients if two optimal AED schedules (known as the mono or polytherapy) do

not stop the occurrence of the seizure[8]. As such, this category of patients (drug-resistant epilepsy patients) needs an alternative therapeutic intervention that will address the issues of unprovoked seizures to improve their quality of life. AEDs and surgery are the traditional therapeutic approach for epilepsy. Other alternative treatments and potential future treatments include transcranial magnetic stimulation(TMS), external trigeminal nerve stimulation, minimally invasive surgery using MRI-guided focused ultrasound, and subthreshold stimulation(continuous stimulation of seizure onset zones)[9]. Epilepsy can affect people of all ages, and its prevalence is equal in both sexes, however, it is more common in very young and elderly populations. The most critical step towards addressing this disease is proper diagnosis and localization of seizure onset zones.

The most common diagnostic tool used for seizures is electroencephalography (EEG), also known as scalp EEG. This is a technique used to record brain activity by placing electrodes on the surface of the scalp. It is used clinically for the diagnosis of diseases such as sleep apnea[10], seizures[11], and for brain-machine interfacing (Brain-computer interface) commercially[12]. EEG has poor resolution due to the loss of signals as it traverses through different layers of the brain tissue, dura mater, and skull. EEG is capable of diagnosing seizures but due to limited resolution, it is not able to pinpoint seizure onset zones. Another clinically used tool for seizure localization is electrocorticography(ECoG). ECoG, also known as intracranial electroencephalography(iEEG) was pioneered in the 1950s at the Montreal Neurological Institute by neurosurgeons Wilder Penfield and Herbert Jasper for the study of epilepsy[13]. This method makes use of electrodes placed directly on the surface of the cerebral cortex to record the electrical activity of the brain. Although the brain tissue is not penetrated, ECoG requires a craniotomy to surgically implant the device, as a result,

it is considered an invasive procedure. Since ECoG records signal directly from the brain cortex with minimal loss of information, This makes it has superior resolution over scalp EEG. Many approaches and technologies have been used to improve prosthetic intervention due to the complexity of the chronic integration of an electronic device with neural tissue. This includes the utilization of different biocompatible materials like certain polymers such as PCL, PLLA, and PLGA among others to enhance its performance and comply with soft brain tissue. Similarly, using flexible and biodegradable polymers for the fabrication of the neural interface offers many advantages over conventional materials. The biodegradable materials have a low elastic modulus, making them almost similar to that of the brain tissue and reducing the chance of evoking immune response which ultimately forms a sheath that encapsulates the device and makes it fail. It also eliminates the need for a second surgery for device removal following insertion, which poses the risk of infection and adds additional damage to the brain tissues due to the surgery.

CHAPTER 2

LITERATURE REVIEW

The objective of this literature review section is to give an overview of the important concept of this thesis. This includes an overview of measurable neural signals, model of the electrode-tissue interface which helps in the understanding the electrode and the biological tissue interface, importance of neural interface in epilepsy, recording challenges, biodegradable materials used for neural prosthetic devices, commercially available ECoG devices, printing technologies and ink characteristics and finally nanoparticles in microfabrication.

2.1. Measurable Neural signals

The study of the electrical activity of neurons and the molecular and cellular processes governing their signaling is known as *electrophysiology*. This can be done at the level of a single cell, or it can include measurements from hundreds or even thousands of cells at the same time. Electrophysiology techniques are categorized mainly into three main types based on the location of the electrode or recording probe placement in the neural specimen. It is termed extracellular recording when the electrode is placed outside and close to the neuron of interest, an intracellular recording when the electrode is inserted inside of the neuron, and lastly, patch clamp recording when the electrode and neural membrane are closely apposed and makes a very tight seal with the membrane patch[14].

Activities of neurons in the brain generate transmembrane currents which can be measured or recorded in the extracellular medium. Although the synaptic transmembrane current is the primary source of extracellular signal, other sources such as Ca^{+} and Na^{2+}

spikes, ionic fluxes through ligand- and voltage-gated channels, as well as intrinsic membrane oscillations can all significantly shape the extracellular field. The extracellular field is influenced by any excitable membrane, whether it is an axon, dendrite, soma, or axon terminal, as well as any type of transmembrane current. All ionic processes, from the slowest fluctuations in glia to the fast action potentials are superimposed in the field. superimpose at any given point in space to yield V_e (electric potential) at that location. Thus, any transmembrane current, irrespective of its origin, leads to an intracellular as well as an extracellular voltage deflection. The specific characteristics of a measured extracellular waveform such as its frequency and amplitude depend on the brain tissue properties and multiple sources contributing to the recorded electric potential. V_e can be measured with electrodes placed either on surface of the scalp(EEG), surface of the cerebral cortex (ECoG), or even from depth surfaces using depth penetrating electrodes in the brain. In general, the smaller the distance from the electrode to the source of the signals, the higher the information recorded and vice versa[15]. Extracellular field recording techniques have a major advantage over other methods for brain activity networks in that the biophysics associated with these measurements is well understood. This has allowed for the development of quantitative and reliable mathematical models that explain how transmembrane currents generate the recorded electric potential[15].

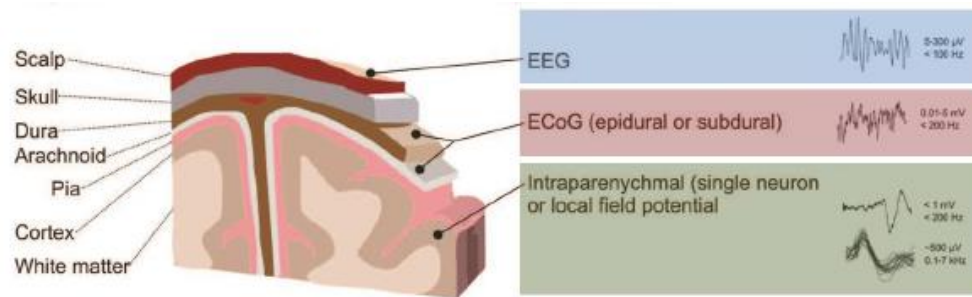


Figure 1. Placement of electrodes for extracellular recording at different depths. Over the scalp(EEG), onto the surface of the cerebral cortex (ECoG), and intracranial/intraparenchymal (Using depth electrodes).

Intracellular recordings on the other hand are used to study the physiology of individual cells. It measures the potential difference (voltage) or current produced by ion movement across a cell membrane typically using a glass capillary electrode containing an electrolyte solution[16]. Intracellular recordings from individual neurons provide the highest temporal and spatial resolution of any known technique for monitoring the brain. They have several major advantages over extracellular recordings such as the ability to record subthreshold brain dynamic events such as membrane potential oscillations and synaptic, that have been identified to play a critical role in neural coding. It also gives information about the large dynamic range of signals up to 80-100 mV and the ability to obtain structural information about the recorded neurons (via dye labeling)[17-20]. Glass micropipettes with cumbersome micromanipulators and very bulk positioning systems were used traditionally used to record intracellularly from neurons. Despite their extensive use in in vitro studies, using this system for in vivo studies has been limited because of the technological large form factor[21].

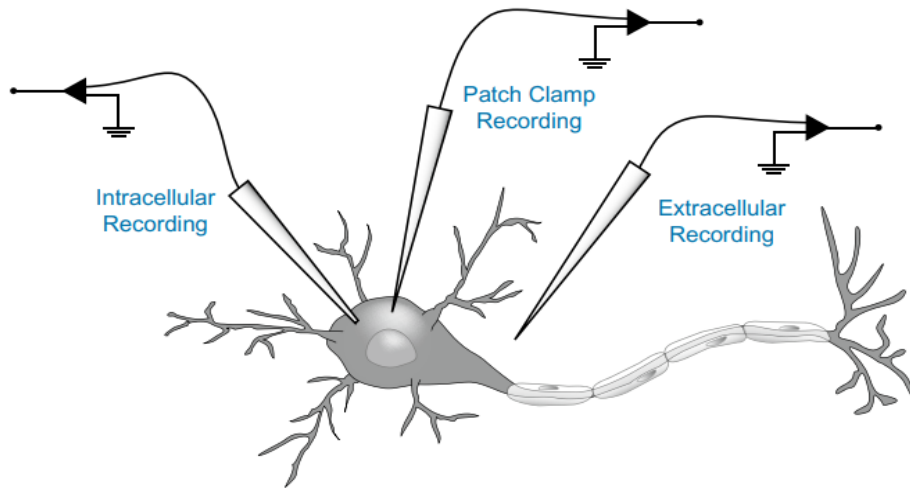


Figure 2. The three methods of electrophysiological recordings. Each method of signal recording is defined by the placement of the electrode: extracellular recording(outside the neuron), intracellular recording (inside the neuron), and patch clamp recording. Adapted from [14].

2.2. Neuron-electrode interface model

To better understand the electrophysiological signals, and physiological interaction during brain signal recording and to improve the neural interface, neuron-electrode interface models are created to simulate what is measured or recorded. Figure 1. Below shows an equivalent circuit model with three main components: A neuron, a cleft (between the neuron and electrode recording site), and the electrode device. In this represented equivalent circuit model, the membrane of the neuron facing the electrode contact site is referred to as the *junctional membrane* and the neural membrane that is away from the electrode contact site(not facing the electrode site) is called the *non-junctional membrane*. Both membranes are represented by a resistance (R_j and R_{nj}), where R_j is the resistance of the junctional membrane and R_{nj} is the resistance of the non-junctional membrane. The membranes also have a capacitance in parallel (C_j and C_{nj}), where C_j is the capacitance of the junctional membrane and C_{nj} is the capacitance of the non-junctional membrane. The cleft, which is the second component of the equivalent circuit model represents a space filled with physiological solutions and generates what is called the *seal resistance*. It has an influence on the flow of current across the electrode

site. Finally, the resulting current at the site of the electrode is represented with resistance and capacitance arranged in parallel (R_e and C_e).

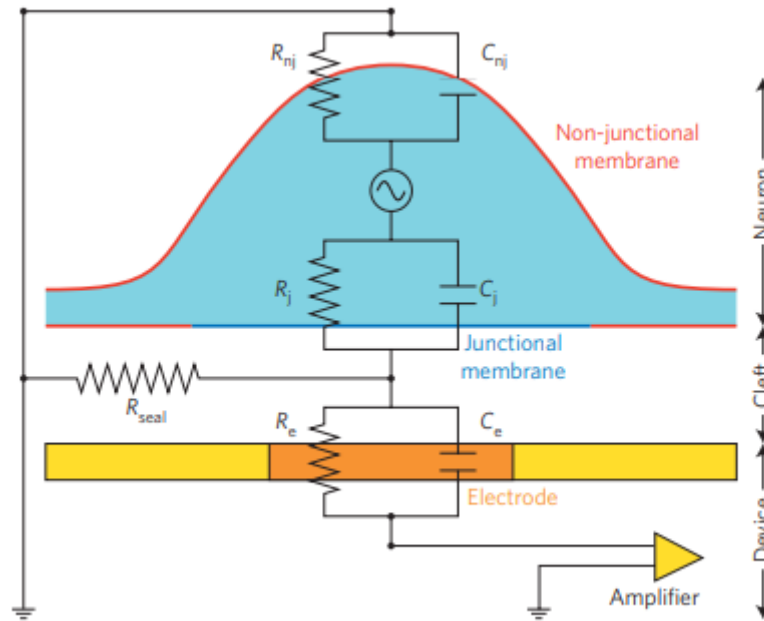


Figure 3. Equivalent circuit model explaining measured extracellular brain signals. Adapted from [22]. The schematic diagram shows a neuron (blue color) on a recording device (yellow) with one electrode contact site (orange). The recorded signals are sourced from the transmembrane currents, that flow through a seal resistance containing cleft, which ultimately results in the flow of current at the electrode site.

2.3. Neural Interface in Epilepsy

The neural interface is an integral part of a prosthetic device that is in direct contact with the brain tissues and plays a vital role in the application of neural prosthesis for diagnosis, treatment, and management of neurological disorders [23-25]. This technology has been shown to be very effective and useful in the treatment of several neurological diseases such as epilepsy, Parkinson's disease, dystonia, essential tremor, and other movement disorders. It works by either injecting an electrical charge into the brain tissue (neural stimulation), recording neural activities from the brain tissue, or technically integrated to do both neural recording and neural stimulation [25, 26]. Electrocorticography (ECOG) electrodes are extensively used in the brain-computer interface for patients with neurological defects to enhance their quality of life. It offers an advantage over penetrating electrodes because it is minimally invasive, hence posing

less damage to the brain tissue. It also has superior spatial resolution and signal-to-noise ratio (SNR) over the conventionally used electroencephalography electrodes (EEG). This makes it a very attractive tool for neural signal acquisition [6, 27, 28]. ECoG electrodes usually have a diameter of about 1-2.33 mm diameter, 10mm inter-electrode spacing, and are embedded in a silastic base of about 0.4-0.6mm in thickness [29, 30]. Smaller high-density electrodes with micro-scale diameters (70–1500 μm) and 1-4 mm inter-electrode spacing have been employed for research in humans [31, 32]. Below is a diagram showing different neural interfaces and materials used for their designs.

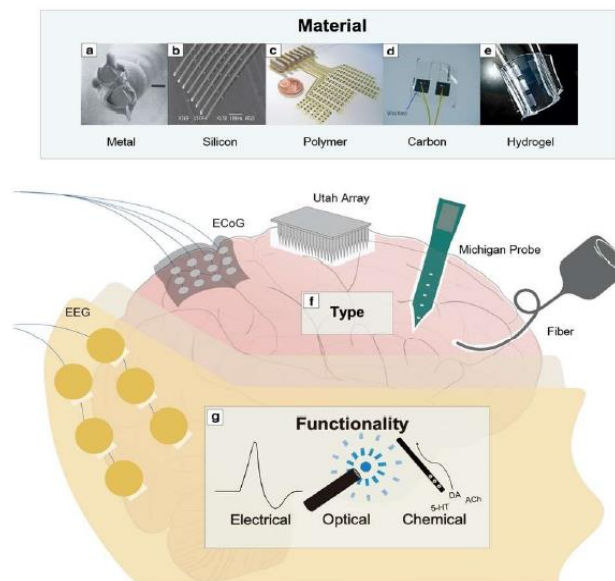


Figure 4. Schematic diagram of neural interfaces and different electrode materials [33]

2.4. Neural Recording Challenges

Neural recording devices act as a bridge that allows communication between the brain and external devices. However, because of the complex nature of these devices, several challenges arise during recording. Classical challenges being faced include the biomechanical mismatch between the device and the soft brain tissue. Conventional brain electrodes are made on rigid silicon substrates with an elastic modulus of approximately 160GPa which is very high compared to the brain tissues' elastic modulus (typically

between 3-100KPa)[34]. Consequences arising due to mechanical mismatch lead to three unfavorable incidents; one, the rigidity of the electrodes over the brain tissue creates shear motion at the recording side, changing the position between the neural interface and the recorded neurons, leading to instability in chronic recording in vivo. Secondly, a very rigid implant causes recurrent damage to the brain tissue and neurons proximal to the electrodes, which triggers an immune reaction in response to the injury and glial cells proliferation (astroglia and microglia) which forms a glial sheath (about 100 μm thick) that ultimately encapsulate the electrode, creating a barrier between the implants and the device, thereby impeding signal recording[35]. Lastly, triggered immune response leads to the disruption of the normal distribution of neurons and glia at the electrode side. Owing to the cooperative effect of glial cells in delineating the functional transformation of neural networks [36, 37], this disruption in neuron-glial distribution deters the studying of individual neuron activities and neural circuits. Other challenges are implant and tissue damage due to abnormal chemical reactions at the site of the electrodes and device damage during secondary surgery in patients that require postoperative monitoring [23]. To address these challenges in neural interfacing, attention has been focused on new materials that will outperform the conventional ones both in terms of mechanical compliance with the brain tissue and recording stability. The development of a flexible and biodegradable ECoG device will open room to addressing the limitations associated with the conventional devices.

2.5. Biodegradable/Bioresorbable Materials for Neural Prosthetics

Material selection for the fabrication of neural prosthetics is a critical factor for its success; this plays a vital role in the performance of the device and its long-term use.

Bioresorbable materials for the fabrication of neural interfaces are a great choice because they offer several advantages over conventional ones. It allows the fabrication of devices that conform to the brain surface and eliminates the mechanical mismatch between the electrode and the brain that arises from using conventional substrates. In many cases, in order to localize the brain region where the epileptic seizure originates, ECoG electrodes are surgically placed on the brain for about one to three weeks for monitoring[38]. Subsequently, a second surgery is needed for the removal of the device along with brain resection of the areas generating the seizure, while in some cases, electrodes are left even after resection for a certain time in preparation for the placement of neural prosthetics. According to recent research, ambulatory intracranial recording for 1-3 months may be required for adequate localization of seizures for epilepsy surgery or placement of devices [39]. This period is very long to be adopted for use in hospital settings. Currently used ECoG devices in hospitals are non-bioresorbable and will require surgery for removal at the end of monitoring. The use of bioresorbable devices will eliminate the risk associated with device retrieval surgery and an additional cost to patients at the end of the recording period. By the end of the recording period, conventional devices would have been adhered to the underlying tissues or encapsulated by glial cells, where retrieving them will cause injury at the implantation site. An ideal device for such an application will be a bioresorbable ECoG array that is capable of recording brain activities over a certain period before it degrades and stops working. With the advent of bioresorbable ECoG devices, the use of ECoG will easily be extended from pre-operative to a desired post-operative monitoring period without the need for any additional surgery. Varieties of biodegradable and bioresorbable materials have been explored for neural interfacing. For example, A recent study has used polycaprolactone (PCL) and a copolymer of poly(l-

lactic acid and poly(trimethylene carbonate)(PLLA-PTMC) substrate to fabricate a fully degradable device that injects electrical cues for peripheral nerve regeneration, where a successful recovery of the motor function was achieved in rodents. Using biodegradable materials eliminates the need for subsequent surgery that would have been done in the conventional procedure for retrieval[40]. Other studies have used poly(lactic-co-glycolic acid) (PLGA) substrate to fabricate a device that map cortical electrical activities [25], poly(l-lactide) (PLLA) and polycaprolactone (PCL) composite (PLLA/ PCL)[41, 42]. Polyethylene glycol (PEG) was also recently explored as a substrate material where cortical signals were recorded from the brain of a cat[43]. In a recent study using inkjet printing technology, electrodes were printed on agarose and gelatin substrates, neuronal spikes were recorded from cardio myocyte like HL-1 cells[44], and more recently PCL substrate was used to print microelectrodes that were tested in vitro on rat isolated neural retina and PC12 cells[45].

Polycaprolactone (PCL) is one of the members of the biodegradable polyester family (others are PGA and PLA) with a relatively low melting temperature of about 60°C and a glass transition temperature of -60°C [46]. It is biocompatible and non-toxic to tissue, hence widely used as a scaffolds material for tissue engineering, drug delivery applications, and bioresorbable sutures is relatively hydrophobic and exhibits a longer degradation time (2 to 3 years) [47]. The FDA recently approved PCL for use in medical devices[48]. To our knowledge, there is only one study that used inkjet-printing technology to fabricate microelectrodes on PCL for in-vitro extracellular recording[45]. Moreover, no studies have been done to develop gold microelectrodes on PCL using inkjet printing technology. Our study will present one of the first fully degradable and

bioresorbable inkjet-printed microelectrode arrays based on gold nanoparticles printed on polycaprolactone (PCL).

2.6. Commercially available ECoG devices

We have summarized some of the state-of-the-art electrocorticography devices that are commercially available for human use and research purposes below (Table 1). In this table, we have considered materials used for the fabrication of the device, measurements such as electrode diameter (contact exposure), Inter-electrode spacing (pitch), and application. All devices listed are non-biodegradable and will require retrieval surgery if chronically implanted for seizure lateralization. Based on our search, there are no commercially available biodegradable/bioresorbable microelectrode arrays at the time being. Below is the table showing the commercially available ECoG devices and their materials:

Table 1. Commercially available state-of-the-art ECoG devices

ECoG Device	Company	Substrate material	Electrode Site Material	Channel Count	Spacing/pitch	Contact exposure	Application	
Auragen TM Cortical grid	Integralife	Property-specific silicones	Platinum/iridium	2 to 64	1 cm	1.5mm	Humans	[49]
Neuronexus ECoG	Neuronexus	Polyimide	Platinum	16, 32, 64	Not disclosed	Not disclosed	Humans	[50]
PMT Cortac Intracranial electrodes	Cortac	Not disclosed	Platinum or stainless steel	8-64	4mm-7.5mm	1.0, 2.0mm, 3.0mm, 4.5mm	Humans	[51]
CORTEC silicone-based °AirRay research electrodes	Cortec	Silicones	platinum: iridium contact	4 to 64	10mm	2.7mm	Humans	[52]
Ad-Tech Medical Subdural Cortical Electrodes	Ad-Tech	Silicone	90:10 Platinum: iridium or Stainless Steel	3-128	10 mm	1.17, 1.8 mm, 5 mm	Humans	[53]
AirRay research micro 8 hexagonal	Cortec	Silicone	Platinum Iridium	8	1.2mm	0.3mm	Large animals	[54]
Cambridge NeuroTech ECOG 32A	Cambridge NeuroTech	Silicon	Not disclosed	32	350 µm	20 µm	Rats	[55]
Cambridge NeuroTech ECOG 32B	Cambridge NeuroTech	Silicon	Not disclosed	32	700 µm	20 µm	Rats	[55]
Cambridge NeuroTech ECOG 64A	Cambridge NeuroTech	Silicon	Not disclosed	64	30 µm	12 µm	Rats	[55]
Cambridge NeuroTech ECOG 64B	Cambridge NeuroTech	Silicon	Not disclosed	64	250 µm	80 µm	Rats	[55]
ATLASNeuro silicon probes: E16+R-250-S1-L8 NT	ATLASNeuro	Silicon	Platinum (Pt), Iridium Oxide (IrOx), or Gold (Au)	16	250 µm	35 µm	Rats	[56]
Neuropixels 1.0	Neuropixels	Silicon	TiN	960	16 µm (column), 20 µm (row)	<16 µm	Small animals	[57]
Neuropixels 2.0	Neuropixels	Silicon	TiN	1,280	15 µm	<16 µm	Small animals	[58]
EcoFlexMea36	Multichannel systems	Polyimide (Kapton)	Gold	32 recording, 2 ground, 2 ref	300 µm	50 µm	Small animals	[59]
EcoFlexMea24	Multichannel systems	Polyimide (Kapton)	Gold	23 recording, 2 ground, 2 ref	30 µm	80 µm	Small animals	[60]
FlexMEA72	Multichannel systems	Polyimide (Kapton)	TiN	64 rec, 4 ref, 4 ground	625 µm horizontal and 750 µm vertical	100 µm	Small animals	[61]
FlexMEA36	Multichannel systems	Polyimide (Kapton)	TiN	36rec, 2ref, 2 ground	300µm	30µm	Small animals	[62]
FlexMEA36-Om	Multichannel systems	Polyimide (Kapton)	TiN	32rec, 2ref, 2 ground	300µm	30 µm	Small animals	[63]
Blackrock microsystem Microflex Array	Blackrock microsystem	Polyimide	Pt, IrOx	12, 16, 24, customizable	10-500µm	15-100µm	Large and small animals	[64]

2.7. Printing Technologies

Conventional fabrication methods such as Lithography fabrication techniques are the standard, well-established methods for the fabrication of bioelectronic devices. However, this fabrication method is time-consuming as it involves several steps: a simple electrode fabrication (described in the figure 5) requires metal deposition on a substrate, spin coating of photoresist, and soft baking (at 60 °C to 100 °C for up to 30 minutes), exposing the sample with light through a mask, Photoresist development and hard baking (at 120 °C to 180°C for 20 to 30 minutes), etching of exposed metal areas(in case of positive photoresist), and finally the removal of photoresist and leaving the patterned metal on the substrate. It also involves the use of expensive equipment and a dedicated clean room for fabrication. The use of high temperature and harsh processing chemicals in photolithography limits the use of certain materials in this fabrication technique. Flexible and biodegradable substrates made from polymers with low melting points such as PCL, PLLA, and PLGA, among others can't withstand the conditions materials are subjected to in this fabrication process.

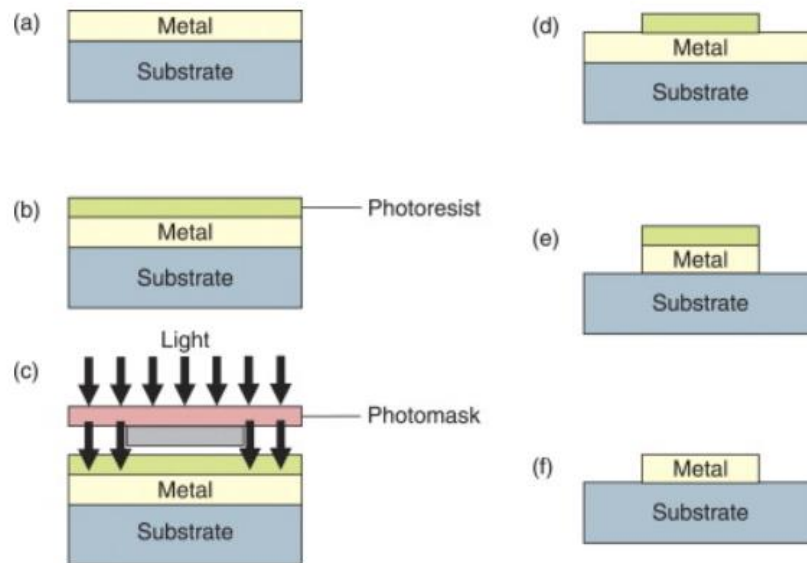


Figure 5. Photolithography fabrication process using a positive photoresist. (a) Metal deposition, (b) spin coating of photoresist, (c) mask alignment and exposure of light, followed by resist development and hard baking, (d) etching of exposed metal, (e) removal of the remaining resist, (f) patterned metal on the substrate. Adapted from [65]

Because of the limitations of lithography techniques, alternative fabrication methods that allow the versatile handling of materials during the fabrication process are being investigated [66-69]. There are basically two methods of printing, described as contact printing in which an image carrier comes in physical contact with the substrate to be printed on, and non-contact printing, where no physical contact is made with the substrate. Contact printing methods are the most common printing technologies. Examples of contact printing techniques include screen printing, gravure printing, flexography, and offset printing [70]. The ink requirement for contact printing differs from that of other printing technologies. Contact printing ink is required to have higher viscosity because of the mechanical stresses it is subjected to during printing.

In non-contact printing methods, only the deposited material contacts the substrate. Non-contact printing technologies examples are aerosol jet printing and inkjet printing. Both aerosol jet printing technologies (AJP) and inkjet printing technologies (IJP) are being

used in several industries such as graphics, textiles, and medicine, but they are in greater use in the field of printed electronics[71, 72].

2.8. Inkjet Printing technology

Inkjet printing is a contactless and additive method that employs the use of a small volume of ink droplets (~ 1–1000 pL) jetted out of nozzles to create a precise well-defined pattern on a substrate. There are two types of inkjet printers: Drop-on-demand (DOD) inkjet and continuous inkjet printers.

Continuous inkjet printer (CIJ) is named as such because a continuous stream of droplets is generated that is directed towards the substrate by an electric field when printing is required. Since this technique involves the continuous release of droplets, Unused droplets are captured into a gutter which is then recycled back into the reservoir for further printing[73]. The disadvantage of this technique is the potential contamination of the recycled unused droplets and inefficient use of energy because of the continuous production of droplets stream when not needed.

On the other hand, drop-on-demand inkjet printer produces droplets that are jetted on the substrate only where needed. Here, energy is efficiently utilized and the potential contamination due to unused ink recycling is eliminated. The problem encountered with DOD inkjet printer is usually clogging of nozzles of the ink cartridge when it is left idle. This can be addressed while using Fujifilm dimatix printer by running sessions of cleaning cycles, wetting the cartridge nozzle side with the particular ink solvent that is being used, or gently rinsing the tube that leads the ink from the ink bag to the nozzles with the ink solvent. In some cases, a new cartridge will be needed if all efforts didn't yield a positive result.

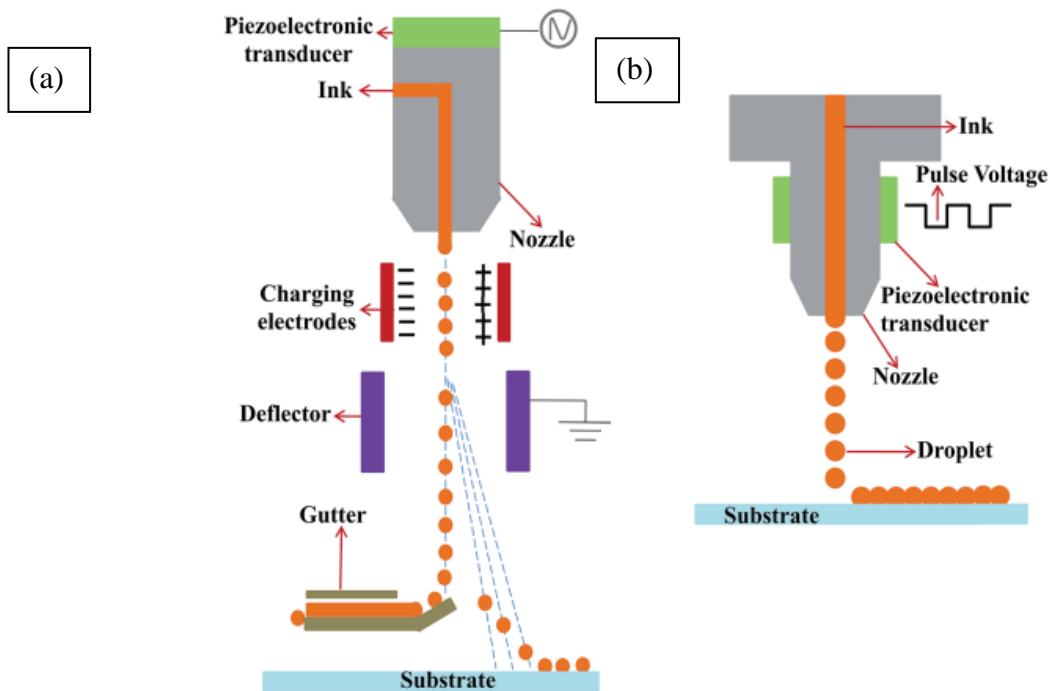


Figure 6. Schematic diagram of inkjet printing methods. (a) continuous inkjet printing and drop-on-demand-inkjet printing method(b).Adapted from[74]

2.9.Drop Spacing

Unlike graphic printing where images of objects are formed from isolated drops on the substrate or photographic paper used, in functional materials printing, drops are required to overlap with each other forming a continuous line. Figure 4 shows a typical behavior of inkjet printed lines on a substrate relative to drop spacing [75]. At the initial stage, isolated droplets were formed on the substrate (Figure 4a), with a decrease in the drop spacing, the isolated drops begin to coalesce with each other forming a scalloped line (Figure 4b), and a further decrease in the drop spacing forms a smooth line with fine edges (Figure 4c), additional decrease in drop spacing from here yields bulging due to a very small drop spacing (Figure 4d), the line takes a stacked coin like morphology when the evaporation time of a single drop is less than the subsequent drop deposition jetting period (Figure 4e).

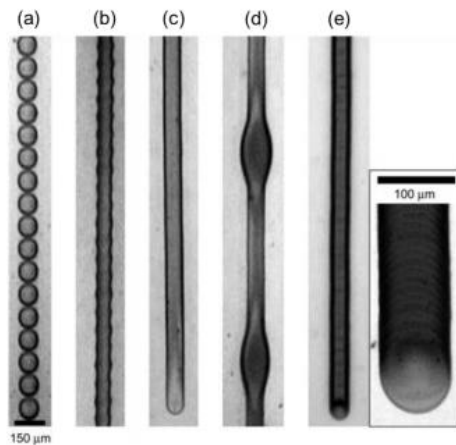


Figure 7. Typical behavior of printed lines on a substrate. Individual drops(a), scalloped line(b), uniform line(c), bulging(d), and stacked coins (e). Drop spacing decreases from left to right (a-e). Adopted from [75]

2.10. Nanoparticles

Nanoparticles are defined as particles of matter having a dimension within the range of 1-100nm [76]. They exhibit a large portion of surface atoms and reduced area-to-volume ratio, which makes them have very unique and significantly different physical, chemical, and biological properties when compared to bulk materials. Many of them exhibit enhanced reactivity as well as unique optical, electronic, and magnetic properties [77].

Among the several nanoparticles available, silver nanoparticles have been extensively studied and remain one of the best options due to their characteristic high electrical

conductivity, cost-effectiveness when compared to gold nanoparticles, resistance to oxidation, and due to their antimicrobial/biocidal properties [78, 79]. Additionally, silver nanoparticles have a low melting point, which enables the formation of conductive thin films using a relatively low temperature. This is crucial for applications using flexible substrates such as papers and polymers [80-82] because of their low melting temperature.

2.10.1 Biocompatibility of Nanoparticles in Biomedical Applications

In terms of biomedical applications, gold nanoparticles (AuNPs) are the most researched nanomaterials (NMs). AuNPs are thought to be the least toxic metal nanoparticles, making them ideal for biological/medical applications. However, their slow clearance rate from circulation streams and tissues may cause health issues[83]. As a result, focusing on the cytotoxicity and biocompatibility of AuNPs is very crucial. Although AuNPs are chemically inert, they are sometimes functionalized with biologically active materials to interact with nucleic acids, proteins, DNA, antibodies, enzymes, and drugs, thus having unique characteristics[84]. There is a growing need to assess the health impact of these materials and to discover more about their toxicity and biocompatibility[85]. Cytotoxicity is defined as the alteration of basic cellular function. Whenever a new nanomaterial is developed for biological application, its cytotoxicity is first evaluated. However, the absence of cytotoxicity does not imply that these materials are biocompatible, the biocompatibility of the nanomaterial must be assessed as a separate criterion[86]. Biocompatibility is the material ability to elicit an appropriate host response in a given situation. The body responds to nanoparticles in the same way it does to any foreign substance that enters it by initiating biological responses that result in nanoparticle clearance. When these biological responses are not desired, they can cause

toxicity and bio-incompatibility. When a material interacts with the body without causing unacceptable toxic, thrombogenic, immunogenic, or carcinogenic responses, it is said to have a high degree of biocompatibility. Prior to in vivo testing, cytotoxicity is usually assessed using specific in vitro assays. Whether in vitro and in vivo models are used, the results of studies on the cytotoxic effects of AuNPs are currently contradictory[87].

2.10.2. Inkjettable Nanoparticles Ink Characteristics

While using an inkjet printer, the nano ink must possess certain characteristics to attain adequate print quality. For this reason, it is of great importance to start with the characterization of an ink prior fabrication of devices. Three key factors need to be taken into consideration when developing an ink, which are dispersion, surface tension, and viscosity. Optimum dispersion of nanoparticles in the ink is very important to avoid clogging of nozzles. Nozzle clogging leads to a waste of time during printing or results in discarding a cartridge. This is commonly experienced when using water-based inks and less common when using solvent-based inks. Optimum dispersion also leads to a uniform network of printed patterns. The second important factor to be considered is for the ink to have low surface tension. The inkjet printing technology is designed to eject a small volume of ink from the nozzles onto a substrate, thus, the surface tension of the ink in use plays a critical role in the printing process. Good ink should have low surface tension. Surface tension problem mostly arises when using water-based ink. Typically, solvents have inherently low surface tension and as a result, a solvent-based ink needs no additional modification. For water-based inks, the addition of ionic surfactant can reduce the surface tension. The last factor to be considered is viscosity. This is typically not an issue for both two categories of inks (water and solvent-based) since viscosity depends

on the additives used for the ink formulation. The viscosity of the ink should always be taken into consideration for proper printing[88].

2.10.3. Synthesis of Nanoparticles

Several methods are employed for the synthesis of nanoparticles, however, they are generally classified into physical, chemical, and biological methods[89]. The choice of synthetic method used strongly dictates the physical, chemical, and biological properties as well as the shape, size, uniformity, and stability of the silver nanoparticles. Varieties of nanoparticles are available for use in inkjet printing, ranging from self-synthesized to commercially available one, some of these are gold nanoparticles, silver nanoparticles, carbon black nanoparticles, copper nanoparticles, and copper oxide nanoparticles,

2.10.4. Post-Printing Treatments of Nanoparticles ink

Following the printing of patterns using a nanoparticle ink for electronic use, they are subjected to an additional step called “sintering” to form a well conductive path. Sintering is a treatment process where nanoparticles are subjected to coalesce and form a continuous and conductive path.

Generally, nanoparticles are coated with a protective covering called the “capping agent” or “stabilizers” which prevents the agglomeration of nanoparticles and are dispensed in an aqueous or organic solution[90]. This capping agent acts as an insulator and requires sintering to be removed and make printed Nano inks to be conductive. Removal of the capping agent/stabilizer causes solid non-coated nanoparticles to coalesce and form necks

with the adjacent nanoparticles. There are several types of the sintering process, such as thermal sintering; used when dealing with non-temperature sensitive substrates, also the temperature employed depends mainly on the type of stabilizers/capping agents used to coat the nanoparticles[91], electrical sintering, chemical sintering, plasma sintering and photonic sintering[90]. Photonic sintering is employed when dealing with temperature-sensitive substrates such as polylactic acid (PLA) substrate, and polycaprolactone(PCL) among others. The diagram below illustrates the process of nanoparticle sintering (post-printing treatment).

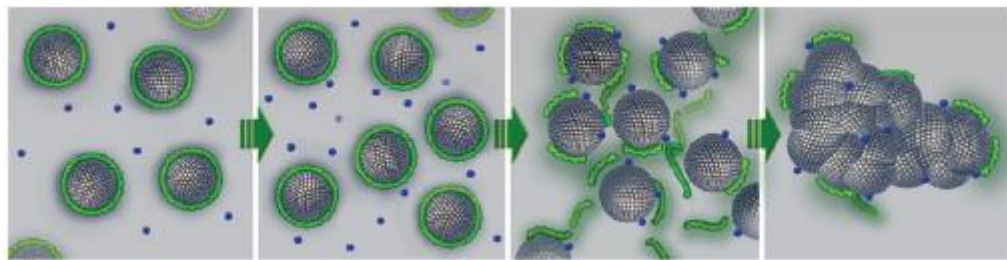
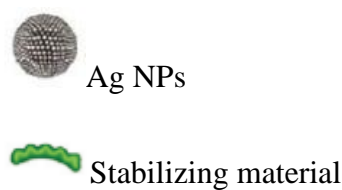


Figure 8.Schematic illustration of the sintering process of nanoparticles[92]



2.11. Dielectrics

Dielectrics are required for the insulation of printed conductive patterns following sintering. Dielectrics are materials that prevent current flow (insulators). When the conductive electrode pattern is printed on a substrate, the whole electrode arrays track is insulated except for the contact site which will interface with the biological tissues and

the contact pads that make contacts with a connector or ZIF board to the electronic system for recording. Several printable insulators are available such as PDMS, SU-8, aluminum oxide-resin composite [73], and PVPh dielectric ink [45]. In this thesis, a commercially available inkjettable polyimide ink was purchased from UT Dots (UTDPI-IJ) to be used as the passivation layer over the printed pattern following the ink characterization. Detailed information about the characterization is discussed in the fabrication section of this thesis.

CHAPTER 3

SPECIFIC AIMS

Aim #1: Inkjet printing of a highly flexible and biodegradable microelectrode array using electrode materials that are compliant with the brain tissue.

Hypothesis A: We will test the hypothesis that gold nanoparticle ink can be print conductive lines and electrodes onto a flexible polymer substrate (polyimide, non-biodegradable).

Hypothesis B: We will test the hypothesis that gold nanoparticle ink can be print print conductive lines and electrodes onto a flexible and biodegradable polymer substrate polycaprolactone (PCL).

Approach:

Impact: Fabrication of highly flexible and biodegradable devices offers an advantage over the conventional devices that uses a rigid base which triggers an immune response in the brain, micro motion, and ultimately leading to instability in the recording. It will also eliminate the need for a second surgery after implantation of the device, reducing the possible chances of impacting the brain tissues and also the introduction of infections.

Aim #2: Test the electrochemical performance and capability of our inkjet-printed highly flexible and biodegradable microelectrode arrays in recording epileptiform activities in vivo from rat cortex.

Hypothesis A: We hypothesize that gold electrodes printed on a flexible polyimide substrate and biodegradable polycaprolactone substrate have excellent electrochemical performance.

Hypothesis B: We hypothesize that our inkjet-printed gold electrodes are capable of stable recording epileptiform activities in vivo from the rat cortex.

Challenge: Identifying optimum parameters and conditions for recording epileptiform activities in vivo in rats

Approach: We will make a craniotomy in rats, implant the device, and induce seizures using a chemo-convulsant to test the feasibility of recording epileptiform seizures using the device. We will also track recording over a certain period to assess the stability of recording with the device. Device noise level, ability to record different brain rhythms, and ultimately epileptiform activities will be assessed. Additionally, the electrochemical impedance of the electrodes before and after experiments will be assessed.

Aim #3: Assess the biodegradability of the device over time.

Hypothesis : We hypothesize that the device comprised of PCL substrate and inkjet-printed electrodes is capable of degrading over time.

Approach: An accelerated degradation test will be performed in vitro to assess the degradability of the device.

Impact: knowing the device degradation rate will help in monitoring the patient's condition, as well as help in knowing if any possible neurological changes occurring at a specific time are related to the degradation of the device.

CHAPTER 4

METHODOLOGY

Aim #1: Inkjet printing of a highly flexible and biodegradable microelectrode array using electrode materials that are compliant with the brain tissue.

In this part, we took advantage of drop-on-demand inkjet printing technology to develop highly flexible and biodegradable microelectrode arrays for ECoG recordings.

Aim #1A: Testing the hypothesis that gold nanoparticle ink can be printed onto a flexible polymer substrate (polyimide, non-biodegradable)

The device fabrication process was done using a commercially available drop-on-demand inkjet printer (DMP-2850, Fujifilm Dimatix, USA). This is a printing system that is easy to use and cost-effective. It offers a range of applications which includes evaluation of substrate and fluid interaction, digital patterns optimization and evaluation, development and optimization of fluid and materials, prototype generation, and product development. The DMP-2850 uses a piezo inkjet cartridge and allows materials deposition on an 8x11 inch platen. With an adjustable Z height, this printer can create patterns over an area of approximately 200 x 300 mm and handles substrates of up to 25mm thick. The vacuum platen secures the substrate to avoid movement during the printing process, it also has an adjustable temperature technology up to 60 °C . Using a pattern editor, the DMP-2850 provides a variety of patterns. Additionally, the printer is equipped with a waveform editor, which allows for the manipulation of electronic pulses to the piezo jetting device for optimization of the drop characteristics as they are ejected from the nozzles, and a drop-watcher camera system that allows for the monitoring of the drops as they are being ejected. This system makes the printing of structures and samples for process validation and prototype creation very simple and cost-

effective. In this study, several layers of gold nanoparticles were patterned onto the substrate and a functional device was developed for testing. In order to achieve optimum performance of printing, the inkjet printer requires the viscosity of the ink to be in the range of 10-12 cps, surface tension between 28-42 dynes/cm at the jetting temperature, recommended particle size of up to 0.2 μ m, and pH value between 4-9. In this work, inkjet-printed arrays were patterned using gold nanoparticle ink and the connection lines were passivated using dielectric ink. The prints on PCL were passivated via heat pressing of a PCL film over the prints on a hot plate.

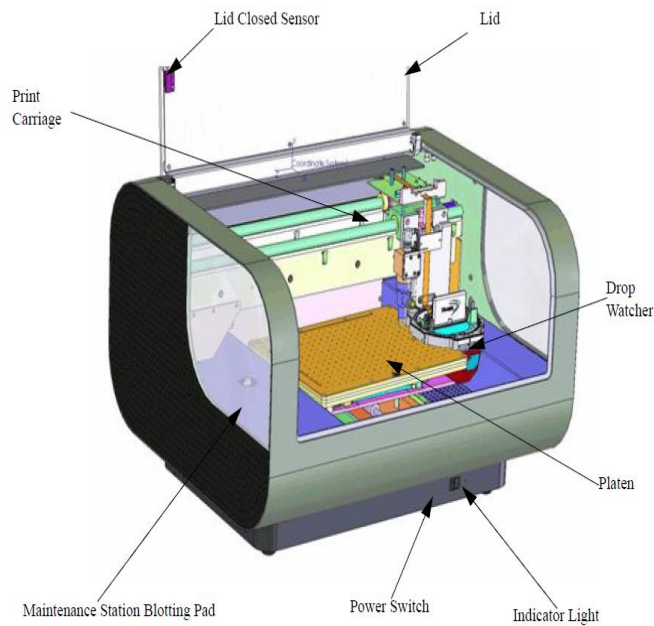


Figure 9. Schematic diagram of DMP-2850 inkjet printer



Figure 10. DMP-2850 inkjet printing workstation

Fabrication process:

Commercially available gold nanoparticle ink was purchased from UT Dots Inc (UTDAuIJ). UTDAuIJ is a suitable, gold nanoparticles-based, inkjet-printing compatible ink with a particle size of approximately 3-5nm and a viscosity in the range of 10-12cP. No modification was done on the ink before use. The gold nanoparticle ink was used to print the conducting patterns of the electrode (Figures 11 and 12). The printer was equipped with a 1pl cartridge filled with gold nanoparticle ink for printing. Electrodes were printed on polyimide (Kapton) substrate purchased from CS Hyde, USA. The PI film has a thickness of about 25 μ m. Before the start of the printing, PI films were cut into the desired size and mounted on a glass slide, which acts as support during printing. The polyimide films were then subjected to oxygen plasma etching for 30 seconds at 100W to modify the wettability of the substrate and achieve optimal print quality. Prints done on plasma etched substrates were observed to have a better resolution and no discontinuities along the tracks of the electrodes, as compared to prints done on the non-etched PI substrate. The gold electrodes were sintered at 300 $^{\circ}$ C

for 35 minutes to obtain maximum conductivity. This was based on the initial sheet resistance measurement done using the four-point probe system (Ossila, UK) before the start of the main electrode printing. For the passivation of the gold electrode leads, a commercially available inkjet suitable polyimide ink was purchased from UT Dots Inc (UTD-PI-AJ). No modification was done to the ink. A waveform was developed for the ink to allow for a good drop formation devoid of satellite drops. Several layers of the PI ink were printed along the interconnects of the electrode arrays except for the electrode contact site and the contact pad area. The printed PI was cured at 180°C on a hot plate for 1 hour. Care should be taken while transferring insulated electrodes from the platen of the DMP inkjet printer to the hot plate for curing to avoid the unwanted spread of ink which may lead to the coverage of the electrodes' active site.

Table 2. Physical properties of the ink used for printing at room temperature.

Properties	Gold ink	Polyimide ink
Particle size	3-5 nm	-
Nanoparticles concentration	25% w/v	-
Solvents	Non-polar solvent formulations	Alcohols and water
Viscosity	7-10 Cp	<1 cP

Table 3. Inkjet printing parameters for ink deposition.

Ink Type	Parameter	Value
Au nanoparticles	Print resolution	725.71 dpi
	Drop separation	30 μm
	Platen temperature	40 $^{\circ}\text{C}$
	Pulse width	6.336 μs
	Jetting voltage	28 V
	Jetting frequency	5 kHz
Polyimide	Print resolution	1693.33 dpi
	Drop separation	15 μm
	Platen temperature	30 $^{\circ}\text{C}$
	Pulse width	11.776 μs
	Jetting voltage	24 V
	Jetting frequency	4 kHz

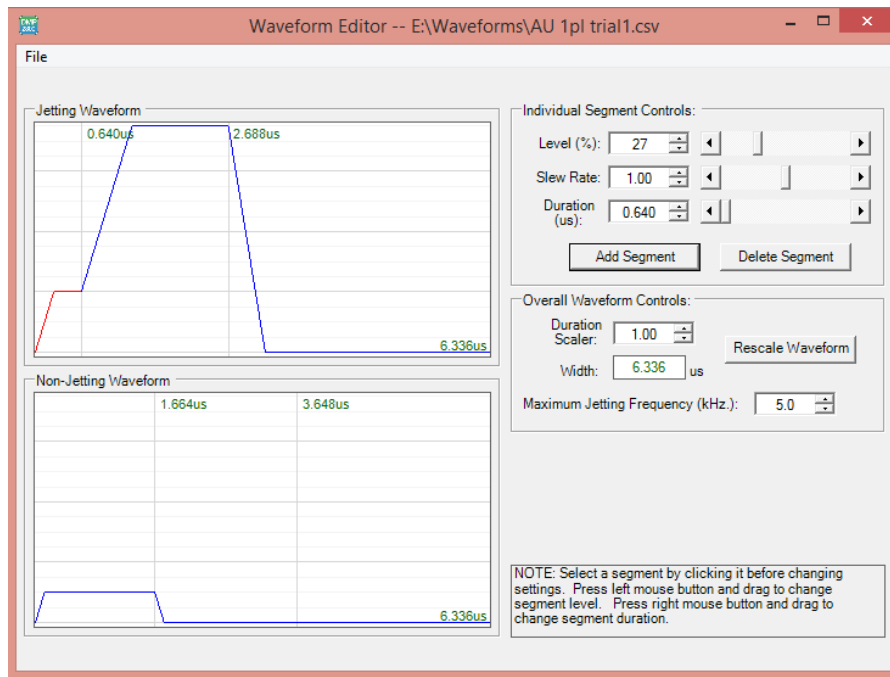


Figure 11. Au in jetting waveform

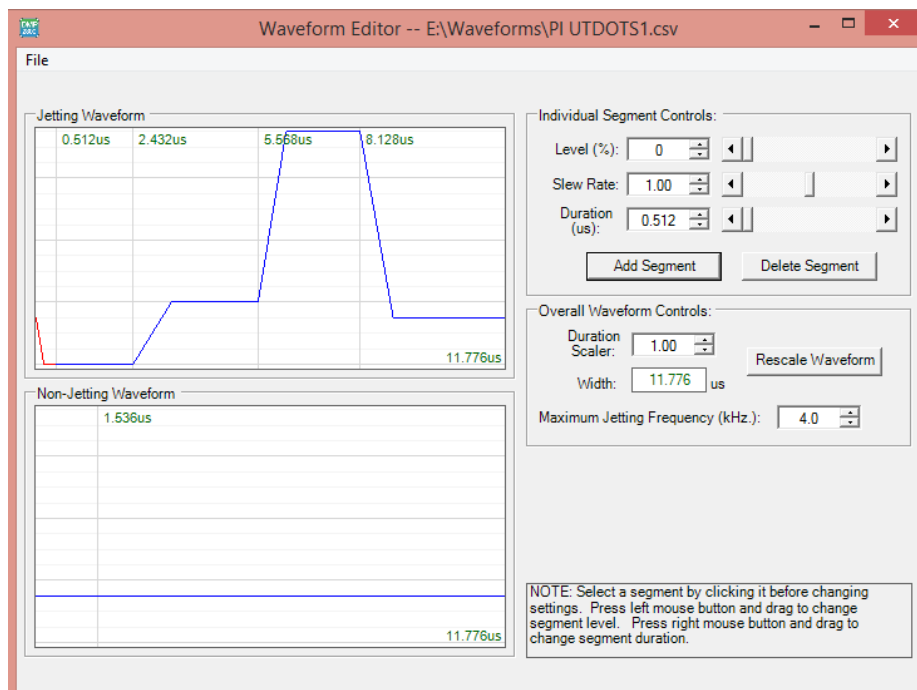


Figure 12. PI ink jetting waveform

Aim #1B: Testing the hypothesis that gold nanoparticle ink can be printed onto a flexible and biodegradable polymer substrate polycaprolactone (PCL).

Several biodegradable materials have been tested in the fabrication of neural interfaces using different fabrication processes [41, 45, 93-95]. However, very limited materials were explored to print devices using inkjet printing technology. In this research, we used a biodegradable polymer, *polycaprolactone* (PCL) as the substrate for our microelectrode arrays. PCL is a biodegradable polymer that is approved by the US food and drug administration (FDA) and has been extensively explored for use as injectable implants for controlled release drug delivery systems and implantable biomaterials [96-101]. PCL has a relatively low melting point of about 60 °C and a glass transition temperature of about -60 °C. Fibers of PCL have shown good properties such as non-

toxicity and biodegradability, making them suitable biomaterial candidates for use in wound dressing and tissue engineering[102, 103].

Fabrication process:

PCL solution was prepared using 20% w/v PCL of 9:1 chloroform to dimethylformamide (DMF). Pellets of PCL (704105 Sigma-Aldrich) with 45000 molecular number were dissolved in chloroform and subjected to magnetic stirring for 30 minutes at 50°C on a hot plate. Following the complete dissolution of PCL in the solution, dimethylformamide (DMF) was added and mixed to form a clear solution of PCL. A glass slide was then cleaned with isopropanol alcohol and rinsed with deionized water in preparation for the deposit of PCL solution for PCL film formation. PCL films were formed by spin coating the deposited PCL solution on the cleaned glass slide using a spin coater (model WS-650MZ-23NPPB, Laurell Technologies Corporation). At 1000 rpm for 5 minutes a flexible PCL film of ~ 15 µm was achieved. A scanning electron microscope (SEM) and the optical microscope were used for surface and morphology investigation. The fabrication process of electrodes on PCL films is slightly different from that on PI substrates. Two major differences were in the substrate preparation and the sintering method used to cure the printed nanoparticle tracks on the surface of the substrate. The polyimide substrate was able to withstand high temperatures, where prints were sintered using the thermal sintering method. However, as earlier stated, PCL has a relatively low melting temperature of about 60°C, so it was subjected to an alternative sintering process that is suitable and effective on printed devices on temperature-sensitive substrates.

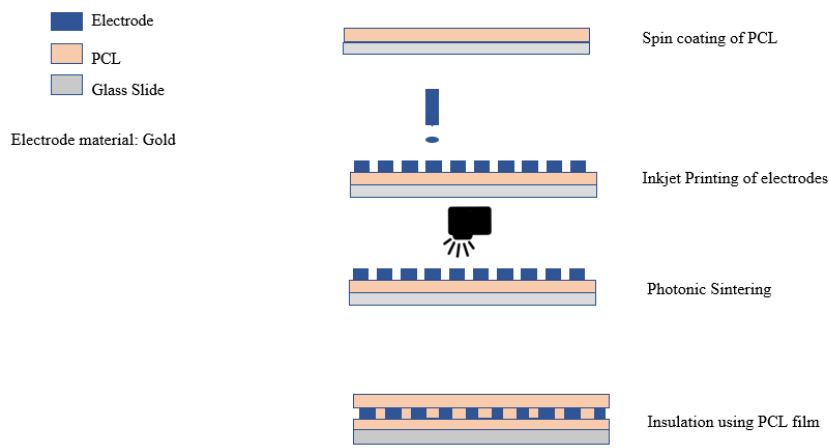


Figure 13.PCL electrode fabrication process

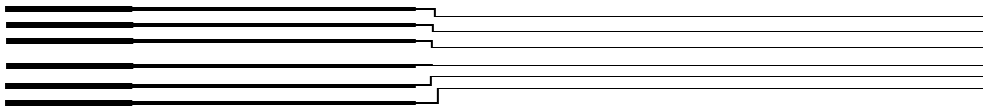


Figure 14.Top view of electrodes pattern 1

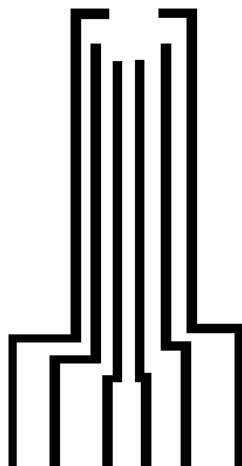


Figure 15.Top view of electrodes pattern 2

As for the printing of devices on PCL, no plasma etching treatment was carried out as prints were optimum without subjecting it to oxygen plasma etching. Both prints at room temperature and an elevated temperature were tried on PCL, however, the printing at room temperature yielded a better result. Several layers of the gold ink purchased from UT Dots were printed on PCL, upon the completion of the printing process, printed electrodes on PCL supported by a glass slide were put inside a petri dish and allowed for solvent evaporation at room temperature overnight before the sintering process. PCL has a very melting point of about 60 °C, and because of this, it cannot be subjected to the thermal sintering process. An alternative sintering process used for temperature-sensitive substrates is flash sintering. This sintering process takes the advantage of enhanced photo thermal effect of nanoparticles to sinter printed nanoparticles on a temperature-sensitive substrate. In this research, we utilize a camera flash (Nikon Speedlight SB-28) to sinter our electrodes. Printed gold electrodes supported on a glass slide were placed on an aluminum foil for reflection and to ensure uniform light distribution. The camera flash was kept about 1cm away from the substrate and two consecutive flashes were incident on the print.



Figure 16. Flash sintering set-up using a camera flash. (a)Schematic diagram of the set-up (b)front view of the set up with Nikon Speedlight SB-28 (c)Lateral view with sample

Once the electrodes get sintered, you can easily identify them by seeing their color change from a pinkish appearance to golden from beneath the substrate and darker from above. The conductivity of printed lines was checked by measuring line resistance using a multimeter, and sheet resistance of printed patterns was evaluated using the four-point probe sheet resistance measurement system.

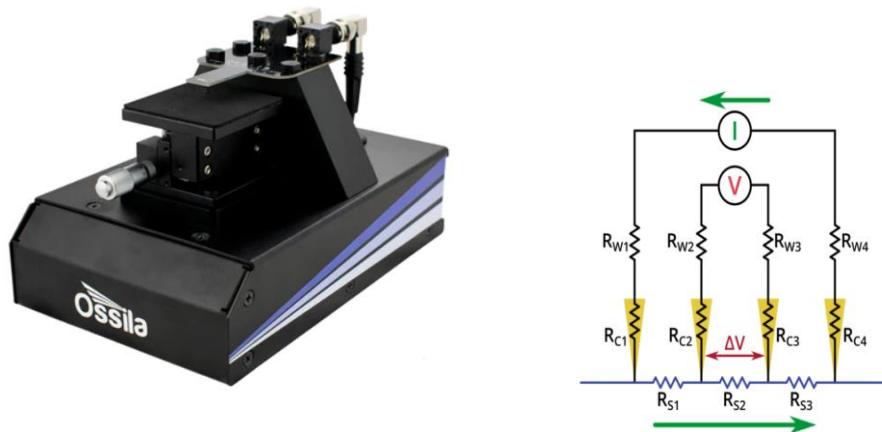


Figure 17. Schematic diagram of four-point probe system (ossila) (a) and its equivalent circuit (b)[104]

The four-point probe sheet resistance measurement technique is also known as the Kelvin technique, it works based on using four equally spaced in a straight line. A current is sourced by the two outer probes, while the inner probes measure the drop in voltage. The sheet resistance of the gold printed films is then calculated from the resultant I-V curve based on the below equation:

$$\text{Sheet resistance} = \frac{\pi}{\ln(2)} \frac{\Delta V}{I}$$

For the passivation of the gold electrodes, electrodes printed on biodegradable PCL films were passivated by heat pressing of PCL films over the printed pattern. This was done on a hot plate at 60 °C for about 2-3 seconds.

Aim #2: Testing the electrochemical performance and capability of inkjet printed highly flexible and biodegradable microelectrode array in recording epileptiform activities in vivo from rat cortex.

This aim serves as a proof of concept of our printed gold electrodes on both polyimide and polycaprolactone in recording seizure activities from the brain.

Aim #2A: Testing the hypothesis that gold electrodes printed on a flexible polymer substrate (polyimide, non-biodegradable) and polycaprolactone (PCL, biodegradable) have excellent electrochemical performance.

Electrochemical Characterization of the electrodes

The electrochemical characterization of the electrodes was done in our lab electrochemical workstation using Potentiostat/Galvanostat/ZRA system (Zero Resistance Ammeter) Gamry Instruments, USA with a three-electrode cell system. Ag/AgCl was used as the reference electrode, platinum (Pt) electrode as the counter electrode, and our printed electrodes as the working electrode. A glass beaker will be filled with phosphate buffer saline (PBS) and electrodes were connected to the ME2100 connector and immersed in the glass beaker-filled PBS solution for characterization. We measured the electrochemical impedance spectroscopy (EIS) of the electrodes and evaluated their impedance at 1KHz. This step of electrode electrochemical characterization is very essential for both recording and stimulating electrodes. Impedance varies inversely with electrode size, the larger the size of an electrode, the lower the impedance, and vice versa. An electrode with a very high impedance tends to introduce thermal noise to the recording and decreases the signal-to-noise ratio, similarly, it decreases the charge injection capacity of an electrode during stimulation and leads to failure of such electrodes due to overloading. Typically, electrodes with impedance less than 5 M Ω don't produce a significant noise level that creates recording problems and leads to poor quality recordings [105-107]

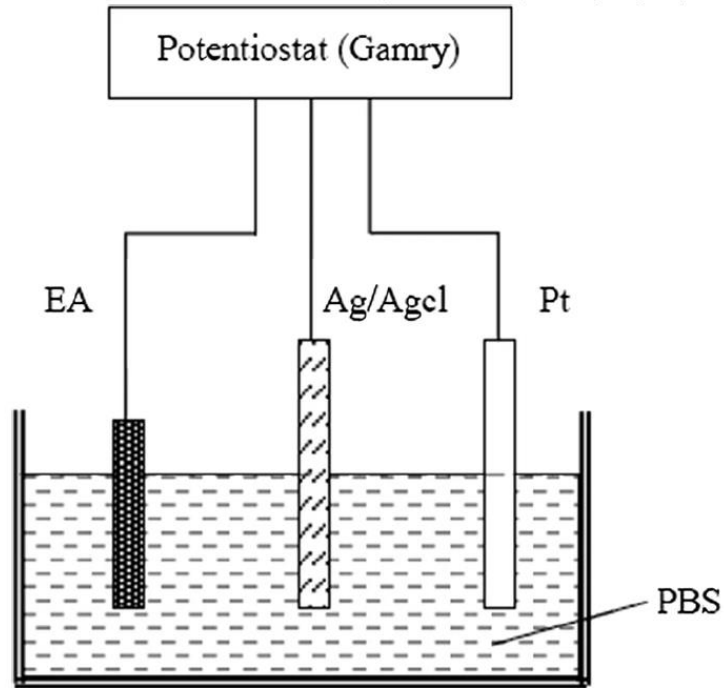


Figure 18. EIS 3 electrode cell system set up. Adapted from [108]

Aim #2B: Testing the hypothesis that our gold electrodes printed on a flexible and biodegradable substrate is capable of recording epileptiform activities in vivo from the rat cortex.

Experimental design

An established animal model of status epilepticus via Intra-amygdala microinjection of kainic acid from our collaborators; Dr. Makram Obeid's lab was adopted and used in our experiment.

Animal Preparation and implantation:

5 to 6 months old female adult Sprague Dawley rats weighing 300g were used for the study. The following steps were followed for the animal preparation and surgery for device implantation and recording.

1. Prepare an Anesthesia injection (Ketamine & Xylazine) according to the rat weight.
2. Using a barber's clipper, shave the head from the region between the eyes down to behind the animal's ears.
3. Apply lubricant to the eyes of the rat to avoid drying.
4. Mount the animal on the stereotaxic device.
 - a) Carefully position the ear bar in the right auditory meatus and position the animal properly.
 - b) Insert the second stereotaxic ear bar, secure it into the animal's left auditory meatus, and ensure it is well fixed.
 - c) Slowly move the mouthpiece anteriorly and tighten it when you feel resistance

(Make sure the height of the mouthpiece is zeroed on the frame for adult rats).
 - d) The proper animal position is confirmed by having a rigid head position after grasping the animal behind the ear and wiggling back and forth.
5. Scrub the head three times with isopropyl alcohol, followed by betadine.
6. Using a scalpel, make an incision down the midline and use a clamp to hold the skin.
7. Use a sterile swab to remove underlying connective tissues adhering to the skull
8. Clean the skull bone using hydrogen peroxide and dry it with a gauze pad.
9. Identify the bregma and insert coordinates into the excel sheet (an excel template for ECOG using 2.8mm AP and 5mm L)

10. Locate the injection site (-2.8 AP, 5 mm L, 7.6 DV measured from the brain surface, or 8.8 DV mm from the skull) to the bregma.
11. Mark the injection site using a marker or by creating a shallow drill.
12. Mark the four corners of the craniotomy site (better to do this with specific coordinates (around the injection site coordinates such as -2.8 +/- 2 mm and 5 mm +/- 2mm, which may have to be slightly modified as there may not be enough room lateral to the injection site)
13. A craniotomy is made of approximately 4x4mm covering the identified injection site.
14. Use #105 drill burr to drill off the bone surface at the craniotomy site down to a transparent layer followed by finishing the edges.
15. Use Rongeurs to lift off the remaining thin transparent bone.
16. Remove the dura using fine scissors.
17. Use a 1 μ L Hamilton syringe mounted on a holder to inject 0.6 μ L Kainic Acid (KA) into the injection site 7.6mm from the surface of the brain surface or 8.8 mm from the skull.
18. To implant, the micro ECoG, Position the stereotaxic arm above the site of the exposed brain tissue.
19. Secure the micro ECoG device to the stereotaxic arm making sure that the contact sites are facing downward.
20. While making sure electrodes are well secured, lower them onto the drilled area above the injection site and make sure the electrodes are in contact with the brain tissue.

system has a signal collector unit (MCS-SCU) that allows the connection for up to four recording head stages, which also has a connector that allows for up to four outputs for optogenetics (optical stimulation). The interface board and the signal collector unit are connected via eSATA cable and up to two signal collector units can be connected to the interface board.

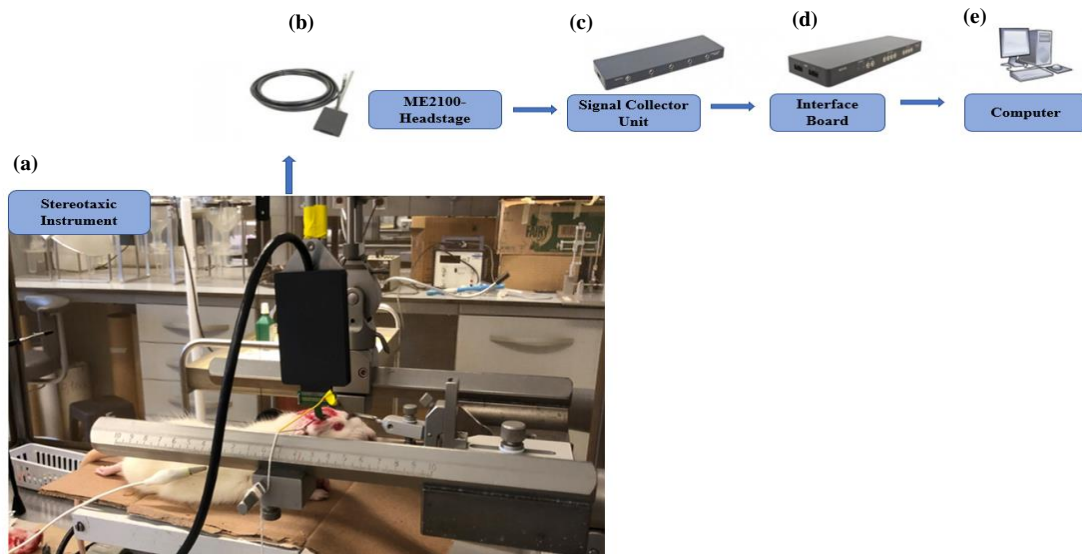


Figure 20. In vivo recording set-up using the ME2100 system from multichannel systems. (a) A stereotaxic instrument, (b) The head stage, (c) A signal collector unit, (d) An Interface board, (e) A computer for data visualization and analysis.

Aim #3: Testing the in vitro degradation of the biodegradable gold microelectrodes printed on PCL.

Aim #3: Testing the hypothesis that our gold electrodes printed on a flexible and biodegradable substrate is capable of biodegrading over time.

Here we tested the in vitro degradation of PCL-based electrodes. PCL is known to have a very long degradation time of up to two years in vivo. This time is very long for this study and that is why accelerated degradation testing is employed electrodes were prepared and immersed into a prepared PBS solution with pH 13 in a petri dish at a controlled temperature of 37°C. A Series of images were taken as shown in figure 49. It

should be noted that the degradation process at this PH of 13 is based on chemical hydrolysis only, the presence of enzymes will accelerate the process.

CHAPTER 5

RESULTS

5.1. Surface Characterization

As mentioned in chapter 4, two materials were chosen as substrates were chosen for our devices, one flexible and biodegradable (PCL) and the second one flexible but not biodegradable (Polyimide). Characterizing the surface morphology and roughness of a substrate is a critical step before printing. The surface characteristics along with that of the ink used during the printing process dictate the quality and resolution of the printed pattern. Characterization also gives information on whether that particular substrate is suitable to be printed on or if it may need further modifications before use. Fig 18 below shows SEM images of the surface topography of spin-coated PCL films and PI films used as substrates for our prints. PCL showed a rough topographical surface. This rough surface topography of PCL films made it very challenging while printing small-scale patterns. It also affects the printing quality and makes electrodes to be prone to cracking upon sintering. This is the main reason why we had to increase the size of the electrodes printed on PCL to be up to 300x400 μ m. On the other hand, PI films presented relatively smooth surfaces and are hence hydrophobic. Printing on the PI was less challenging compared to PCL. However, what affects the quality of print and scaling it to a smaller size here is dominated by the viscosity of the ink used during printing.

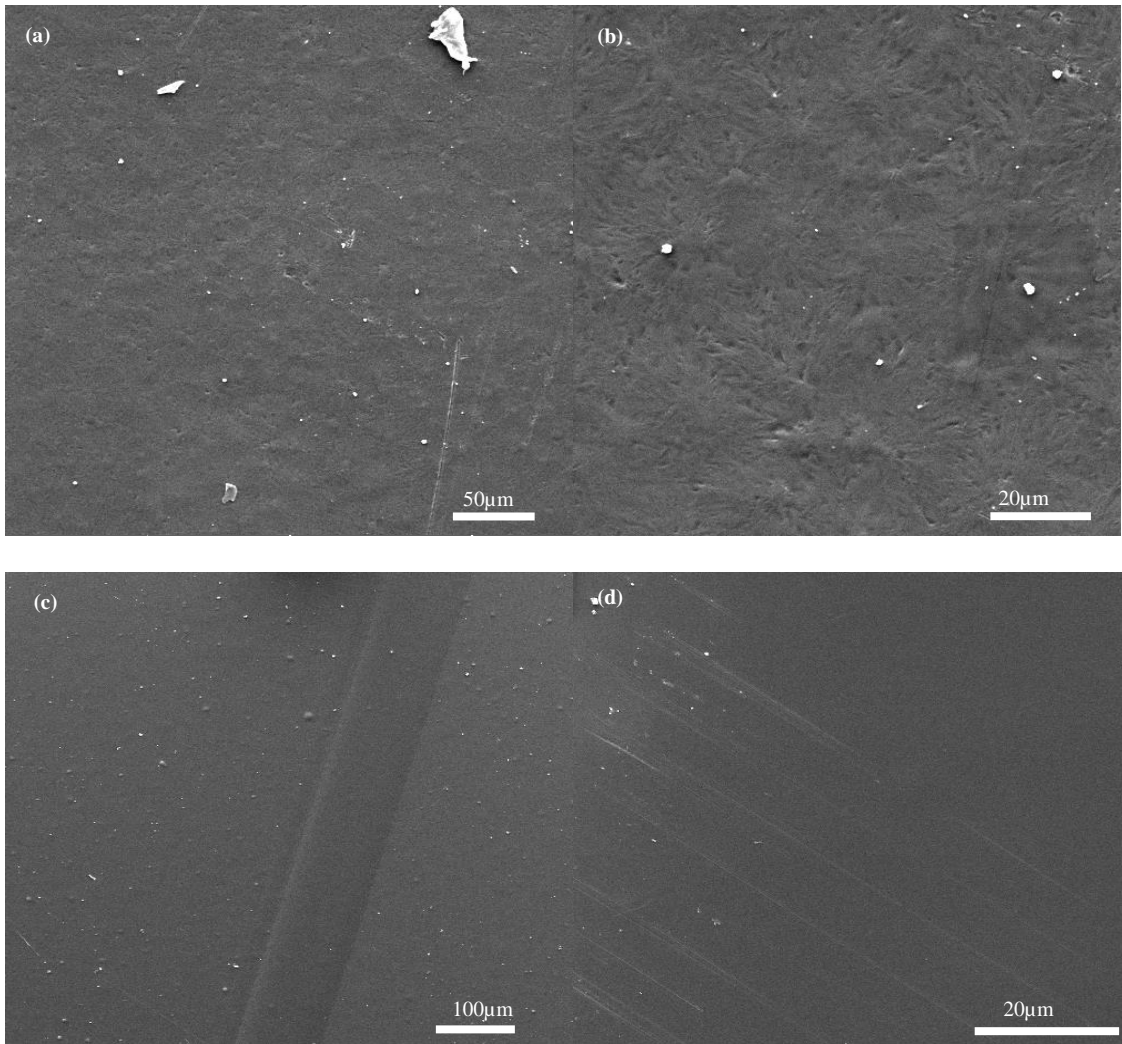


Figure 21. SEM images of PCL films at different scales showing the topographical rough surface (a and b), PI films showing smoother surface(c and d)

Subjecting the PCL films spin-coated on the glass to heat briefly by placing them on a hotplate at 60°C for 2 to 3 seconds modifies its surface causing it to become less rough. This also causes the film to adhere more firmly to the glass slide, which ensures that delamination of the film does not occur until the electrode fabrication processes are done and the substrate is ready for lifting. Figure 19 shows the optical microscopic images of PI with its smoother surface as compared to PCL. Both under an optical microscope (figure 22a and 22b) and fiducial camera (figure 22c and 22d), the effect of heat treatment

of PCL over its glass support is pronounced. This same effect translated to the quality of printing on the PCL where heated PCL gives good quality printed patterns.

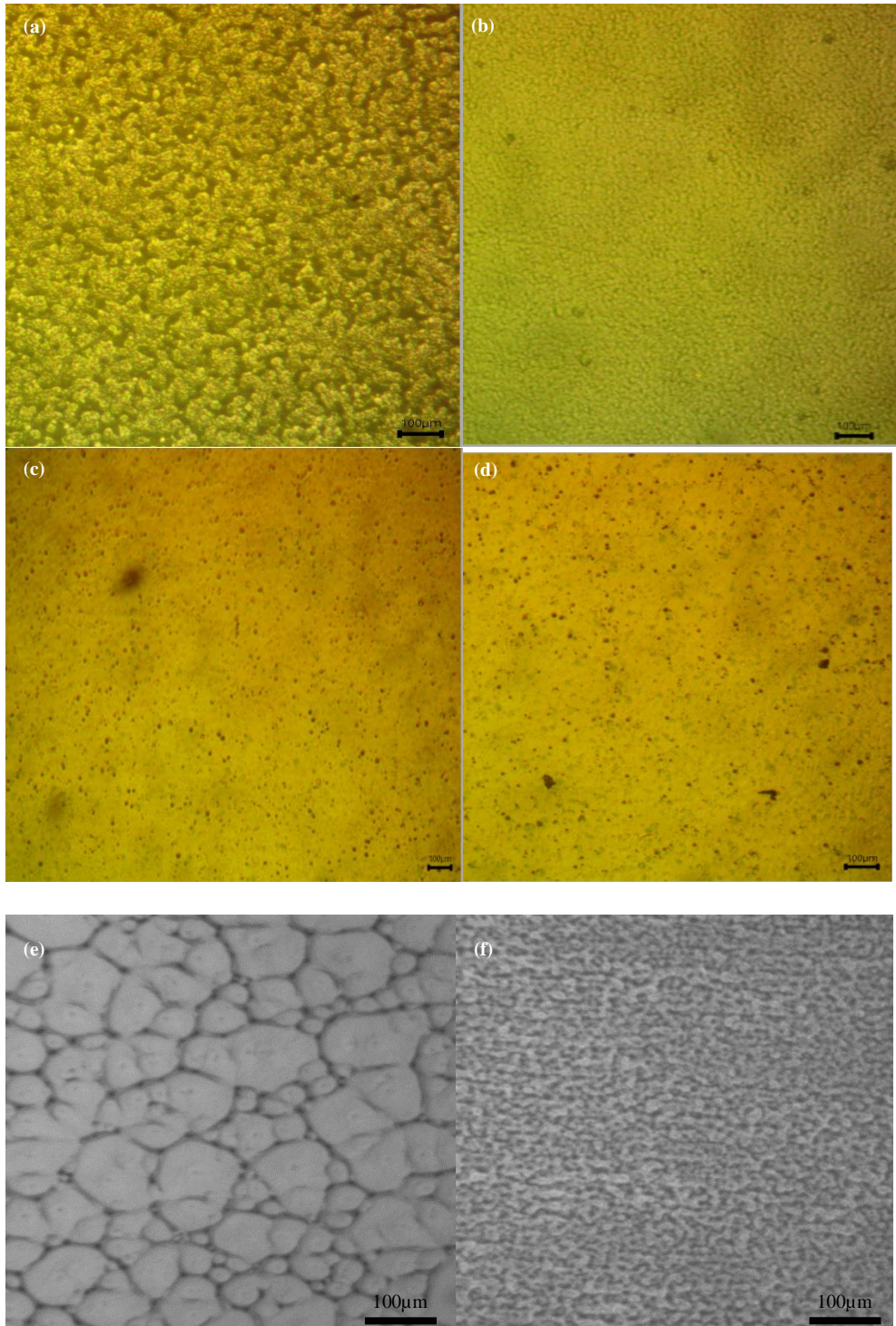


Figure 22. Optical microscopic images of PCL. (a) PCL film briefly subjected to heat on a hotplate having a less rough surface,(b)PCL film not subjected to heat, showing

rougher surface, PI film surfaces(c and d) PCL film surface(pre-heat) under DMP fiducial camera (c) and after heating on a hot plate (d)

5.2. Printing of Gold Nanoparticles Ink on Polyimide substrate

In an attempt to optimize our gold nanoparticle ink, several printing was done on PI at different drop spacing and substrate treatment conditions. Figure 23 (a and b) shows 100um lines of gold printed on non-plasma etched PI substrate, the printed pattern yielded a very poor printing quality and non-uniform distribution of the ink on the substrate. This print was done using the drop spacing of 15 and 20 μm respectively. The poor result from the start of printing necessitates us to modify the surface of our PI substrate. Figure 23 (c,d, and e) shows an image of a 100um printed pattern on 30 seconds etched PI substrate at 50,30, and 20um drop spacing respectively. It could be seen that with surface modification of PI substrate by making it more hydrophilic, there is an even distribution of ink along with a well-defined pattern than the prints on a non-etched hydrophobic surface. Etching of PI substrate greater than 1 minute makes the surface of the PI substrate extremely hydrophilic and electrodes get connected forming short circuits. A drop spacing of 30 was selected for the printing of our devices because it gives a good quality printing and minimum sheet resistance measurement(See electrical characterization). Printing at a drop spacing of 50 μm gives a finer pattern but the sheet resistance was extremely high, making this drop spacing not suitable for printing of electrodes as it will lead to a very high impedance and possible chance of introduction of noise to recorded signals. Drop spacing of 20 μm gives a print with too much spread because of the reduced distance between jetted drops, and as such, the electrodes track will be easily overlapped forming short circuits especially when a small interelectrode spacing is needed, as in our case. Additionally, it will be challenging to get smaller dimensions of electrodes at this

drop spacing. Figure 24 shows different printing quality of 2 layers of gold between 1-minute plasma etching (Figure 24a) and 30 seconds of plasma etching (Figure 24b). High printing quality with well-defined electrodes contact pads, lead, and electrode sites are produced with 30 seconds of etching as compared to 1 minute of PI etching which gave electrodes with a poorly defined pattern.

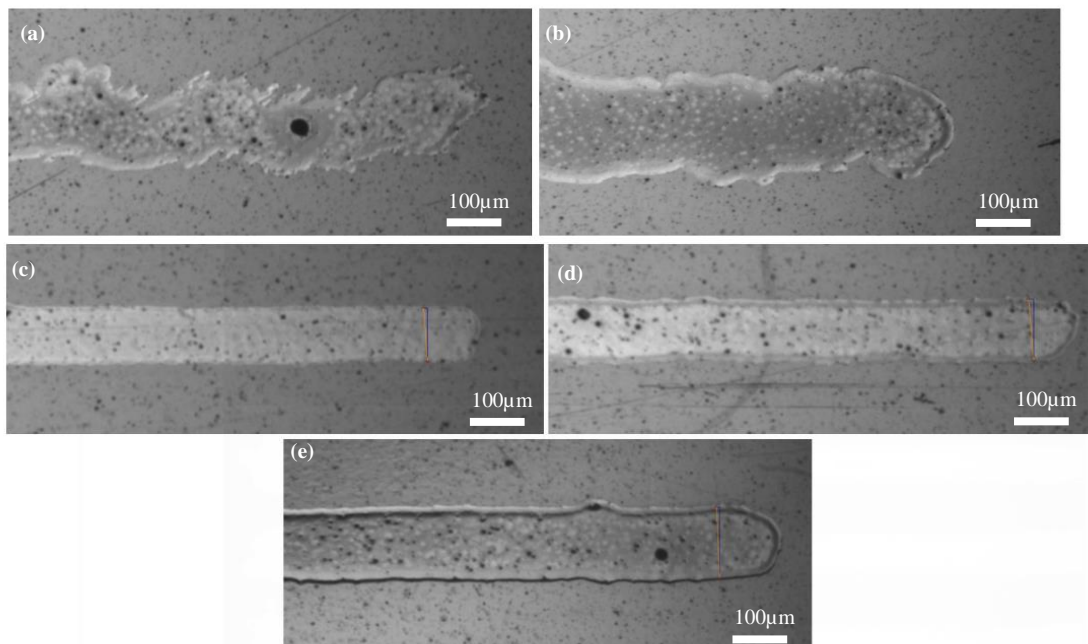


Figure 23. Gold print on non-etched and etched PI substrate. (a and b) 100µm line on the non-etched PI substrate at 20µm and 15µm drop spacing respectively, showing the non-uniform spread of ink and poor printing quality, (c, d, and e) 100 um line on 30 seconds plasma-etched PI substrate at 50µm,30µm and 20µm drop spacing. Printing at this substrate condition yields a well-defined pattern.

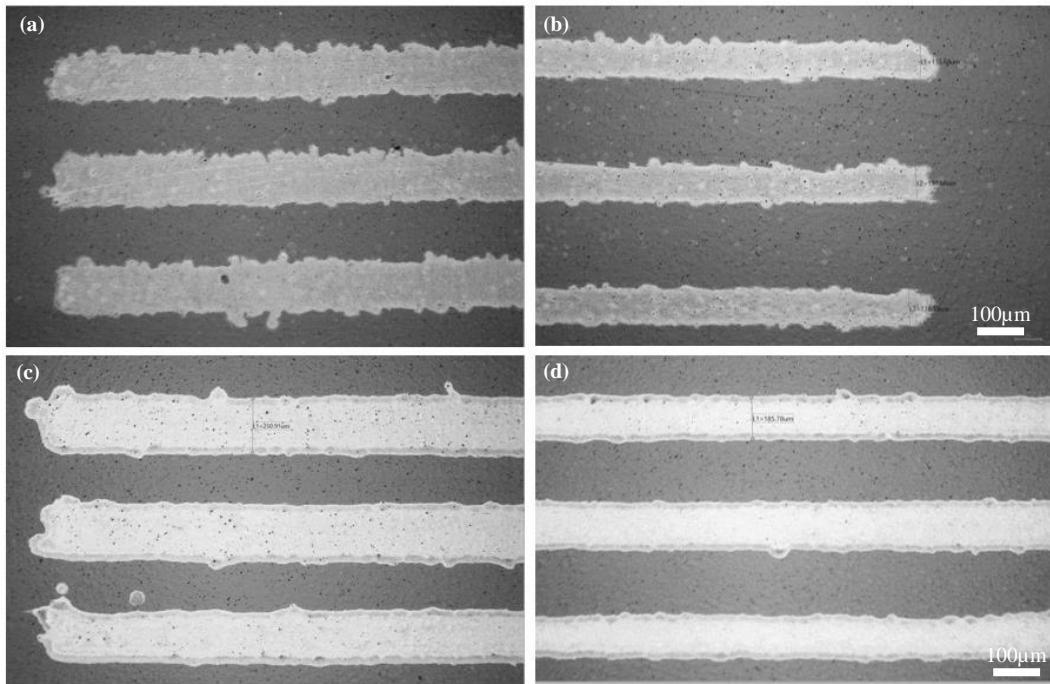


Figure 24. Printing quality of 2 layers of gold between 1-minute (a) and 30 seconds plasma etching(b).

It should be noted that surface modification using plasma was immediately before the printing process, and modified surfaces were not left unattended for a very long time before printing on the substrate. Any substrate left for a very long time before printing was discarded, this is because the modified surface characteristics change with time. The time from the etching of the PI substrate surface to the initiation of the printing process was not more than 5 minutes.

5.3. Polyimide ink for insulation

Before utilizing the PI ink for insulation, it was tested on a bare substrate without an electrode, to begin with the characterization. We printed the PI ink on PI substrates before and after plasma etching to check the spread and adhesion of the dielectric ink. We adapted the drop spacing of 15µm and 35°C platen temperature during printing. We printed 2,4,6,8, and 10 layers of PI ink and assessed the spread and coverage accordingly. At 2 layers the line width of a 100µm pattern yielded 87µm print on the PI substrate,

showing that the substrate is relatively hydrophobic, and the ink isn't spreading excessively. At 4 layers the line width of the 100 μ m pattern yield 106 μ m, this can be clearly seen in the below figure as the increase in the number of layers causes an increase in thickness and additional spread. Furthermore, at 8 and 10 layers, the 100 μ m line width pattern produced 106 μ m and 114 μ m respectively.

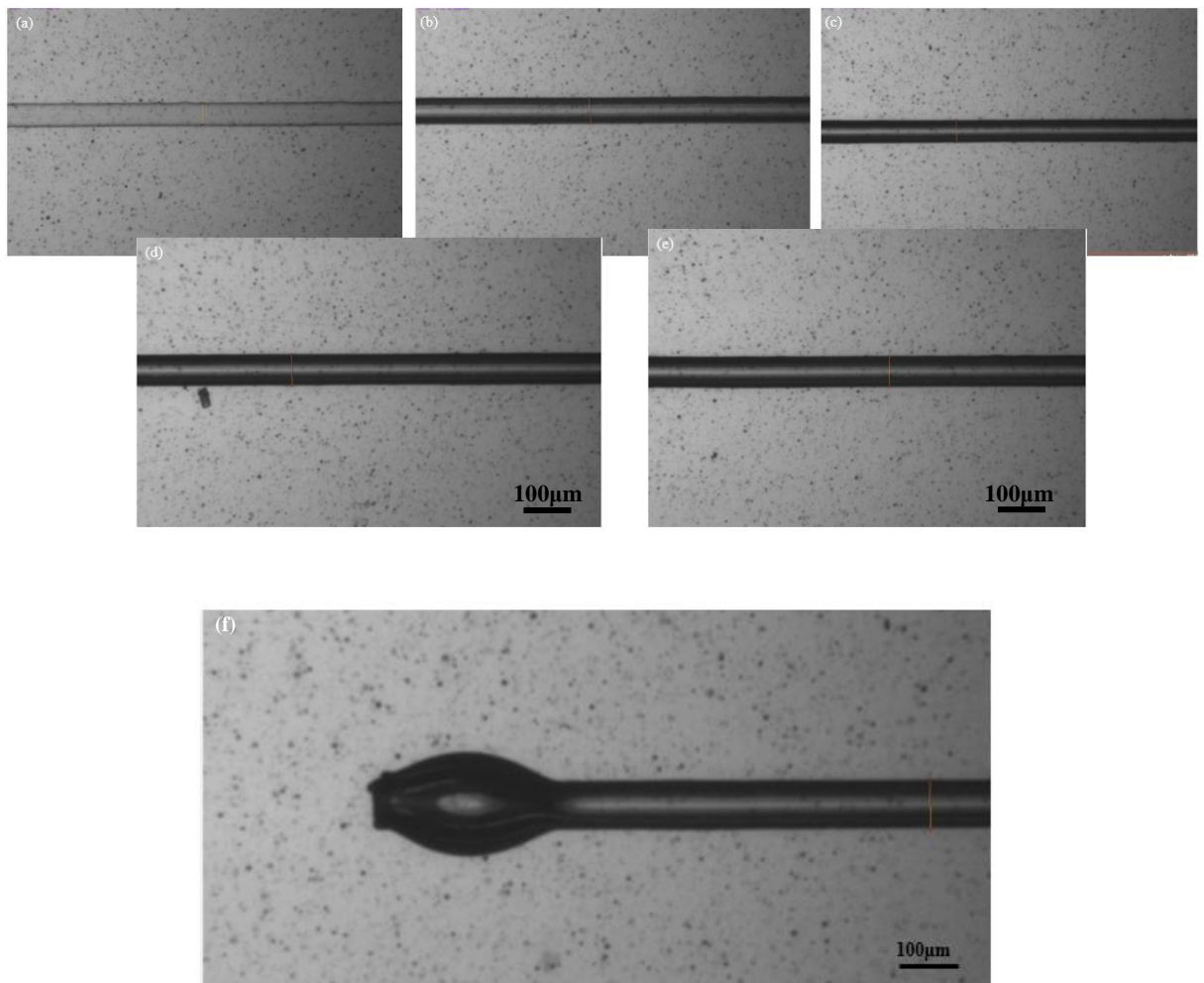


Figure 25. Several layers of PI ink on a non-etched PI substrate at 15 μ m Drop spacing. (a) 2 layers,(b) 4 layers, (c) 6 layers, (d) 8 layers,(e) 10 layers, and (f) Bulging at one side of the printed line after 10 layers. Ink spread and concentration increased with an increase in the number of layers.

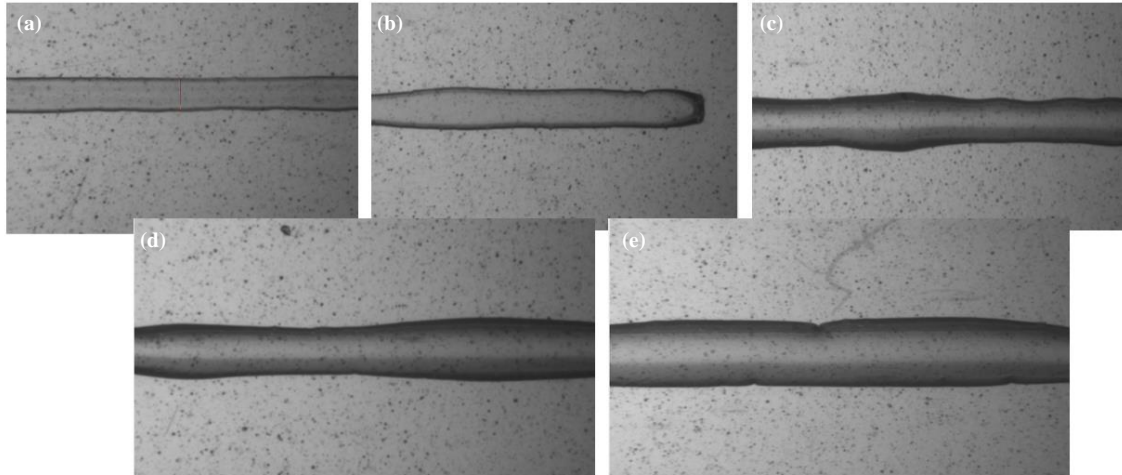


Figure 26. Several layers of PI ink on 10 seconds etched PI substrate at 15 μ m Drop spacing. (a) 2 layers,(b) 4 layers, (c) 6 layers, (d) 8 layers,(e) Ink spread and concentration increased with an increase in the number of layers

After testing the performance of PI ink on PI substrates, PI insulation was done on printed gold electrodes as shown in figure 27. Several layers of PI were printed on the gold electrodes; however, the surface of the gold print was more hydrophobic relative to the PI surface, which prevented the spread of PI ink over gold, causing the accumulation of ink over specific areas, leaving areas devoid of the ink along the electrode track. Because of this, we subjected our printed electrodes to 10 seconds of plasma etching, increasing the surface free energy and rendering the surface more hydrophilic, thus ensuring better insulation as shown in figure 27. A very optimum spread of ink was achieved following the 10 seconds of etching. It should be noted that an increase in plasma etching time more than this leads to the excessive spread of ink which will consequently coat all the electrode tracks including the site that is supposed to be in contact with biological tissues. For this reason, both the plasma etching time, platen temperature, and the cartridge has to be monitored before and during the printing process. Insulated electrodes should be carefully removed from the printer platen after switching off the vacuum to avoid spreading the ink over the electrode active site. The insulating layer is then cured by placing the PI electrodes on a hot plate at 180 $^{\circ}$ C for an hour.

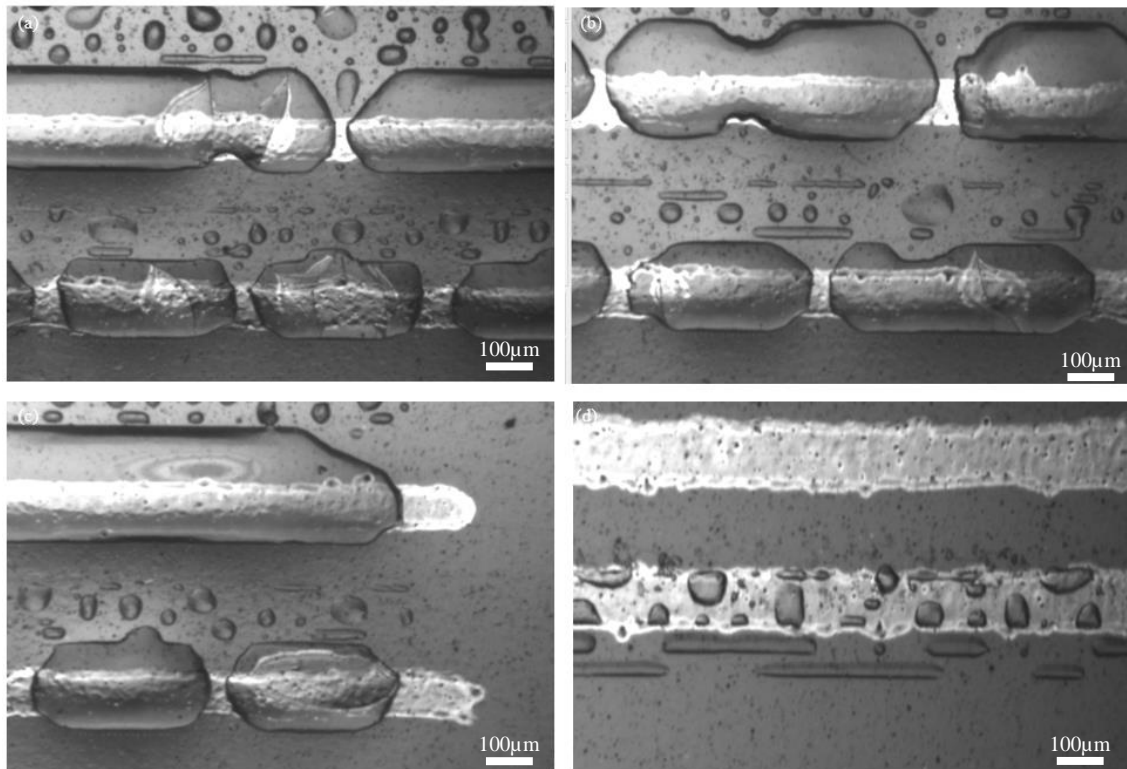


Figure 27. PI ink insulation on electrodes (pre-etched). Non-continuous PI ink deposition with areas devoid of ink due to the hydrophobic nature of the gold printed pattern and non-etched PI substrate surface(a-e).

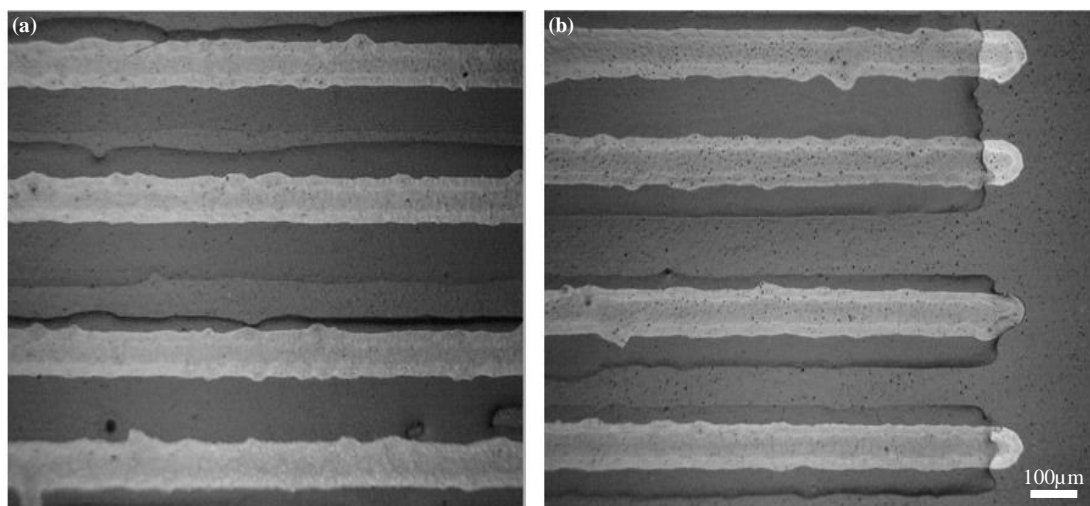


Figure 28. PI ink insulation on electrodes (Etched surface). Uniform and continuous distribution of PI ink. Optimum coverage of PI insulation layer on electrode tracks(a), uniform insulation ink distribution over the electrodes track except for the electrode active contact site (b)

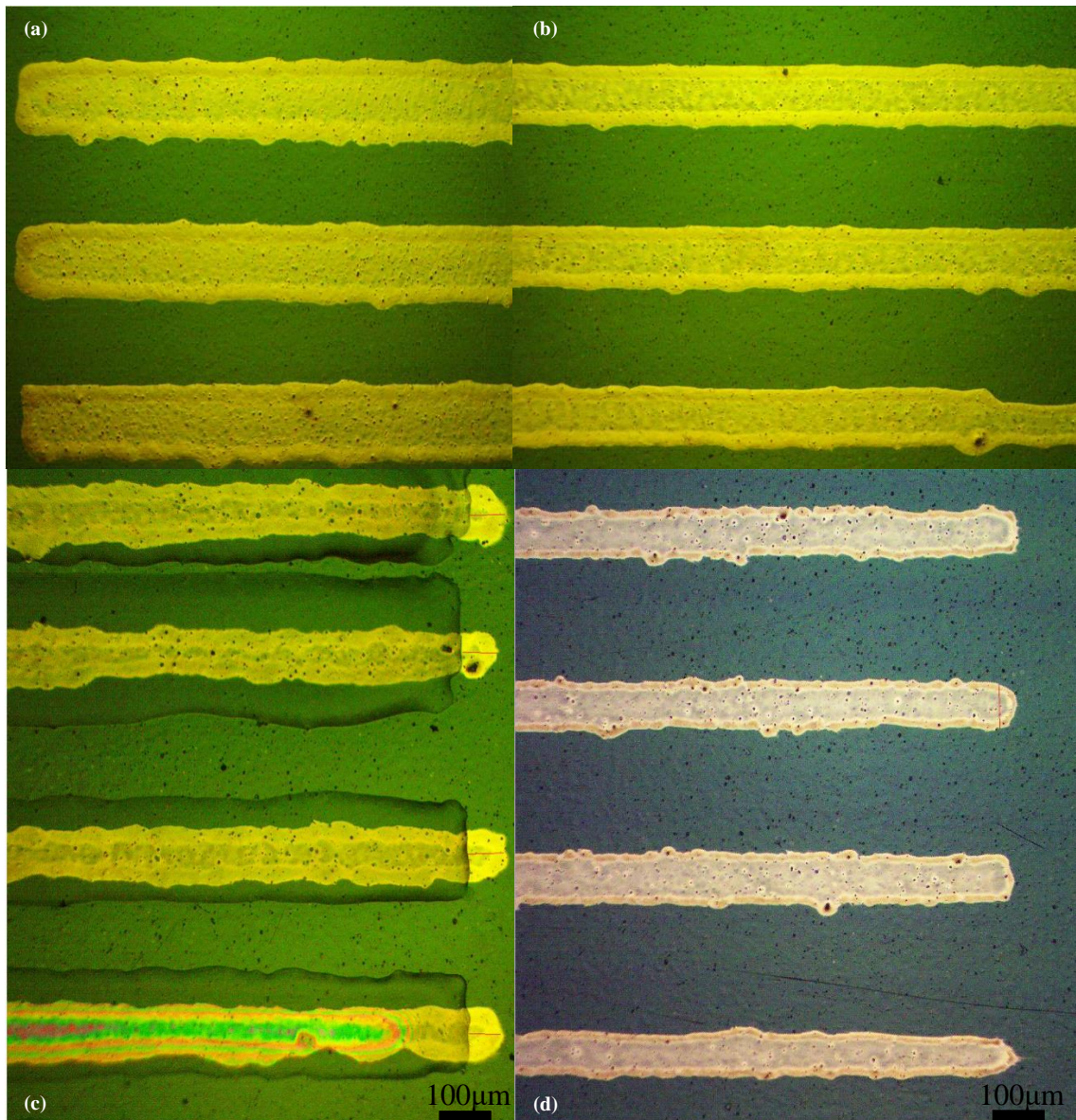


Figure 29. Optical microscopic images of electrodes printed on PI.(a)Contact pads (b)Electrodes track (c)PI insulated electrodes showing exposed site (d) Electrodes without PI insulation

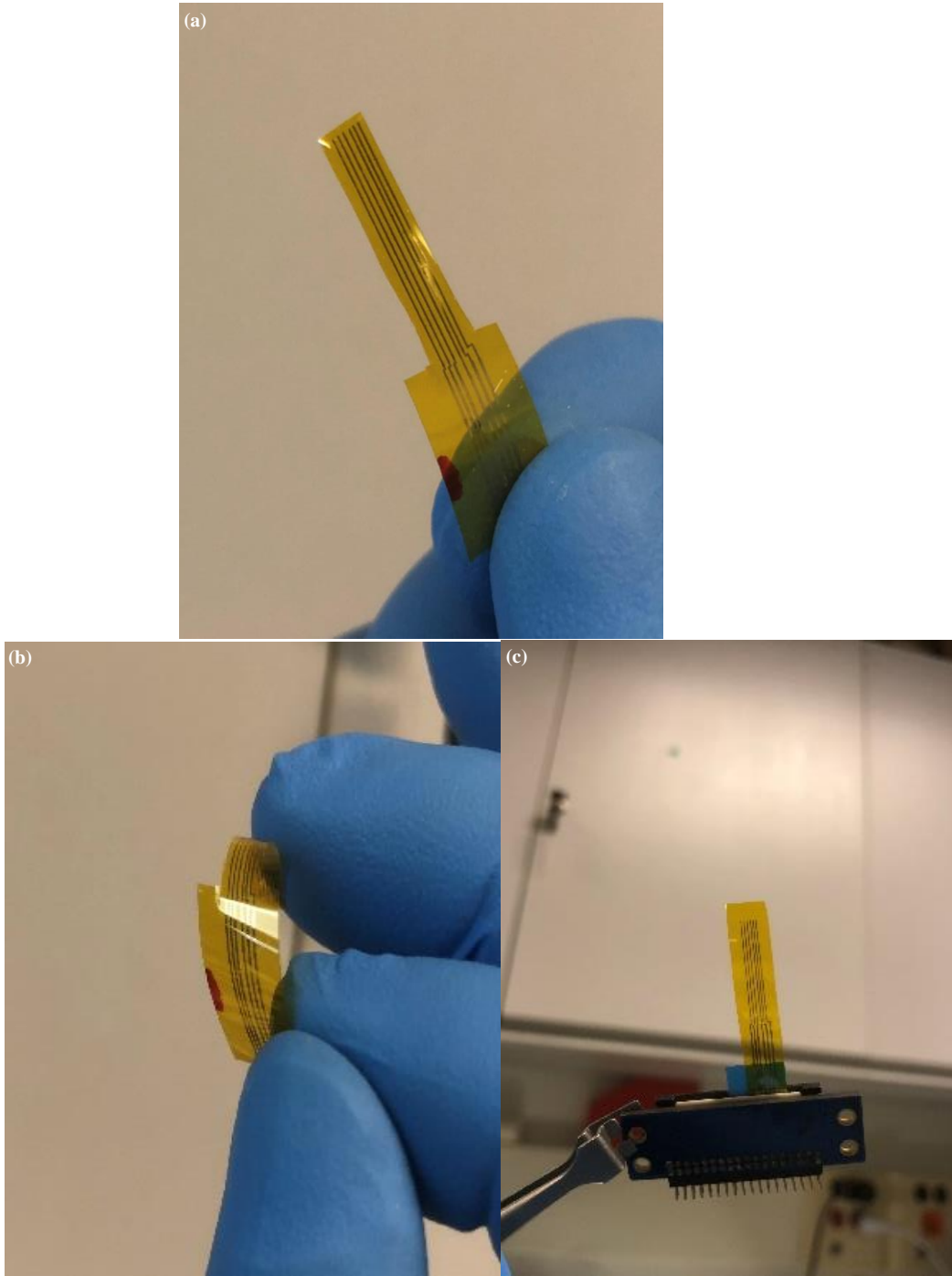


Figure 30. Images of PI electrodes array. PI six electrode array(a), flexed PI-based electrode, PI electrode fixed in the connector for ME2100 head stage.

5.4. Inkjet Printing of electrodes on PCL Substrate

The printing of gold electrodes on PCL is a challenging process as the surface topography of the prepared PCL substrate plays a critical role in obtaining desired electrode dimensions of good quality. Following the spin coating of PCL solution on a clean glass slide, the prepared film was allowed for about 10 minutes for solvent evaporation at room temperature before the printing process. Figure 31 shows the printing of a 100 μm line on a non-modified PCL surface at a drop spacing of 30 μm . This drop spacing was selected after first characterizing the gold ink on PI substrates. It could be seen in figure 31 that printing of gold ink on a non-modified PCL surface gives a non-uniform distribution of ink and it spreads through the ridges of the spherulites on the surface of the PCL. The presence of large spherulites on the PCL surface predisposes PCL electrodes to cracks upon sintering. It also makes getting smaller electrode dimensions practically impossible. It is worth mentioning that the viscosity of the ink used during the fabrication process also has an impact on the quality of the prints. The ink used has a viscosity of about 7-10 centipoise, Using ink with a higher viscosity will decrease the spread of ink as well as cracks upon sintering. Higher viscous ink will also allow for the printing of thicker layers while also minimizing ink spread.

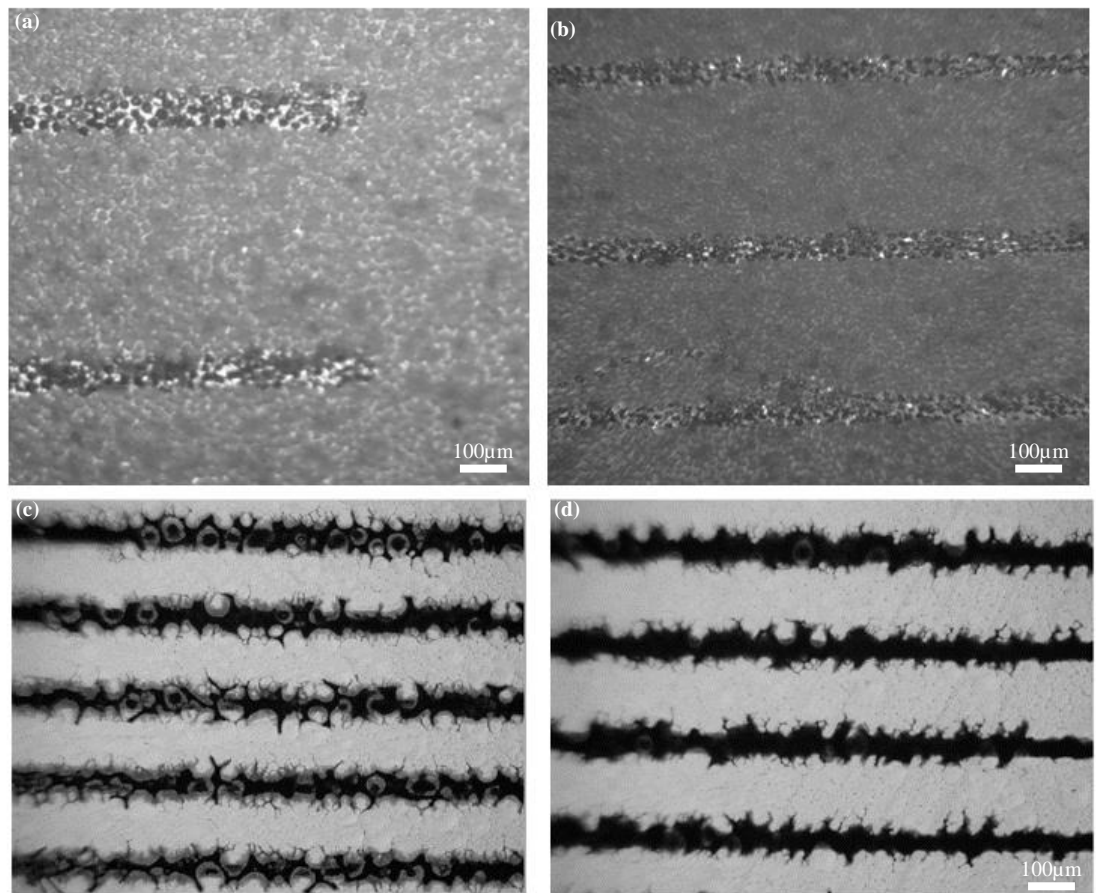


Figure 31. Gold electrodes printed on non-temperature modified PCL substrate. (a) and (b) one layer of gold,(c) 2 layers of gold, and (d) 4 layers of gold. A non-uniform spread of ink and poor-quality print was obtained on a non-pre-heated PCL substrate at different layers.

In an attempt to modify the surface of our PCL substrates and improve the quality of prints, we subjected it to oxygen plasma etching for 30 seconds as shown in figure 32. The printing quality on etched surfaces has improved as it gives well-defined edges of electrodes, however, the presence of the ridges on the surface of the PCL impacted the quality of the printed electrodes. This necessitates further surface modification of the PCL substrate to reduce or eliminate the excessive surface roughness present.

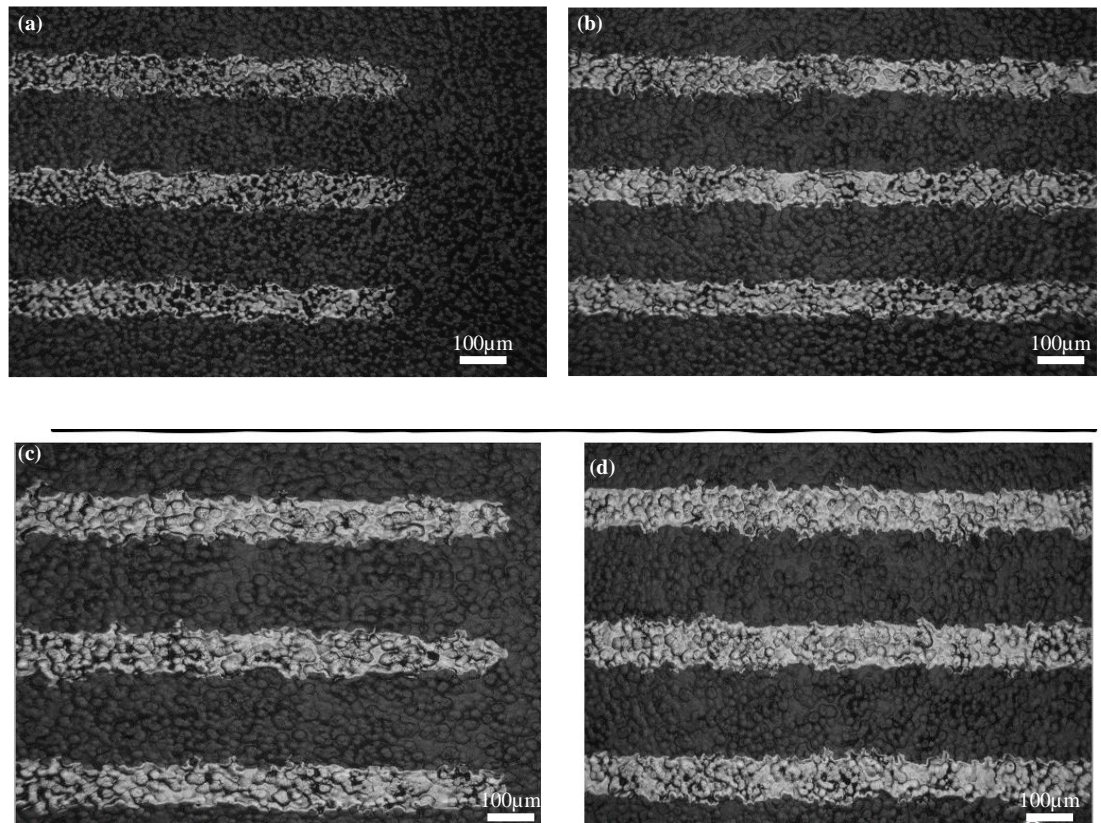


Figure 32. Gold print on 30 seconds plasma etched PCL substrate. (a) and (b) 2 layers of gold on 30 seconds plasma etched PCL substrate, (c) and (d) 4 layers of gold on 30 seconds plasma etched PCL substrate. Plasma etching of PCL substrate improves the quality of printing, however, the coarse surface topography of the substrate makes electrodes to be prone to cracks upon sintering.

Because of the surface roughness issue faced and the delamination of the PCL substrate from the glass support, we placed the PCL films on a hot plate at 60°C for about 2 to 3 seconds. This causes the PCL film to further spread on the glass slide, adhere firmly to the glass support, and reduce the ridges increasing the PCL surface roughness as seen in figure 33. The optical microscopic images of electrodes printed on the temperature-modified PCL substrates are shown in figure 33. Subjecting PCL substrate longer than 3 seconds excessively melts the substrate, making it stick firmly on the glass support layer and become very difficult to lift off following the printing process. Ensure complete evaporation of solvents before heat treatment, spin-coated PCL subjected to heat prior to

evaporation doesn't adhere to the glass support layer and is likely going to delaminate during the printing process.

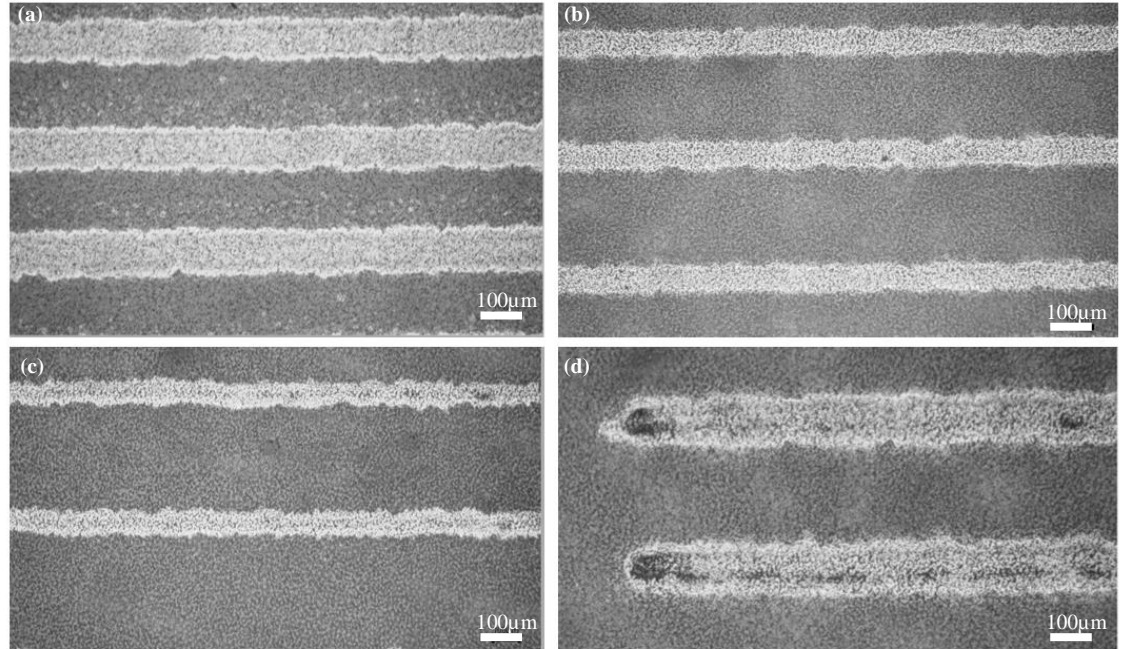


Figure 33. Gold electrodes on 3 seconds pre-heated PCL substrate. (a),(b),and(c) electrode tracks, (d) electrode active site. Pre-heated PCL substrate improves printing quality and reduces the coarse topography seen on non-preheated PCL substrate

5.5. Photonic Sintering of Gold electrodes on PCL:

As explained in the methodology section, PCL is a temperature-sensitive substrate and because of this reason gold nanoparticles printed on PCL substrate need a specialized method to render the continuous electrode track conductive. We employed a photonic sintering method using a camera flash to deliver an intense pulse of light to the printed electrodes. The camera flash was suspended at different heights from the inkjet-printed electrodes and several tests were done. At a height greater than 1cm electrodes don't become sintered even at an increased number of flashes. At 1 cm source-to-substrate distance, the optimum flash intensity is delivered and gold nanoparticles printed on the PCL substrate become

cured and conductive. One major challenge faced was the dimension of electrodes to be sintered. Camera flash offers limited parameters, and the flash intensity can only be modified by increasing the source-to-substrate distance. A dedicated sintering machine offers several sintering options including the desired energy of light that incidents on electrodes. Small dimensions electrodes were observed to completely crack even with an increase in the number of layers of gold, making printed electrodes non-conductive. We then increased the dimensions of our electrodes as well as the number of layers and subjected the printed electrodes to a different number of flashes. We observed that less or no cracks were obtained with larger electrodes dimension of about 300 μm and above. Additionally, conductive electrodes can be obtained at 3 layers and above.

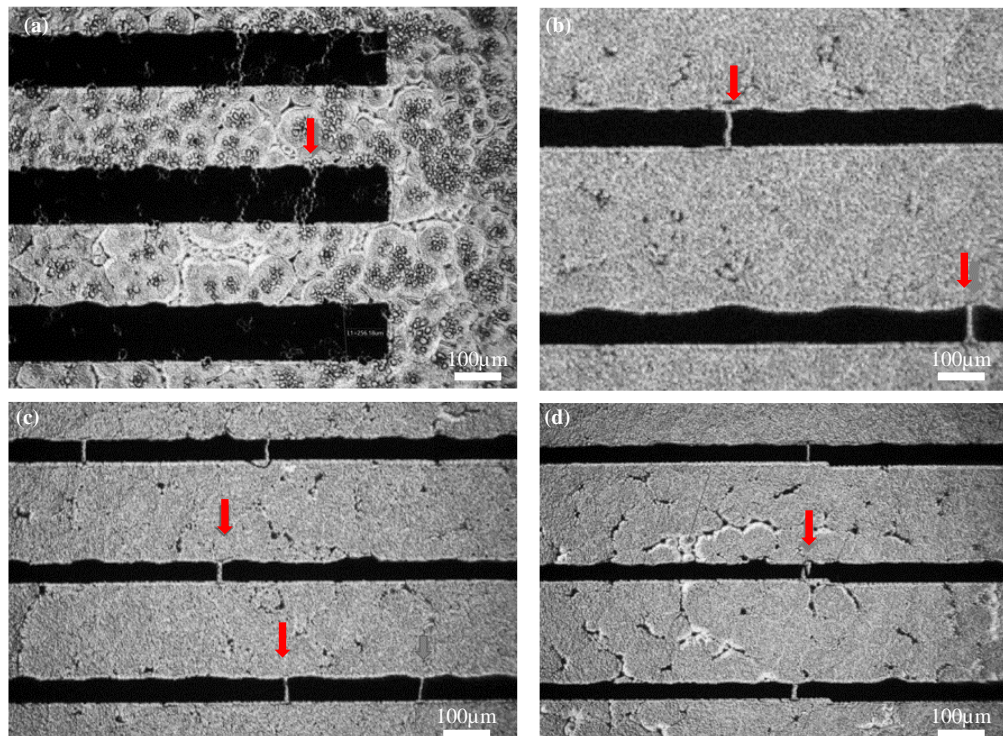


Figure 34. Crack upon sintering smaller dimension of gold electrodes printed on PCL substrate. (a) and (b) 2 flashes,(c) and (d)3 flashes. Red arrows indicate cracks along the electrode track.

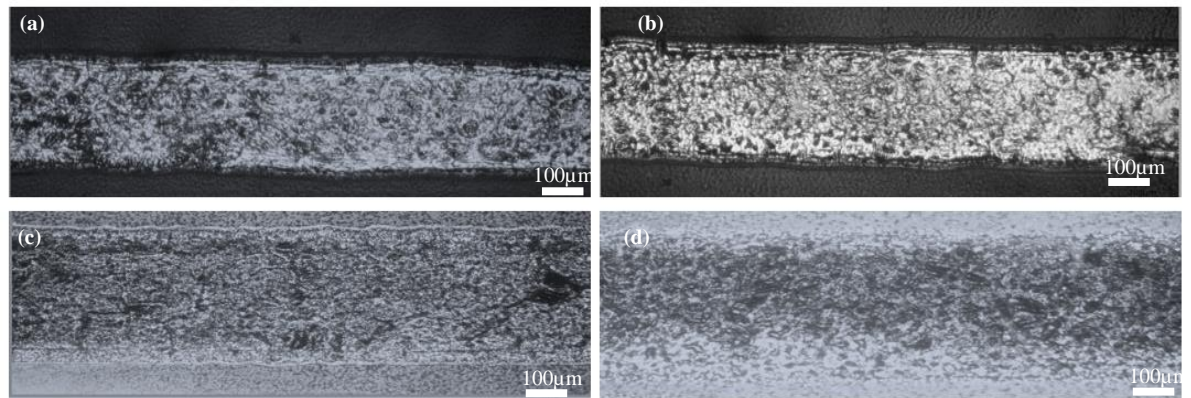


Figure 35. Larger dimension electrodes with no cracks along the electrode tracks. (a) and (b) 4 layers of gold,(c) and (d) 8 layers of gold. Electrodes of dimensions greater than $300\mu\text{m}$ fewer or no cracks, and micro-cracks reduce with an increase in the number of layers of electrodes.

As for the final electrodes printed on PCL, a drop spacing of $30\mu\text{m}$ was used on heat-treated PCL films. These parameters were adopted following the characterization of ink and using different substrate modifications as shown above. Printing at room temperature as well as elevated temperatures was tested. However, better prints were gotten at room temperature. Figure 36 below shows different parts of the 6 electrode arrays on PCL under an optical microscope.

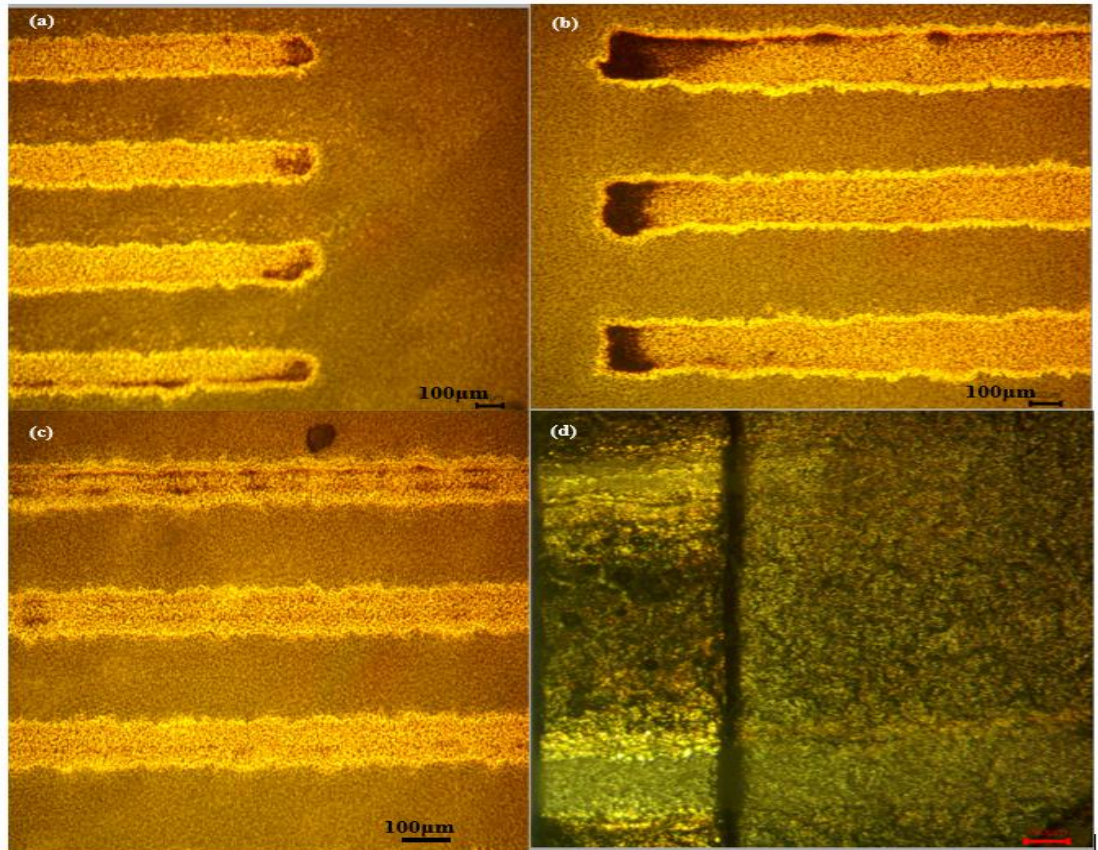


Figure 36. Optical microscopic images of electrodes printed on PCL.(a)Electrodes active site,(b)Contact pads,(c)Electrodes track/leads,(d)PCL heat pressed electrodes with the exposed active site.

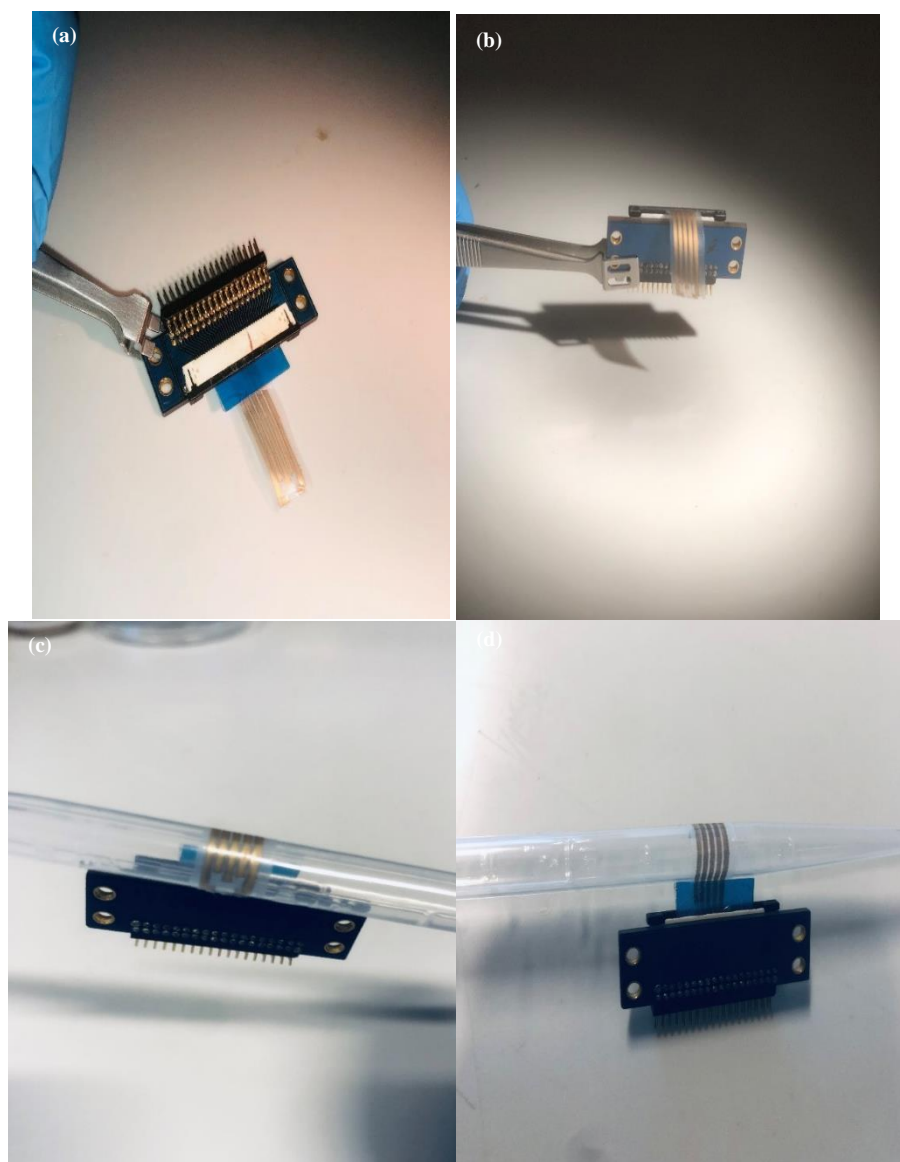


Figure 37. Images of PCL array. (a) and (b) PCL electrode with the connector (c) and (d) PCL electrodes conform on the surface of a pipette

5.6. Electrical characterization

Before device fabrication, various printing parameters are assessed to study their effect on the performance of the printed electrodes. These parameters include the number of layers printed, drop spacing, sintering temperature in case of thermal sintering, and the number of flashes in case of photonic sintering. This step allows us to achieve electrodes with optimal conductivity and electrochemical performance. Figure 38 shows the effect

of the number of gold layers on the obtained sheet resistance. The sheet resistance of 1, 2, and 3 layers of gold nanoparticles structures printed on PI and sintered at 300°C for 35 minutes was 18.3, 2.85, and 2.84 $\Omega.\square^{-1}$ respectively. This sintering temperature and time were adopted since they yielded the electrodes with the lowest sheet resistance. Sintering at temperatures lower than this yielded mostly non-conductive prints even at an increased sintering time. It was thus observed that sheet resistance decreases for a higher number of layers. Consequently, all prints of our electrodes were done with 3 and 4 layers of gold at the sintering condition of 300°C for 35 mins.

Table 4. The sheet resistance of gold layers on PI

No of Layers	Sheet Resistance ($\Omega.\square^{-1}$)
1 layer	$21.30 \pm 5.889 \times 10^{-2}$
2 layers	$2.85 \pm 1.605 \times 10^{-3}$
3 layers	$2.84 \pm 1.345 \times 10^{-3}$

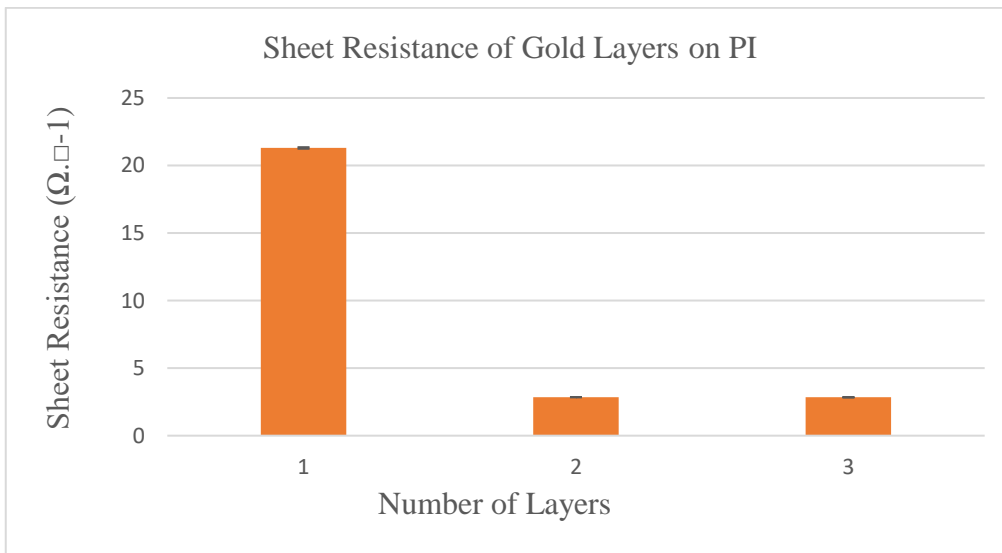


Figure 38. Sheet resistance measurement between different number of gold layers on PI and corresponding electrical resistance.

5.7. Printing on PCL & photonic sintering

As discussed in the methodology section of this study, PCL is a temperature-sensitive substrate with a melting temperature of about 60°C. As a result, it cannot be subjected to the conventional thermal sintering process to render the printed electrode tracks conductive. Consequently, we made use of a camera flash (Nikon Speedlight SB-28) to perform the photonic sintering process. Firstly, 5 x 5 mm squares were printed for sheet resistance evaluation, with the varying number of layers or number of flashes applied. Figure 34 presents the variation of sheet resistance with respect to the number of gold layers printed on PCL. The prints were sintered by applying 3 flashes. Similar to the results presented in Figure 33, an increase in the number of layers leads to a decrease in sheet resistance, hence, better conductivity. Moreover, the application of a single flash at these numbers of layers didn't achieve the sintering of the printed pattern, leaving it non-conductive. Figure 39 shows the effect of 3 flashes and the number of gold layers on sheet resistance.

Table 5. Sheet resistance measurement between the different number of gold layers on PCL at 3 flashes sintering condition.

No of Layers	Number of flashes	Sheet Resistance ($\Omega \cdot \square^{-1}$)
2	3	$9.91 \pm 7.964 \times 10^{-2}$
3	3	$6.12 \pm 5.957 \times 10^{-3}$
4	3	$4.23 \pm 3.664 \times 10^{-3}$
9	3	$2.54 \pm 1.258 \times 10^{-2}$

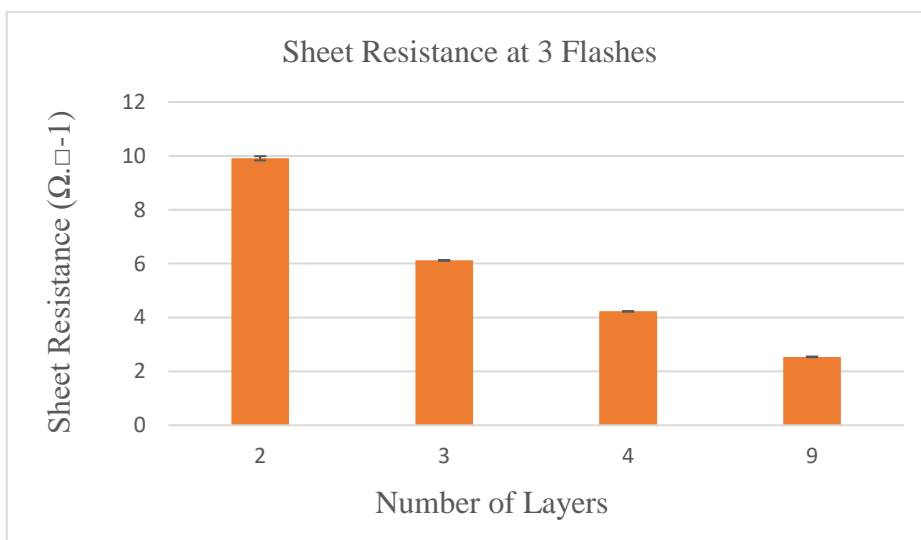


Figure 39. Sheet resistance measurement between different number of gold layers on PCL at 3 flashes sintering condition.

The previous result showed that an increase in the number of layers leads to a decrease in sheet resistance when sintering is done by delivering 3 flashes. We further investigated the effect of the number of flashes delivered on the obtained sheet resistance. Figure 40 shows that at 9 layers of gold, 2 flashes achieved a sheet resistance of $3.24 \pm 7.868 \times 10^{-3} \Omega \cdot \square^{-1}$. At 3 flashes, the sheet resistance decreased to $2.54 \pm 1.258 \times 10^{-2} \Omega \cdot \square^{-1}$, and at 4 flashes, an increase in sheet resistance to $4.63 \pm 1.839 \times 10^{-2}$ was noted. This could be that after delivering 3 flashes, the gold nanoparticles are fully sintered and any additional flash leads to cracking and introduction of defects on the print, which decreases its conductivity, thereby increasing the sheet resistance.

Table 6. Sheet resistance measurement of 9 layers of gold layers on PCL at 2, 3, and 4 flashes.

No of Layers	Number of flashes	Sheet Resistance ($\Omega \cdot \square^{-1}$)
9	2	$3.24 \pm 7.868 \times 10^{-3}$
9	3	$2.54 \pm 1.258 \times 10^{-2}$
9	4	$4.63 \pm 1.839 \times 10^{-2}$

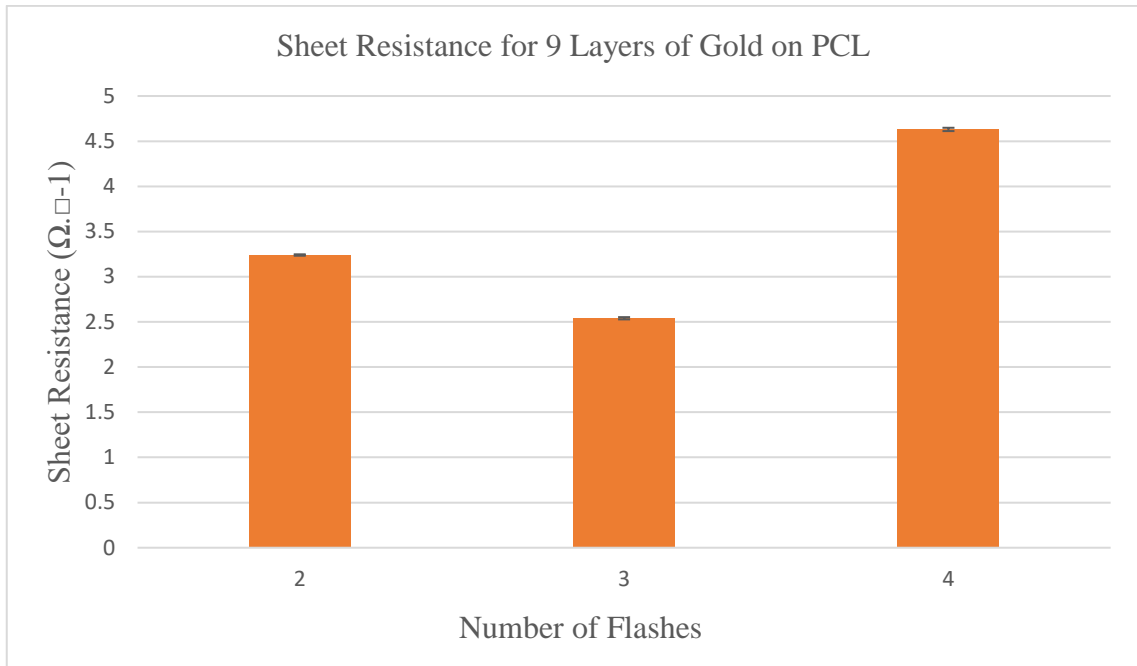


Figure 40. Sheet resistance measurement of 9 layers of gold layers on PCL at 2, 3, and 4 flashes.

Furthermore, the same comparison was conducted on prints made with 5 layers of gold, and the results are depicted in figure 41. Ultimately, prints done with 9 layers of gold and sintered by delivering 3 flashes yielded the best results.

Table 7. Sheet resistance measurement of 5 layers of gold on PCL at 2, 3, and 4 flashes.

No of Layers	No of flashes	Sheet Resistance
5	2	$12.5 \pm 2.610 \times 10^{-2}$
5	3	$7.85 \pm 2.806 \times 10^{-2}$
5	4	$13.4 \pm 5.750 \times 10^{-3}$

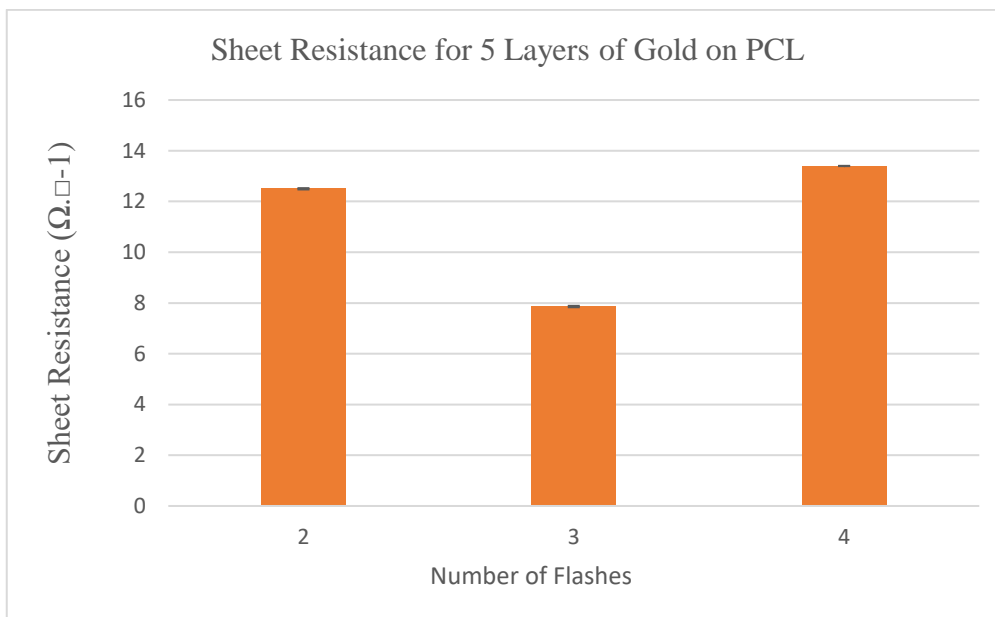


Figure 41. Sheet resistance measurement of 5 layers of gold on PCL at 2, 3, and 4 flashes.

5.8. Electrochemical Characterization

In this work, gold nanoparticles were printed on polyimide and PCL substrates following the electrical characterization of the materials and determining the optimum parameters that yield good conductivity. Up to four layers of gold were printed for the electrodes on polyimide and the electrodes measured about 100 μ m in diameter. As for the electrodes printed on PCL, up to 9 layers of gold were layered on the substrate, and our electrodes measured about 300 x 400 μ m in diameter. The increased dimension of electrodes in the case of PCL substrates was due to the challenges faced in obtaining conductive prints on this substrate. PCL has a rough surface with ridges as compared to PI. Hence, upon photonic sintering, cracks were observed along the prints, rendering them non-functional. It was thus noted that electrodes with larger dimensions did not pose this issue as compared to smaller prints. Another factor that plays a very vital role in getting good prints on PCL is the viscosity of the ink used. A less viscous ink will give a tough

time in getting good prints. On the other hand, ink with a medium-range viscosity tends to spread less and makes prints appear good, and allows for easy scale-down of electrode diameter. But it should be noted that while using a dimatix inkjet printer, a very viscous ink makes nozzles get clogged very easily. This is time-consuming and you may end up spending almost half of the time dedicated to printing running several cleaning cycles to open clogged nozzles.

5.9. Electrochemical impedance of gold electrodes on PI

Figure 42 shows the mean impedance of electrodes of 100 μ m electrodes printed on PI at 1KHz before and after the experiment. This is done to assess the electrochemical stability of our electrodes when used during recording. As we are only testing the feasibility of our electrodes in vivo by acute recording, it will give us an idea of how stable our electrodes could be when used for long-term chronic recording. The mean impedance of our electrodes (n=4) is 34.4k Ω before the experiment and 36.6k Ω post-experiment. The impedance of the electrodes slightly rose by just 2k Ω . This result indicated that our gold microelectrodes have a very low impedance and good stability when used for recording. As discussed in chapter 4, the acceptable impedance limits for electrodes have to be less than 5 M Ω if a high-quality recording of diagnostic quality and devoid of excessive noise is required.

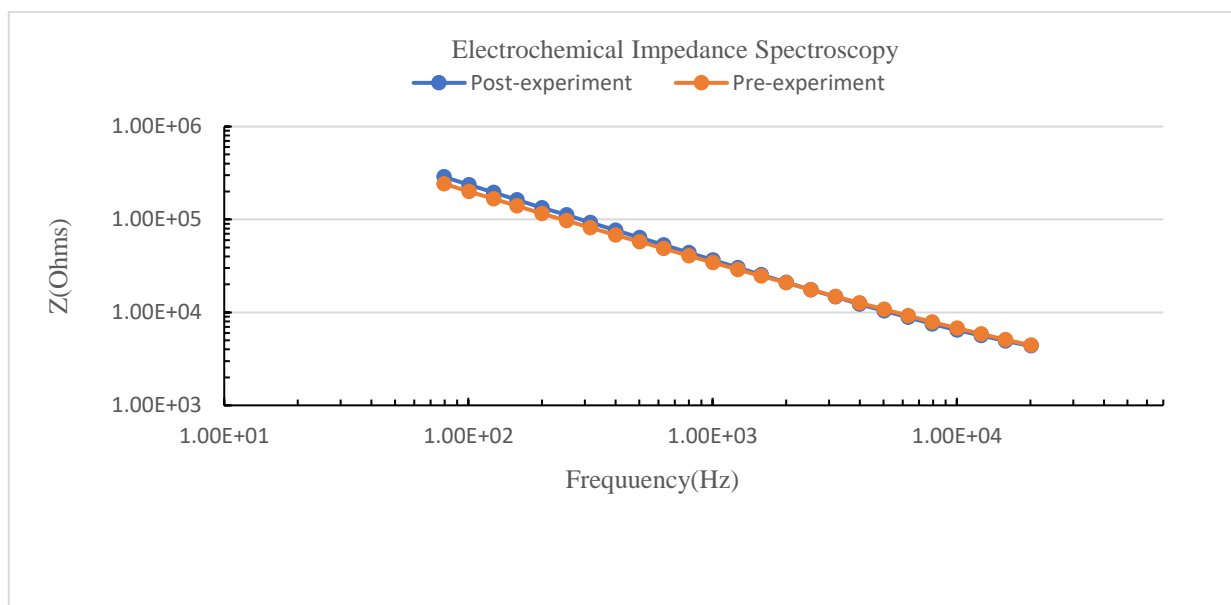


Figure 42. Electrochemical Impedance Spectroscopy of PI electrodes before and after the experiment

5.10. Electrochemical impedance of gold electrodes on PCL electrodes

EIS of electrodes on PCL were assessed before and after experiments to check the electrochemical stability of the gold electrodes on PCL. Electrodes of about 300 x 400 μm as well as higher dimensions, were printed and assessed (n=6). An electrode with 300 x 400 μm yielded a mean impedance of about 30.1 k Ω . This impedance value is slightly lower than that recorded on PI, where the 100 μm electrode gives 34.4 k Ω at 1 kHz. The surface characteristics along with the sintering condition of PCL played a great role in giving this impedance despite the increase in the number of layers of the electrodes. With further surface modification and a dedicated sintering machine, the impedance of the electrodes can be lowered with a smaller-sized electrode. We also measured the impedance of our electrodes after 16 hours in PBS. The mean impedance of our electrodes has shown to increase up to 191 k Ω at 1 kHz.

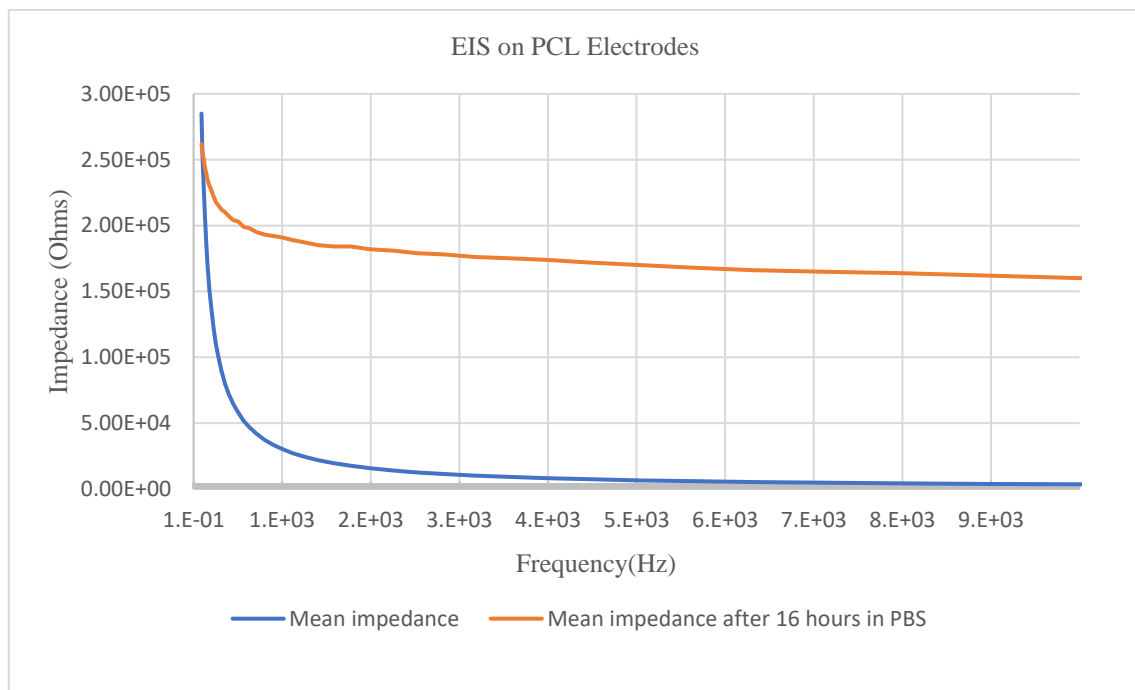


Figure 43. Electrochemical impedance spectroscopy of PCL electrodes before and after 16 hours in PBS.

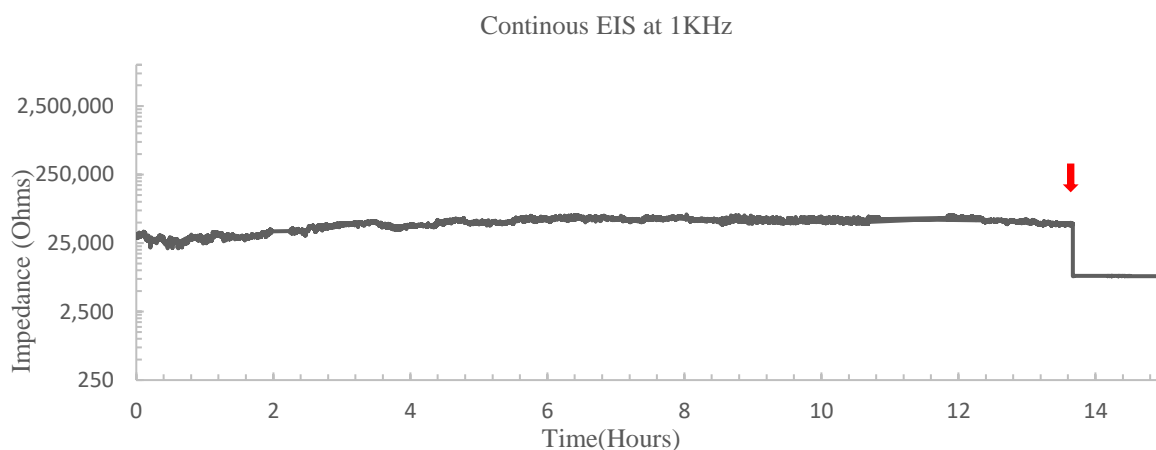


Figure 44. Continuous Electrochemical Impedance Spectroscopy of PCL Electrodes at 1KHz. There was a stable recording for over a period of 14 hours, after that a large drop in impedance was noticed which is likely due to delamination of the encapsulation layer (red arrow)

5.11. In vivo Neurophysiological testing of electrodes

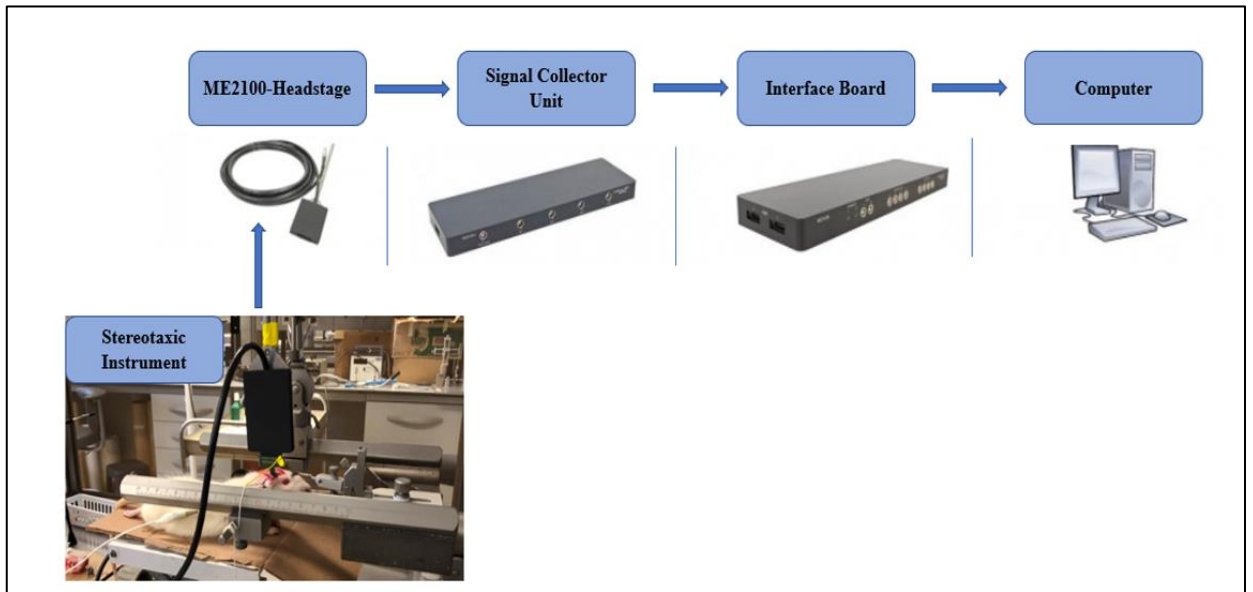
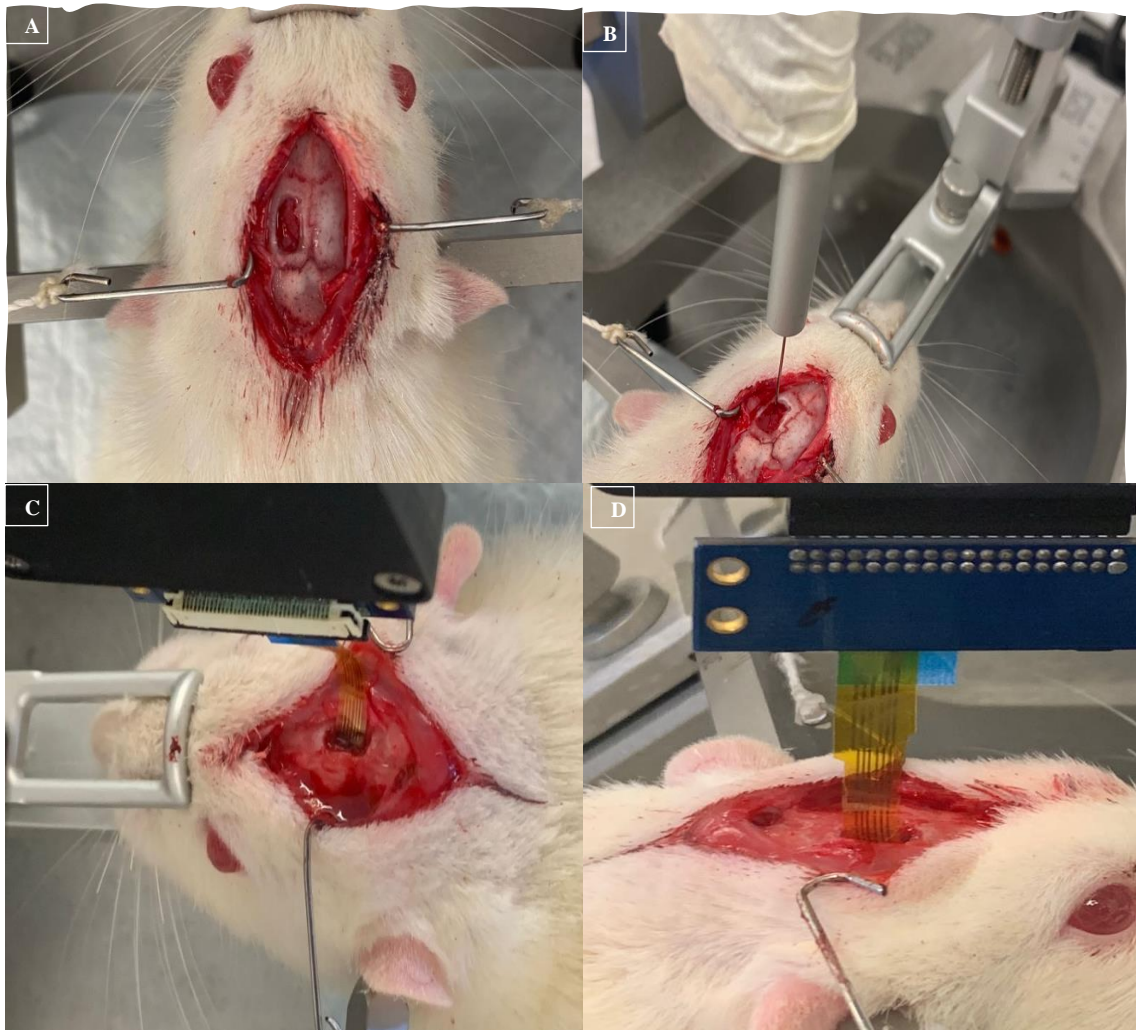


Figure 45. In vivo testing recording set-up

The feasibility testing of our devices in recording epilepsy was carried out using the setup in figure 45. This is an in vivo recording setup described in chapter 4. It consists of the stereotaxic instrument, where the animal is placed and the craniotomy performed, the head stage where our inkjet printed microelectrodes are fixed in, and the signal collector unit which receives the amplified signals from the head stage and sends it to the interface board, which is connected to a computer for the visualization of data both in real-time and for further offline analysis after the recording.

Following the initial animal preparation and placement in the stereotaxic instrument, a craniotomy of about 4mmx4mm was done on the left side of the skull before KA injection and electrode placement as shown in figure 46 (a). We then further locate the BLA which is the micro-injection site of the KA. This site corresponds to (-2.8 AP, 5 mm L, 7.6 DV measured from the brain surface, or 8.8 DV mm from the skull) to the bregma. Figure 46 (b) Shows the point where a 1 μ l Hamilton syringe is positioned over the injection site after getting the coordinates based on the atlas. Right after that, electrodes are placed over

the exposed part of the brain, and saline-soaked gel foam is placed over the electrode for proper contact with the brain and to ensure stability in the recording. The acute recording was done and monitored until several episodes of seizures are detected. Figure 46 (c) shows an axial view of polyimide electrodes fixed in the ME2100 system head stage and placed over the exposed part of the brain in good contact with the cerebral cortex for recording. The PI electrodes are easily distinguishable from the PCL electrodes because of the yellowish color of the polyimide substrate. Figure 46 (d) shows a lateral view of the same polyimide electrode placed on the surface of the brain during the recording process.



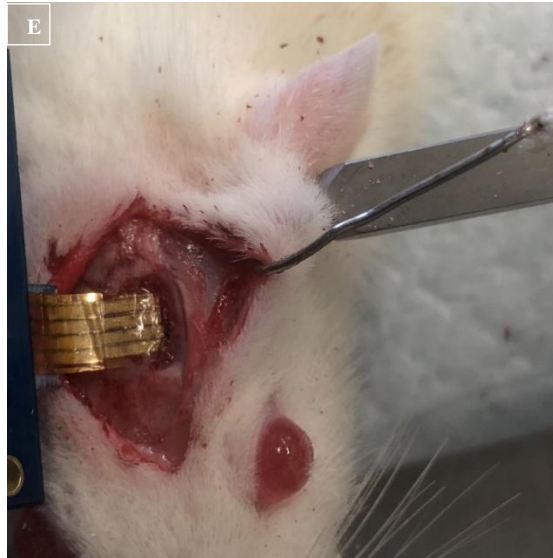


Figure 46. Microelectrode arrays implantation procedures in the rat brain. 4mmx4mm craniotomy on the left side of the skull (a), where a 1µl Hamilton syringe is positioned over the injection site (b), axial view of polyimide electrodes over the exposed brain tissue (c), lateral view of electrode placement (d), Axial view of PCL electrodes placement (e)

When the brain is in a certain state, qualified ECoG electrodes should be capable of recording oscillatory signals in the characteristic frequency ranges for that particular state. To test the quality and recording stability of our device, we treated rats with kainic acid through intra-amygdala micro-injection. This is a widely used method to induce status epilepticus (SE) and subsequently the development of mesial temporal lobe epilepsy (MTLE). The method was first demonstrated in the late 1970s [110, 111] and was also adapted for use in mice in the early 2000s [112, 113]. Unlike models that employ the systemic injection of KA, which leads to widespread damage, micro-injection of KA has been reported to cause unilateral limited damage to the hippocampus which is similar to human MTLE [114]. It has also been reported to have a short latency period for SRSs. Our flexible and biodegradable microelectrodes were implanted to check their capability in recording physiological and pathological brain waves. Before every recording using both the PI and PCL electrodes, the noise level of the electrodes was assessed using the ME2100 system we used for recording. Both our PCL and PI electrodes exhibited noise

levels with amplitude not greater than $20\mu\text{v}$ peak to peak. Five in vivo experiments were done to test the feasibility of our devices. The result presented below highlights an acute recording that was done over an hour. At the resting and anesthetized state of the rats, the amplitude of the baseline recording measured about $20\mu\text{v}$ (Figure 47). This baseline recording was done over a period of about 20 minutes in order to ensure the stability of our recording and also capture the time when abnormal seizure activities start. It should also be noted that our device was able to capture spontaneous physiological activities, as well as evoked potentials after grasping the toe of rats in real-time. Following the protocol used to induce seizure by intra-amygdala micro-injection of kainic acid as explained in detail in chapter 4 of this thesis, our rats developed seizures at around 20 to 30 mins post-injection. The first episode was seen for around 20 minutes, followed by subsequent episodes of seizure discharge with a decrease in the latency period. More than 5 episodes of seizures were recorded in 20 minutes. Seizure on ECoG recording is presented as an area of high synchronous activities and spike-wave discharge with an increase in both amplitude and frequency. Figure 42 shows a signal recorded from four channels of our electrodes, where the hypersynchronous activities of the seizure burst started. This was around 20 minutes after the injection of KA. The pattern of the seizure initiation first starts with a large sharp wave, which is followed by high-frequency sharp waves as seen in figure 48, this evolved as the seizure progresses into hypersynchronous, high amplitude, and frequency polyspikes. The amplitude of our signals during seizure activities went up to $800\mu\text{V}$ peak to peak. Figure 49 shows the transition from one episode of seizure discharge to the next one. Furthermore, we assessed the local field potentials (LFP), these are key signals in studying the communications of neurons in the brain. We used a low pass filter at 200Hz to generate our signals and its corresponding Time-

frequency power spectrogram (figure 50). This time-frequency power spectrogram is a commonly used method in the analysis of LFP in the frequency domain. It transforms electrical signals recorded into a broad spectrum whose power changes with frequency.

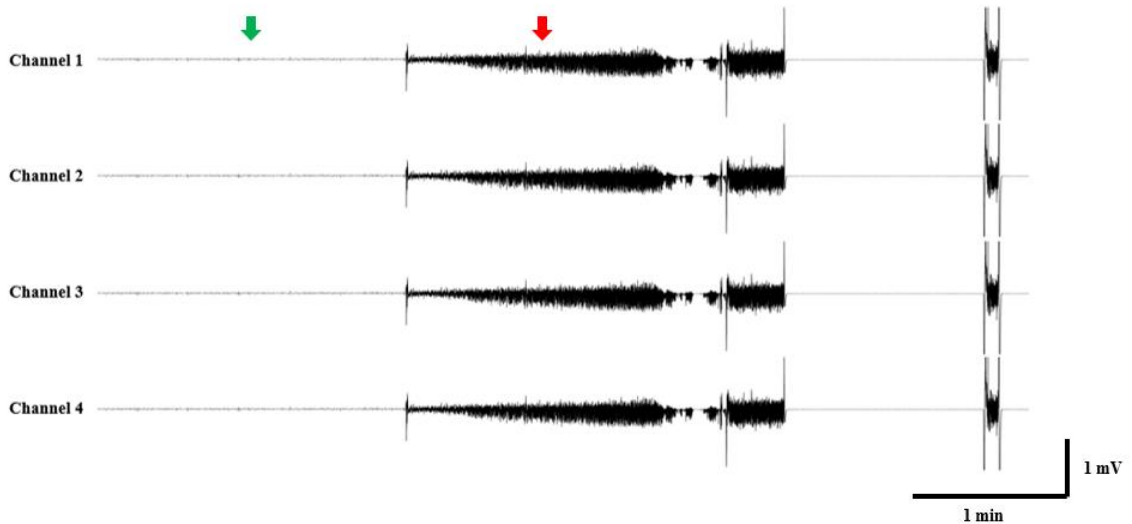


Figure 47. Signals from 4 different channels. The baseline signal during the normal activity of rats under anesthesia (green arrow) had a maximum amplitude of $20\mu\text{V}$ peak to peak, and the signal during seizure discharge (red arrow) had a maximum amplitude of up to $800\mu\text{V}$. The large sharp Spike before a seizure burst was about 1mV and increases as the seizure progresses and more bursts are discharged.

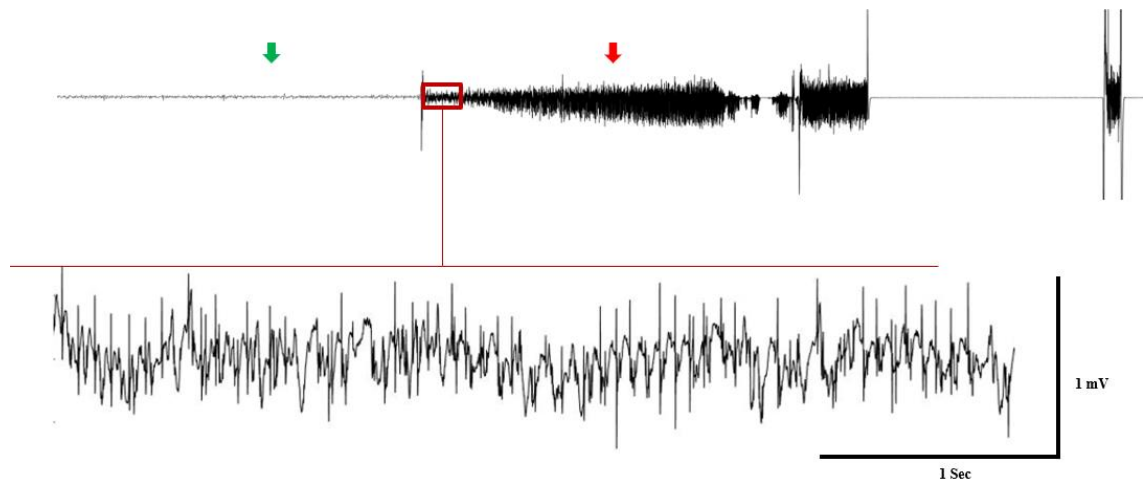


Figure 48. High frequency rhythmic sharp waves over the period of 4 seconds right after the large sharp wave as the point of seizure initiation (red arrow). This continues and evolves to the next stage of the seizure discharge as it progresses.

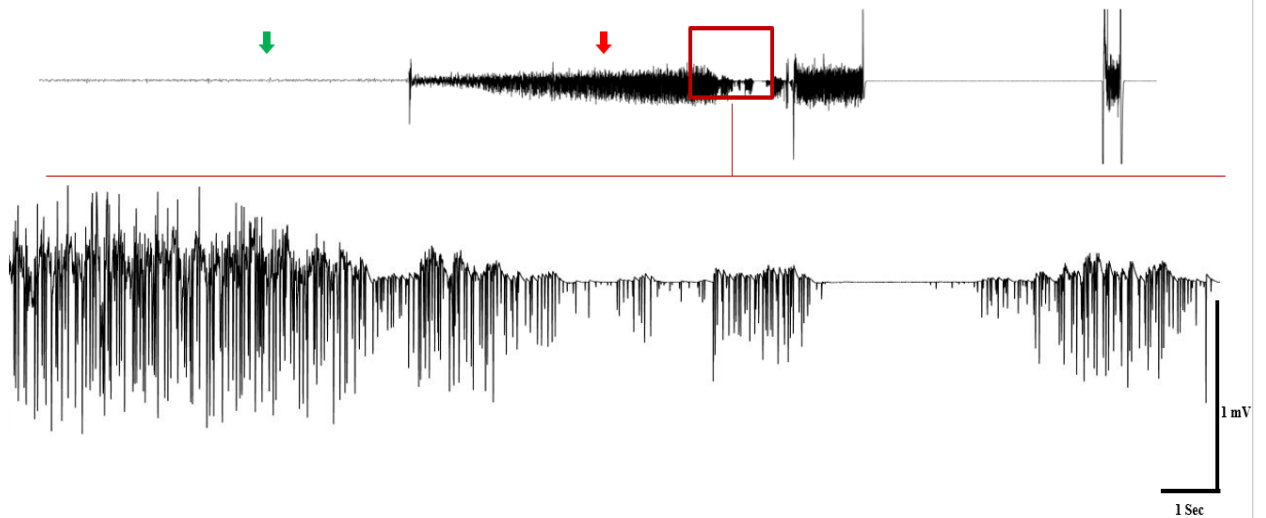


Figure 49. Magnified image of high-frequency poly-spike-like seizure discharge and transition from one burst of spikes to the next one. This is the third stage of our seizure discharge, and it is the continuous evolution of the high-frequency rhythmic sharp waves which occur immediately after the initial large sharp wave indicating the seizure initiation.

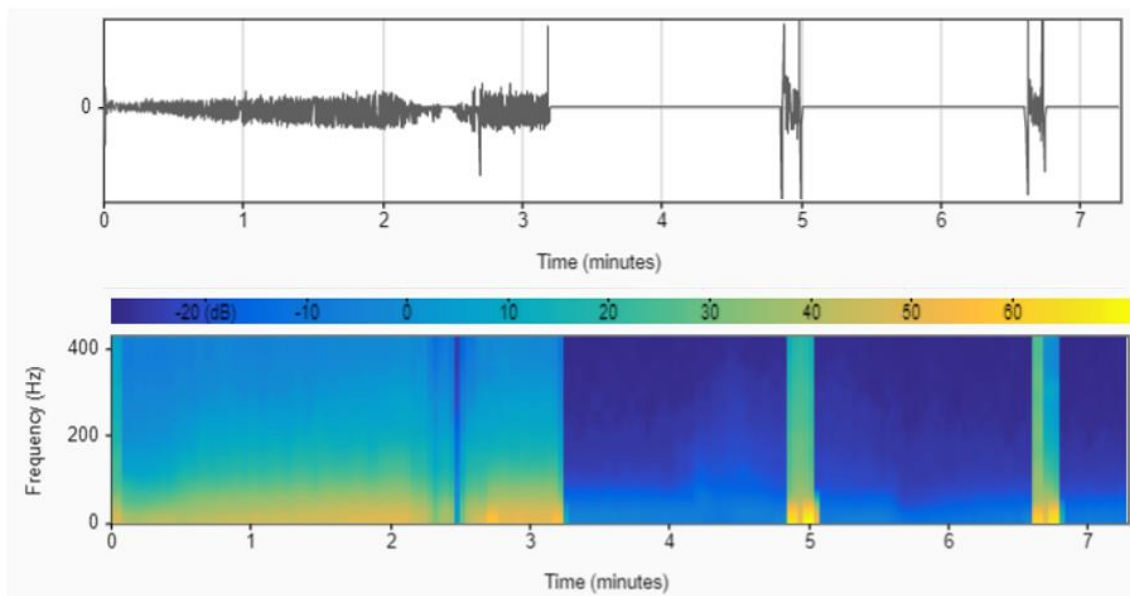


Figure 50. Figure. Low pass filtered signal at 200Hz and spectrogram over the period of 7 minutes. Seizure areas are seen as segments of increased activity and power (yellow) on the spectrogram, while the area of normal activities or baseline appear blue.

HFOs recently become of more interest as they have shown potential to be used as biomarkers for seizures. They have been shown to have a direct link with seizure onset zones and the removal of HFOs generating regions has been correlated with a seizure-free post-surgical outcome[115]. While mostly HFOs are recorded on intracranial EEG, recent studies suggest that it is possible for HFOs to be identified on scalp EEG or MEG. We generated HFOs by band-passing our signals between 80-600Hz (figure 51a). we further zoomed in on one of the short episodes of seizure discharge and evaluate the signal for three seconds (figure 51b).HFOs up to $800\ \mu\text{V}$ were seen during the seizure discharge. We also generated its spectrogram using the inbuilt MATLAB signal analyzer tool used for signal processing.

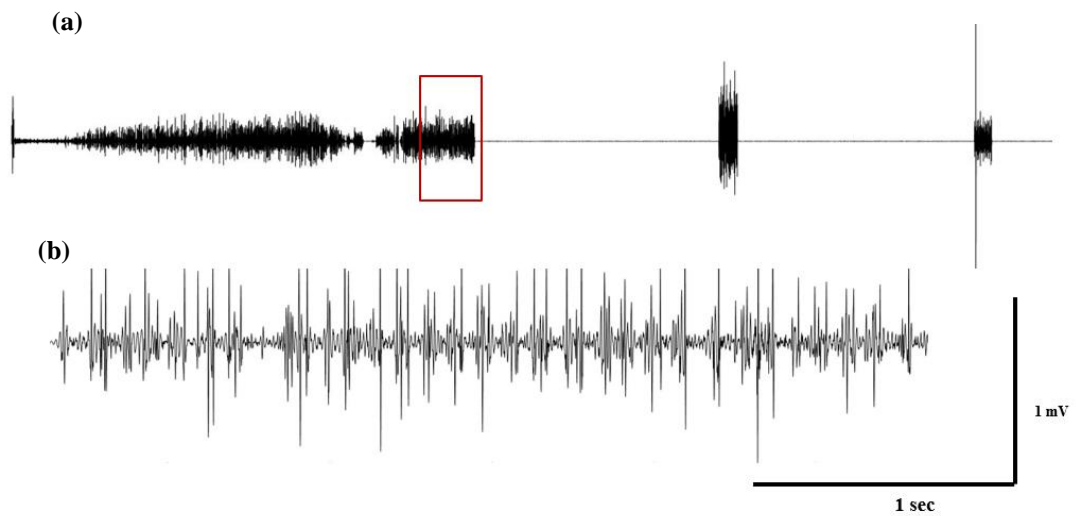


Figure 51. High-frequency oscillations (HFOs). Band passed signal between 80-600Hz Band passed signal between 80-600Hz for 6 minutes(a), magnified HFOs from one of the seizure bursts showing high amplitude seizure discharge(b)

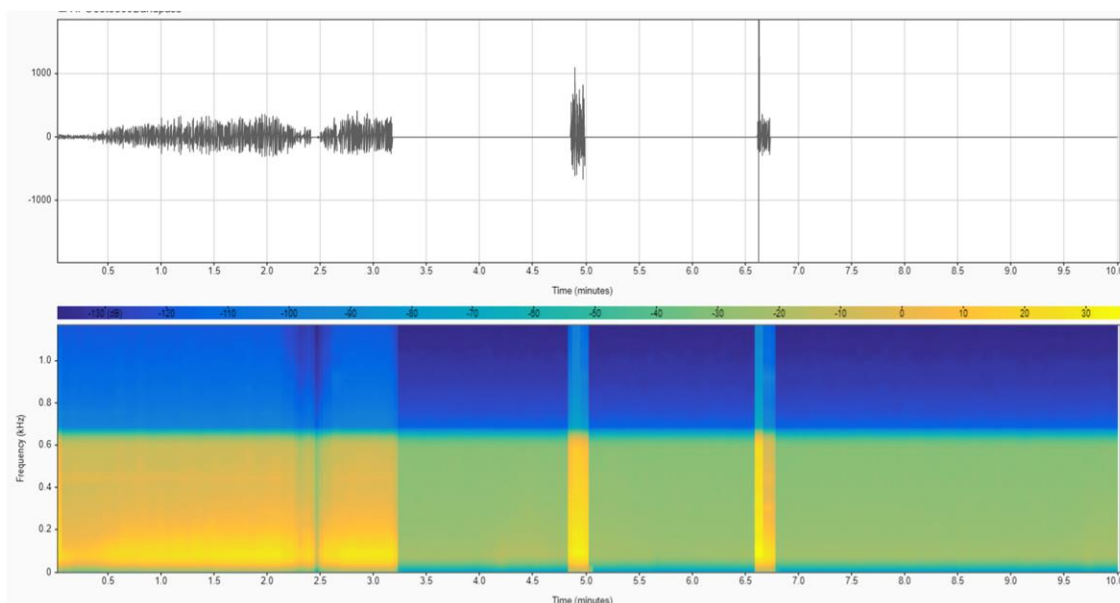


Figure 52. High-frequency oscillations (HFOs) and their corresponding spectrogram. The baseline area is represented as an area of low activity (blue), while the area of seizure discharge is seen as an area of increased activity (yellow).



Figure 53. Spike and wave discharge. This is a characteristic manifestation of seizure. It appears as a sharp wave that is accompanied by an intermittent slow wave.

5.12. Degradation Test

An accelerated degradation test was performed on the degradable substrates (PCL) to simulate their degradation behavior. Degradation of the biodegradable microelectrode arrays occurred in 10ml PBS pH 13 at 37°C. Figure 54 shows a series of images captured at several stages of the accelerated degradation test. The gold printed on the electrodes started to lift off the substrate 22 hours following its immersion in the PBS solution, at 46 hours the substrate became more attacked and started to break off into big

fragments while the dissolution of the gold pattern continuous, at 72 hours, the large fragments of the PCL disintegrated into smaller pieces, at 120 hours the samples completely degraded in the solution. The degradation rate of such substrates can be altered by modifying the substrate by blending it with other polymers to increase or decrease the degradation time of the substrate depending on the applications used. An example of such blending is the combination of PCL/PLLA co-polymer or PCL/PLGA blending. This in vitro degradation process of biodegradable polymer substrates at high pH conditions while simulating physiological temperature conditions at 37°C is based on chemical hydrolysis only and no enzyme participation was involved. The Presence of enzymes will make the process even faster. In the body, several factors affect the degradation rate of implantable devices such as hydrolysis or reaction with water molecules, oxidation as the result of oxidants produced by the tissues, physical degradation due to swelling and mechanical loading as well as wearing, and enzymatic degradation [116]. Based on the previous studies[41, 45] we postulated that the PCL-based microelectrode arrays will degrade completely in two years. To ascertain the accurate degradation rate and time, in vivo experiments are needed. While considering the thickness and dimensions of the electrodes as they play a major role in the degradation time of the arrays.

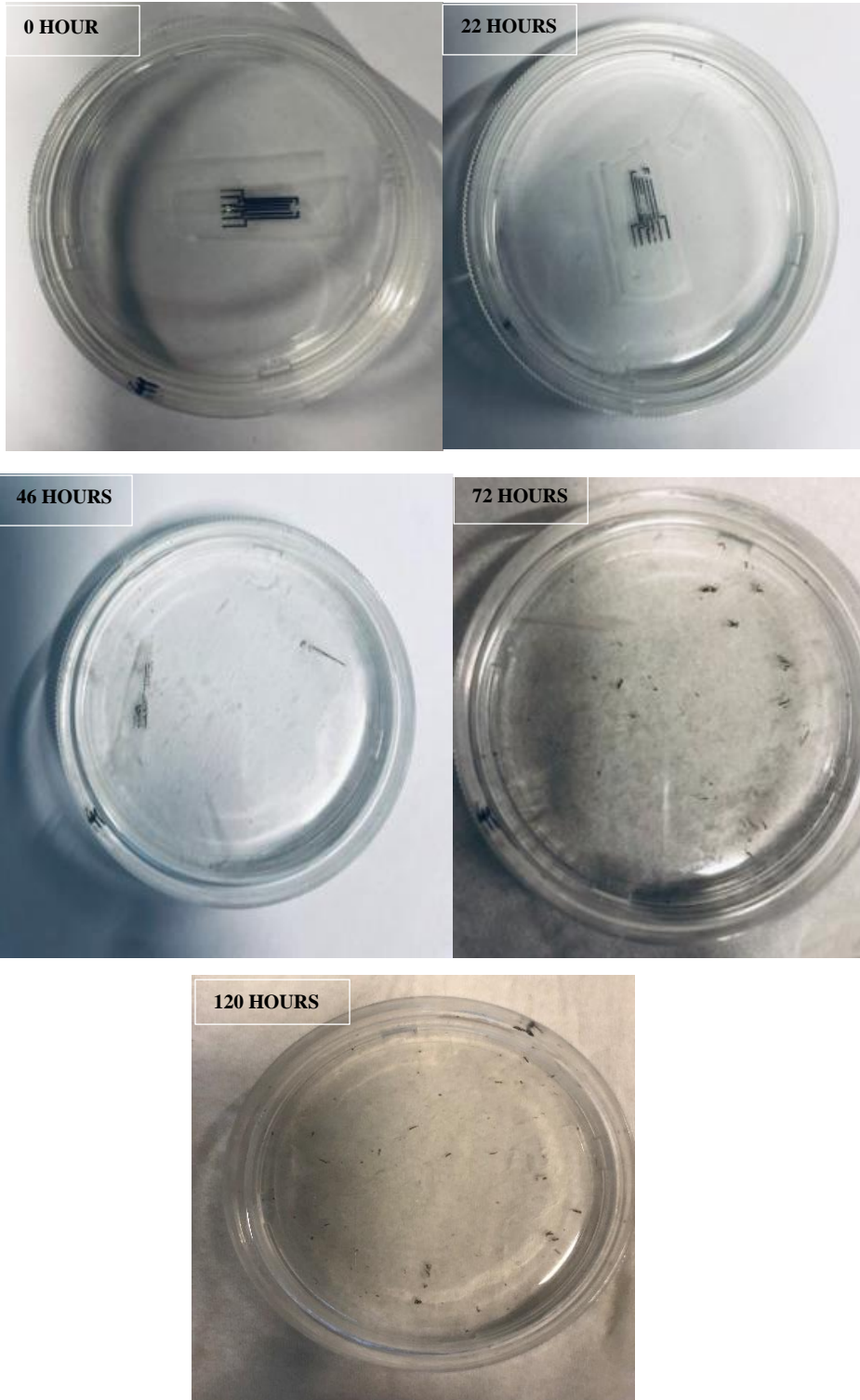


Figure 54. Series of images captured at different stages of accelerated degradation testing of PCL-based microelectrodes in buffer solution (pH 13) at 37 °C

CHAPTER 6

DISCUSSION

Neurophysiologic monitoring is a commonly used tool for diagnosing and treating certain neurological diseases such as epilepsy, Parkinson's disease, dystonia, essential tremors, and many more. Currently, available brain microelectrodes are made on rigid substrates or flexible substrates with elastic modulus extremely higher than that of the brain, this causes a biomechanical mismatch between the implanted device and the brain tissues, causing injuries to the site of implantation and also limiting the functional lifespan of the implanted devices as the result of gliosis and device failure. In the case of epilepsy, where the microelectrodes are required to be put in place for several months, patients are exposed to high-risk second surgery for device retrieval at the end of the monitoring period when conventional microelectrodes are used. It also adds additional cost to the patient and consumes time for both the patients and their caregivers. Additionally, there is a risk of infection associated with the invasive procedure and other possible complications. Intracranial microelectrodes for postoperative seizures and brain function recovery would be useful as well, and potentially more sensitive than scalp monitoring, this clinical need drives efforts to develop neurophysiological monitoring devices that will meet the clinical demands. To overcome the limitations of the currently available brain microelectrodes, the use of biodegradable polymers has been proposed to develop devices on a very soft, flexible, and biodegradable substrate. These proposed polymers however have a very low melting point and low mechanical stability as compared to the substrate materials used in conventional devices. They also not be able

to withstand some steps of the conventional fabrication processes that involve the use of high temperatures and harsh chemical processing conditions. With current technological advancements in the field of microfabrication, other alternative technologies are made available to eliminate such harsh and unbearable conditions of bioresorbable polymers, making it possible to be able to fabricate devices on such polymers, however, there are still limited studies that explored different substrate materials as well as the electrode materials. There is also no work done to integrate gold on such substrates despite it being a very good conductive and biocompatible electrode material using cost-effective and efficient technologies that allows the development of flexible and biodegradable brain microelectrodes. The main purpose of our work is to develop a biodegradable microelectrode array using a drop-on-demand inkjet printing technology, with a very good electrochemical performance and flexibility, that can be used for physiological monitoring over a certain period and eliminates the need for a second surgery for device retrieval. Additionally, the device being flexible will enhance the stability of recording, less or no micro motion and triggering of immune response which causes device failure. We tested two different substrates one biodegradable and the second one non-biodegradable. For the non-biodegradable device, PI substrate was used. This is one of the state-of-the-art materials used in the microfabrication of devices and has proven to be a very good candidate for neural interfacing because of its chemical stability and biocompatibility. We also used polyimide ink to passivate the gold electrodes printed on the substrate. To our knowledge, this is the first flexible gold electrode printed on polyimide and passivated with polyimide ink using an inkjet printing technology and tested in vivo as a proof of concept to check its feasibility in recording epilepsy from the brain.

Beginning with the PI, our study showed that gold nanoparticle inks are suitable for use as an electrode material on PI using inkjet printing technology. We have also demonstrated that polyimide ink, having satisfied some of the inkjettable ink requirements for the jetting properties of a cartridge can be printed as a passivation layer on the electrodes. This material combination has shown that the electrodes printed have good electrochemical performance and stability in recording physiological activities. Additionally, the printed patterns showed good adhesion and good mechanical properties. The materials used have proven to be biocompatible in several research [117-121]. As for the biodegradable electrodes, we demonstrated that PCL, which is an FDA-approved polymer for use in medical applications is a good candidate for use as a substrate material for microelectrode arrays. This is in support of a study previously conducted using silver nanoparticles on PCL substrate[45]. Additionally, it has been shown to be a good material for the insulation of electrodes on PCL substrate via the heat pressing condition. A similar technique of heat pressing encapsulation of electrodes on PCL has been shown in studies conducted by [41, 93]. PCL has shown a very good mechanical properties and optimum ink adhesion due to the surface roughness of the PCL films and its hydrophobic nature. However, the bumpy island-like raisings and spherulitic appearance on the surface of the substrate affected the printing quality, making it a challenge to scale down the line width of the track of our electrodes and the exposed site. The gold ink viscosity also participated in this because its viscosity is within the lower range of the ink requirements for inkjet printing. A very moderate ink is needed to address this challenge.

Additionally, our study has also shown the difference in sheet resistance between electrodes printed on PI and PCL, the difference in the number of layers and its effect on sheet resistance, as well as the effect of the number of flashes on sheet resistance as in

the case of PCL where photonic sintering was employed. We found out that an increase in the number of layers of gold is inversely proportional to the sheet resistance. The higher the number of layers the better lowers the sheet resistance. This is due to the fact that an increase in the number of layers of the gold nanoparticles leads to the formation of dense gold print with fewer or no cracks upon sintering, and its conductivity is less affected by the nature of the substrate. This finding is in support of a study conducted by [122] where gold electrodes were printed on PI using inkjet printing technology. As for the photonic sintering, a dedicated photonic sintering machine will provide control over many sintering parameters such as the light-to-substrate distance, pulse width, number of pulses, and the interval between each pulse while maintaining the desired power of the light to be incident on the print, this is a challenge while using a simple camera flash because you don't get the exact flash output anytime you trigger the flash. The battery energy affects the output of the flash, and you have less control over other parameters. This makes setting up a certain condition for sintering very challenging and time-consuming, and you are prone to either underexposing or overexposing the printed electrodes, which in the latter causes cracks and eventually discontinuity of the printed electrodes track, rendering it to be a non-conductive and hence non-functional electrode. Printing several layers of conductive ink has been a remedy to over-exposure in our condition and it has proven to give a very high conductivity and low resistance.

As for the insulation of the PI-based control electrodes, a commercially available PI ink was used for the insulation layer. Printing PI ink over gold sintered electrodes is a challenging step. Due to the nature of the ink, it clogs the nozzles very easily necessitating several cleaning cycles during the printing. It is also very hydrophobic on the sintered gold electrodes, creating a non-uniform coverage and discontinuous printed lines on the

electrode track. This led to the introduction of an additional step of plasma etching to increase the wettability of the surface before printing the polyimide ink for insulation. It is also worth mentioning that a slight increase in the temperature of the platen or cartridge leads to abnormal spread which can cause whole electrodes to be coated with the ink, including the initially planned site to be exposed. To address this issue a polyimide ink with slightly increased viscosity is suggested.

Regarding the stability of electrodes printed on PI and PCL, our work demonstrated that gold electrodes printed on the substrates used to have good stable electrochemical performance, where the impedance of electrodes both before and after in vivo studies was assessed. This is a good method of assessing the stability of recording devices when only acute recording is done. To better assess the stability of electrodes, the impedance over a long period following implantation, as well as its ability to record physiological signals need to be evaluated.

Seizure recordings gotten from the control and biodegradable electrodes shows the potential of low-cost degradable devices in recording neurophysiological signals. It is worth mentioning that recordings were gotten from 6 channels electrodes on 32 channels head stage. However, we were able to print up to 16 channels of functional electrodes. The reason for this is because of the challenges in making proper contact between the ribbon cable and the ME2100 connector for the head stage. Using a conductive epoxy will enable further experiments to be done on a denser number of channels. This will also make connections to be proper when a chronic recording is to be done while ensuring stability in signal and good SNR.

CHAPTER 7

CONCLUSION

In this thesis, an advanced microfabrication technology, a drop-on-demand inkjet printer was used to develop highly flexible and biodegradable microelectrode arrays for monitoring neurophysiologic signals. The inkjet printing process for gold electrodes on PI and PCL has been optimized to obtain good electrical conductivity and electrochemical performance as well as stable neurophysiological signals with high SNR. Our work has provided comprehensive information about the fabrication process of a high-performance flexible and biodegradable brain microelectrodes array and electrophysiological recording of epilepsy *in vivo* from the brain. Among other microelectrodes developed, our work stands out as exceptional because we integrated materials known to be non-toxic, chemically stable, and biocompatible to develop a fully flexible and biodegradable microelectrode array using a cost-effective and versatile fabrication process. The proof of concept of our work demonstrated that PCL-based microelectrodes arrays have the potential to be used as a tool for long-term monitoring of epilepsy both in the preclinical phase and clinical phase.

Future work will involve the assessment of chronic neurophysiological recording stability over a long period, *in vivo* biodegradability evaluation, and the assessment of the degradation rate, additionally, a biocompatibility test of the microelectrodes is needed at the end of the monitoring period to assess its compatibility or rejection by the body. This is a critical step toward the translation of implantable devices for clinical use. A further test could also be done to evaluate the capability of biodegradable microelectrodes in stimulating the nervous system. Other gold inks and conductive inks of different

materials can be tested and optimized to scale down the size of electrodes and print very dense microelectrodes for dense recording and stimulation.

The fabrication and testing concept introduced in this work shows a solid foundation of the potential of bioresorbable microelectrode arrays for use in several clinical applications ranging from preoperative monitoring to postoperative monitoring of neurophysiological signals while minimizing mechanical injuries to the brain, foreign body response, and ensuring stable chronic use.

REFERENCES

1. Healthline. *Epilepsy*. 2017 [cited 2021 19th November]; Available from: <https://www.healthline.com/health/epilepsy#facts-and-statistics>.
2. WHO. *Epilepsy*. 2022 [cited 2022 10th March]; Available from: <https://www.who.int/news-room/fact-sheets/detail/epilepsy#:~:text=Seizure%20episodes%20are%20a%20result,to%20severe%20and%20prolonged%20convulsions>.
3. Amara, S.G. and A.C. Fontana, *Excitatory amino acid transporters: keeping up with glutamate*. *Neurochem Int*, 2002. **41**(5): p. 313-8.
4. Burke, J.P. and J.J. Hablitz, *Metabotropic glutamate receptor activation decreases epileptiform activity in rat neocortex*. *Neurosci Lett*, 1994. **174**(1): p. 29-33.
5. Vrinda, M., et al., *Enriched environment attenuates behavioral seizures and depression in chronic temporal lobe epilepsy*. *Epilepsia*, 2017. **58**(7): p. 1148-1158.
6. Rogawski, M.A. and W. Löscher, *The neurobiology of antiepileptic drugs*. *Nat Rev Neurosci*, 2004. **5**(7): p. 553-64.
7. Sisodiya, S., *Etiology and management of refractory epilepsies*. *Nat Clin Pract Neurol*, 2007. **3**(6): p. 320-30.
8. Kwan, P., et al., *Definition of drug resistant epilepsy: consensus proposal by the ad hoc Task Force of the ILAE Commission on Therapeutic Strategies*. *Epilepsia*, 2010. **51**(6): p. 1069-77.
9. MayoClinic. *Epilepsy*. 2021 [cited 2021 20th November]; Available from: <https://www.mayoclinic.org/diseases-conditions/epilepsy/diagnosis-treatment/drc-20350098>.
10. Karakis, I., et al., *The utility of routine EEG in the diagnosis of sleep disordered breathing*. *J Clin Neurophysiol*, 2012. **29**(4): p. 333-8.
11. Smith, S.J., *EEG in the diagnosis, classification, and management of patients with epilepsy*. *J Neurol Neurosurg Psychiatry*, 2005. **76 Suppl 2**(Suppl 2): p. ii2-7.
12. Emotiv. *Brain Controlled Technology*. 2021 [cited 2021 20th November]; Available from: <https://www.emotiv.com/brain-controlled-technology/>.
13. Jasper, H.H., *Electrical signs of epileptic discharge*. *Electroencephalogr Clin Neurophysiol*, 1949. **1**(1): p. 11-8.
14. Carter, M. and J.C. Shieh, *Chapter 4 - Electrophysiology*, in *Guide to Research Techniques in Neuroscience*, M. Carter and J.C. Shieh, Editors. 2010, Academic Press: New York. p. 91-118.
15. Buzsáki, G., C.A. Anastassiou, and C. Koch, *The origin of extracellular fields and currents--EEG, ECoG, LFP and spikes*. *Nat Rev Neurosci*, 2012. **13**(6): p. 407-20.
16. Lalley, P.M., *Intracellular Recording*, in *Encyclopedia of Neuroscience*, M.D. Binder, N. Hirokawa, and U. Windhorst, Editors. 2009, Springer Berlin Heidelberg: Berlin, Heidelberg. p. 2019-2026.
17. Crochet, S. and C.C. Petersen, *Correlating whisker behavior with membrane potential in barrel cortex of awake mice*. *Nat Neurosci*, 2006. **9**(5): p. 608-10.

18. Crochet, S., et al., *Synaptic mechanisms underlying sparse coding of active touch*. *Neuron*, 2011. **69**(6): p. 1160-75.
19. Epsztein, J., et al., *Impact of spikelets on hippocampal CA1 pyramidal cell activity during spatial exploration*. *Science*, 2010. **327**(5964): p. 474-7.
20. Long, M.A., D.Z. Jin, and M.S. Fee, *Support for a synaptic chain model of neuronal sequence generation*. *Nature*, 2010. **468**(7322): p. 394-9.
21. Kumar, S.S., et al., *Engineering microscale systems for fully autonomous intracellular neural interfaces*. *Microsyst Nanoeng*, 2020. **6**: p. 1.
22. Spira, M.E. and A. Hai, *Multi-electrode array technologies for neuroscience and cardiology*. *Nature Nanotechnology*, 2013. **8**(2): p. 83-94.
23. Oxley, T.J., et al., *Minimally invasive endovascular stent-electrode array for high-fidelity, chronic recordings of cortical neural activity*. *Nat Biotechnol*, 2016. **34**(3): p. 320-7.
24. Stacey, W.C. and B. Litt, *Technology insight: neuroengineering and epilepsy-designing devices for seizure control*. *Nat Clin Pract Neurol*, 2008. **4**(4): p. 190-201.
25. Yu, K.J., et al., *Bioresorbable silicon electronics for transient spatiotemporal mapping of electrical activity from the cerebral cortex*. *Nat Mater*, 2016. **15**(7): p. 782-791.
26. Kim, D.H., et al., *Dissolvable films of silk fibroin for ultrathin conformal bio-integrated electronics*. *Nat Mater*, 2010. **9**(6): p. 511-7.
27. Hinterberger, T., et al., *Voluntary brain regulation and communication with electrocorticogram signals*. *Epilepsy Behav*, 2008. **13**(2): p. 300-6.
28. Wang, W., et al., *An electrocorticographic brain interface in an individual with tetraplegia*. *PLoS One*, 2013. **8**(2): p. e55344.
29. Bullara, L.A., et al., *Evaluation of electrode array material for neural prostheses*. *Neurosurgery*, 1979. **5**(6): p. 681-6.
30. Schalk, G. and E.C. Leuthardt, *Brain-computer interfaces using electrocorticographic signals*. *IEEE Rev Biomed Eng*, 2011. **4**: p. 140-54.
31. Blakely, T., et al., *Robust, long-term control of an electrocorticographic brain-computer interface with fixed parameters*. *Neurosurg Focus*, 2009. **27**(1): p. E13.
32. Kellis, S.S., et al., *Human neocortical electrical activity recorded on nonpenetrating microwire arrays: applicability for neuroprostheses*. *Neurosurg Focus*, 2009. **27**(1): p. E9.
33. Sung, C., et al., *Multimaterial and multifunctional neural interfaces: from surface-type and implantable electrodes to fiber-based devices*. *Journal of Materials Chemistry B*, 2020. **8**(31): p. 6624-6666.
34. Lecomte, A., E. Descamps, and C. Bergaud, *A review on mechanical considerations for chronically-implanted neural probes*. *J Neural Eng*, 2018. **15**(3): p. 031001.
35. Polikov, V.S., P.A. Tresco, and W.M. Reichert, *Response of brain tissue to chronically implanted neural electrodes*. *J Neurosci Methods*, 2005. **148**(1): p. 1-18.
36. Clarke, L.E. and B.A. Barres, *Emerging roles of astrocytes in neural circuit development*. *Nat Rev Neurosci*, 2013. **14**(5): p. 311-21.
37. Eroglu, C. and B.A. Barres, *Regulation of synaptic connectivity by glia*. *Nature*, 2010. **468**(7321): p. 223-31.

38. Daube, D.I.R.a.J.R., *Clinical Neurophysiology*. 4th ed. 2016: Oxford University Press.
39. King-Stephens, D., et al., *Lateralization of mesial temporal lobe epilepsy with chronic ambulatory electrocorticography*. *Epilepsia*, 2015. **56**(6): p. 959-67.
40. Wang, L., et al., *A fully biodegradable and self-electrified device for neuroregenerative medicine*. *Sci Adv*, 2020. **6**(50).
41. Xu, K., et al., *Bioresorbable Electrode Array for Electrophysiological and Pressure Signal Recording in the Brain*. *Adv Healthc Mater*, 2019. **8**(15): p. e1801649.
42. Can, E., et al., *Investigation of PLLA/PCL blends and paclitaxel release profiles*. *AAPS PharmSciTech*, 2011. **12**(4): p. 1442-53.
43. Wei-Chen Huang, X.C.O., Ik Soo Kwon, Chaitanya Gopinath, Lee E. Fisher, and G.K.F. Haosheng Wu, Robert A. Gaunt,* and Christopher J. Bettinger*, *Ultrasoft Hydrogel-Based Neural Interfaces Fabricated by Aqueous-Phase Microtransfer Printing*. *Advanced Functional Materials*, 2018.
44. Nouran Adly, S.W., Silke Seyock, Fabian Brings, Alexey Yakushenko, Andreas Offenhäusser & Bernhard Wolfrum, *Printed microelectrode arrays on soft materials: from PDMS to hydrogels*. *Nature*, 2018. **2**(15).
45. Almasri, R.M., et al., *Highly Flexible Single-Unit Resolution All Printed Neural Interface on a Bioresorbable Backbone*. *ACS Applied Bio Materials*, 2020. **3**(10): p. 7040-7051.
46. Bezwada, R.S., et al., *Monocryl suture, a new ultra-pliable absorbable monofilament suture*. *Biomaterials*, 1995. **16**(15): p. 1141-8.
47. Shive, M.S. and J.M. Anderson, *Biodegradation and biocompatibility of PLA and PLGA microspheres*. *Adv Drug Deliv Rev*, 1997. **28**(1): p. 5-24.
48. Guarino, V., et al., *Polycaprolactone: Synthesis, properties, and applications*. *Encyclopedia of Polymer Science and Technology*, 2002: p. 1-36.
49. Integralife. *Auragen™ Cortical grid* 2021 [cited 2021 6th January]; Available from: <https://www.integralife.com/auragen-cortical-grid-electrodes/category/brain-mapping-auragen-cortical-grid-electrodes>.
50. Neuronexus. *Neuronexus ECoG*. 2021 [cited 2021 5th January]; Available from: <https://neuronexus.com/products/neural-probes/ecog/>.
51. Cortac. *PMT Cortac Intracranial electrodes*. 2021 [cited 2021 6th January]; Available from: <http://www.pmtcorp.com/cortac.html>.
52. Cortec, *CORTEC silicone-based AirRay research electrodes*. 2021.
53. Electrodes, A.-T.M.S.C., *Ad-Tech Medical Subdural Cortical Electrodes*, FDA, Editor. 2019.
54. Cortec. *AirRay research micro 8 hexagonal*. 2020 [cited 2021 9]; Available from: <https://www.cortec-neuro.com/product-portfolio/airray-research-micro-8-hexagonal/>.
55. NeuroTech, C. *Cambridge NeuroTech ECOG 32A*. 2021 [cited 2021 8th january]; Available from: <https://www.cambridgeneurotech.com/neural-probes>.
56. ATLASNeuro. *ATLASNeuro silicon probes: E16+R-250-S1-L8 NT*. 2021 [cited 2021 6th January]; Available from: <https://www.atlasneuro.com/en/probes/passive-probes>.
57. Neuropixels. *Neuropixels 1.0*. 2021 [cited 2021 5th January]; Available from: <https://www.neuropixels.org/probe>.

58. Neuropixels. *Neuropixels 2.0*. 2021 [cited 2021 6th January]; Available from: <https://www.neuropixels.org/>.
59. systems, M. *EcoFlexMea36*. 2019 [cited 2021 6th January]; Available from: <https://www.multichannelsystems.com/products/ecoflexmea36>.
60. systems, M. *EcoFlexMea24*. 2019 [cited 2021 6th January]; Available from: <https://www.multichannelsystems.com/products/ecoflexmea24>.
61. systems, M. *FlexMEA72*. 2019 [cited 2021 5th January]; Available from: <https://www.multichannelsystems.com/products/flexmea72>.
62. systems, M. *FlexMEA36*. 2019 [cited 2021 5th January]; Available from: <https://www.multichannelsystems.com/products/flexmea36>.
63. systems, M. *FlexMEA36-Om*. 2019 [cited 2021 6th January]; Available from: <https://www.multichannelsystems.com/products/flexmea36>.
64. microsystem, B. *Blackrock microsystem Microflex Array*. 2021 [cited 2021 6th January]; Available from: <https://blackrockneurotech.com/research/products/#electrodes>.
65. Hubenthal, F., *1.13 - Noble Metal Nanoparticles: Synthesis and Optical Properties*, in *Comprehensive Nanoscience and Technology*, D.L. Andrews, G.D. Scholes, and G.P. Wiederrecht, Editors. 2011, Academic Press: Amsterdam. p. 375-435.
66. Chen, S.P., et al., *Inkjet Printed Conductive Tracks for Printed Electronics*. ECS Journal of Solid State Science and Technology, 2015. **4**(4): p. P3026-P3033.
67. Kamyshny, A. and S. Magdassi, *Conductive Nanomaterials for Printed Electronics*. Small, 2014. **10**(17): p. 3515-3535.
68. Singh, M., et al., *Inkjet Printing—Process and Its Applications*. Advanced Materials, 2010. **22**(6): p. 673-685.
69. Sternkiker, C., et al., *Upscaling of the Inkjet Printing Process for the Manufacturing of Passive Electronic Devices*. IEEE Transactions on Electron Devices, 2016. **63**(1): p. 426-431.
70. Lemarchand, J., et al., *Challenges, Prospects, and Emerging Applications of Inkjet-Printed Electronics: A Chemist's Point of View*. Angewandte Chemie International Edition. **n/a**(n/a): p. e202200166.
71. Cummins, G. and M.P.Y. Desmulliez, *Inkjet printing of conductive materials: a review*. Circuit World, 2012. **38**(4): p. 193-213.
72. Wilkinson, N.J., et al., *A review of aerosol jet printing—a non-traditional hybrid process for micro-manufacturing*. The International Journal of Advanced Manufacturing Technology, 2019. **105**(11): p. 4599-4619.
73. Beedasy, V. and P.J. Smith, *Printed Electronics as Prepared by Inkjet Printing*. Materials (Basel, Switzerland), 2020. **13**(3): p. 704.
74. Karunakaran, S.K., et al., *Recent progress in inkjet-printed solar cells*. Journal of Materials Chemistry A, 2019. **7**(23): p. 13873-13902.
75. Soltman, D. and V. Subramanian, *Inkjet-printed line morphologies and temperature control of the coffee ring effect*. Langmuir, 2008. **24**(5): p. 2224-31.
76. Abbasi, E., et al., *Silver nanoparticles: Synthesis methods, bio-applications and properties*. Crit Rev Microbiol, 2016. **42**(2): p. 173-80.
77. Nair, L.S.L., C.T., *Silver Nanoparticles: Synthesis and Therapeutic Applications*. J. Biomed. Nanotechnol, 2007. **3**: p. 301–316.
78. Salomoni, R., et al., *Antibacterial effect of silver nanoparticles in Pseudomonas aeruginosa*. Nanotechnol Sci Appl, 2017. **10**: p. 115-121.

79. Pajor-Świerzy, A.F., Y.; Kamyshny, A.; Magdassi, S., *Air Stable Copper-Silver Core-Shell Submicron Particles: Synthesis and Conductive Ink Formulation*. *Colloids Surf. A Physicochem. Eng. Asp*, 2017: p. 272–280.
80. Black, K., et al., *Silver Ink Formulations for Sinter-free Printing of Conductive Films*. *Sci Rep*, 2016. **6**: p. 20814.
81. Rao, V.K., Venkata, A., Karthik, P. S. & Singh, S. P, *Conductive silver inks and their applications in printed and flexible electronics*. *RSC Adv*, 2015(5): p. 77760–77790.
82. Liu, J., Yu, S., Yin, Y. & Chao, J, *Methods for separation, identification, characterization and quantification of silver nanoparticles*. *TrAC Trends Anal. Chem*, 2012. **33**: p. 95–106.
83. Murali, K., M. Neelakandan, and S. Thomas, *Biomedical applications of gold nanoparticles*. *JSM Nanotechnol Nanomed*, 2018. **6**(1): p. 1064.
84. Hu, X., et al., *Multifunctional Gold Nanoparticles: A Novel Nanomaterial for Various Medical Applications and Biological Activities*. *Front Bioeng Biotechnol*, 2020. **8**: p. 990.
85. Carnovale, C., et al., *Identifying Trends in Gold Nanoparticle Toxicity and Uptake: Size, Shape, Capping Ligand, and Biological Corona*. *ACS Omega*, 2019. **4**(1): p. 242-256.
86. Kohane, D.S. and R. Langer, *Biocompatibility and drug delivery systems*. *Chemical Science*, 2010. **1**(4): p. 441-446.
87. Kus-Liśkiewicz, M., P. Fickers, and I. Ben Tahar, *Biocompatibility and Cytotoxicity of Gold Nanoparticles: Recent Advances in Methodologies and Regulations*. *Int J Mol Sci*, 2021. **22**(20).
88. Tortorich, R.P., H. Shamkhalichenar, and J.-W. Choi, *Inkjet-Printed and Paper-Based Electrochemical Sensors*. *Applied Sciences*, 2018. **8**(2): p. 288.
89. Jorge de Souza, T.A., L.R. Rosa Souza, and L.P. Franchi, *Silver nanoparticles: An integrated view of green synthesis methods, transformation in the environment, and toxicity*. *Ecotoxicology and Environmental Safety*, 2019. **171**: p. 691-700.
90. Zhang, J., et al., *Silver Nanoparticles for Conductive Inks: From Synthesis and Ink Formulation to Their Use in Printing Technologies*. *Metals*, 2022. **12**(2): p. 234.
91. Wünsch, S., et al., *Progress of alternative sintering approaches of inkjet-printed metal inks and their application for manufacturing of flexible electronic devices*. *Journal of Materials Chemistry C*, 2014. **2**(48): p. 10232-10261.
92. Grouchko, M., et al., *Conductive Inks with a “Built-In” Mechanism That Enables Sintering at Room Temperature*. *ACS Nano*, 2011. **5**(4): p. 3354-3359.
93. Ferlauto, L., et al., *All-polymeric transient neural probe for prolonged in-vivo electrophysiological recordings*. *Biomaterials*, 2021. **274**: p. 120889.
94. Adly, N., et al., *Printed microelectrode arrays on soft materials: from PDMS to hydrogels*. *npj Flexible Electronics*, 2018. **2**(1): p. 15.
95. Yu, K.J., et al., *Bioresorbable silicon electronics for transient spatiotemporal mapping of electrical activity from the cerebral cortex*. *Nature materials*, 2016. **15**(7): p. 782-791.
96. Holländer, J., et al., *Three-Dimensional Printed PCL-Based Implantable Prototypes of Medical Devices for Controlled Drug Delivery*. *J Pharm Sci*, 2016. **105**(9): p. 2665-2676.

97. Wang, W., et al., *Dual-functional transdermal drug delivery system with controllable drug loading based on thermosensitive poloxamer hydrogel for atopic dermatitis treatment*. Sci Rep, 2016. **6**: p. 24112.
98. Hu, X., et al., *Electrospinning of polymeric nanofibers for drug delivery applications*. J Control Release, 2014. **185**: p. 12-21.
99. Manoukian, O., et al., *Biomedical Nanotechnology*. 2017, Springer London.
100. Sethuraman, S., U.M. Krishnan, and A. Subramanian, *Biomaterials and nanotechnology for tissue engineering*. 2016: CRC Press.
101. Zajac, F. and J. Bourne, *Critical reviews in biomedical engineering*. Muscle and tendon: properties, models, scaling, and application to biomechanics and motor control. CRC Press, Boca Raton, 1989. **17**(4): p. 359-411.
102. Domingos, M., et al., *Polycaprolactone Scaffolds Fabricated via Bioextrusion for Tissue Engineering Applications*. Int J Biomater, 2009. **2009**: p. 239643.
103. Holzapfel, B.M., et al., *Species-specific homing mechanisms of human prostate cancer metastasis in tissue engineered bone*. Biomaterials, 2014. **35**(13): p. 4108-15.
104. Ossila. *Sheet Resistance Measurements of Thin Films*. 2022 [cited 2022 16 may]; Available from: <https://www.ossila.com/pages/sheet-resistance-measurements-thin-films>.
105. Hetke, J.F., et al., *Silicon ribbon cables for chronically implantable microelectrode arrays*. IEEE Trans Biomed Eng, 1994. **41**(4): p. 314-21.
106. Najafi, K., J. Ji, and K.D. Wise, *Scaling limitations of silicon multichannel recording probes*. IEEE Trans Biomed Eng, 1990. **37**(1): p. 1-11.
107. Neto, J.P., et al., *Does Impedance Matter When Recording Spikes With Polytrodes?* Frontiers in Neuroscience, 2018. **12**.
108. Cui, H., et al., *Electrochemical characteristics of microelectrode designed for electrical stimulation*. BioMedical Engineering OnLine, 2019. **18**(1): p. 86.
109. Paxinos, G. and C. Watson, *WITHDRAWN: Plates and Figures*, in *The Rat Brain in Stereotaxic Coordinates*, G. Paxinos and C. Watson, Editors. 1982, Academic Press. p. 13-153.
110. Ben-Ari, Y., et al., *A new model of focal status epilepticus: intra-amygdaloid application of kainic acid elicits repetitive secondarily generalized convulsive seizures*. Brain Res, 1979. **163**(1): p. 176-9.
111. Ben-Ari, Y., E. Tremblay, and O.P. Ottersen, *Injections of kainic acid into the amygdaloid complex of the rat: An electrographic, clinical and histological study in relation to the pathology of epilepsy*. Neuroscience, 1980. **5**(3): p. 515-528.
112. Araki, T., et al., *Characterization of neuronal death induced by focally evoked limbic seizures in the C57BL/6 mouse*. J Neurosci Res, 2002. **69**(5): p. 614-21.
113. Shinoda, S., et al., *Development of a model of seizure-induced hippocampal injury with features of programmed cell death in the BALB/c mouse*. J Neurosci Res, 2004. **76**(1): p. 121-8.
114. Mouri, G., et al., *Unilateral hippocampal CA3-predominant damage and short latency epileptogenesis after intra-amygdala microinjection of kainic acid in mice*. Brain Res, 2008. **1213**: p. 140-51.
115. Jacobs, J., et al., *High-frequency oscillations (HFOs) in clinical epilepsy*. Prog Neurobiol, 2012. **98**(3): p. 302-15.

116. Lyu, S. and D. Untereker, *Degradability of polymers for implantable biomedical devices*. International journal of molecular sciences, 2009. **10**(9): p. 4033-4065.
117. Valle, J.d., et al. *Biocompatibility evaluation of parylene C and polyimide as substrates for peripheral nerve interfaces*. in *2015 7th International IEEE/EMBS Conference on Neural Engineering (NER)*. 2015.
118. Wurth, S., et al., *Long-term usability and bio-integration of polyimide-based intra-neural stimulating electrodes*. Biomaterials, 2017. **122**: p. 114-129.
119. Heo, D.N., et al., *Flexible and Highly Biocompatible Nanofiber-Based Electrodes for Neural Surface Interfacing*. ACS Nano, 2017. **11**(3): p. 2961-2971.
120. Seo, J.-M., et al., *Biocompatibility of polyimide microelectrode array for retinal stimulation*. Materials Science and Engineering: C, 2004. **24**(1): p. 185-189.
121. Zhou, J.A., et al., *A Suprachoroidal Electrical Retinal Stimulator Design for Long-Term Animal Experiments and In Vivo Assessment of Its Feasibility and Biocompatibility in Rabbits*. Journal of Biomedicine and Biotechnology, 2008. **2008**: p. 547428.
122. Bachmann, B., et al., *All-inkjet-printed gold microelectrode arrays for extracellular recording of action potentials*. Flexible and Printed Electronics, 2017. **2**(3): p. 035003.